University of Alberta

Mitochondria in Vascular Health and Disease

by

Peter Roman Dromparis

A thesis submitted to the Faculty of Graduate Studies and Research
in partial fulfillment of the requirements for the degree of

Doctor of Philosophy

in

Experimental Medicine

Department of Medicine

Dedication

This dissertation is dedicated to my parents, Dianne and Constantin Dromparis, for without their unconditional love and support, encouragement, sacrifice and patience, I would not have been able to accomplish the successes I have achieved. This work is also dedicated to my wife, Kristalee, with whom I hope to share many more of life's milestones.

Abstract

Mitochondria generate reactive oxygen species (mROS) and metabolic substrates like alpha-ketogluterate (αKG), in proportion to oxygen, which target extra-mitochondrial effectors to coordinate a cellular response. For example, acute hypoxia decreases mROS, resulting in pulmonary artery smooth muscle cell (PASMC) contraction and hypoxic pulmonary vasoconstriction. Metabolic suppression can mimic the hypoxic effects, even in normoxia. In cancer, which has suppressed mitochondrial glucose oxidation (GO), reduced mitochondrial-derived signals including mROS and αKG stabilize hypoxia inducible factor 1α (HIF1α), resulting in normoxic activation that contributes to apoptosis resistance and angiogenesis. This metabolic suppression is shared with hyperproliferative and anti-apoptotic cells in the distal pulmonary artery (PA) wall, and is the hallmark of pulmonary arterial hypertension (PHT). Recently, we proposed that endoplasmic reticulum (ER)-stress-induced disruption of an 'ER-mitochondrial unit' as a PHT trigger, since the ER provides Ca^{2+} that is required for many of the key mitochondrial metabolic enzymes like pyruvate dehydrogenase (PDH) and Krebs cycle enzymes like isocitrate dehydrogenase (IDH; produces αKG). We show that like ER-stress, loss of uncoupling protein-2 (UCP2), reduces mitochondrial calcium (Ca^{2+}_m) in PASMCs. This suppresses PDH activity, Krebs cycle function and mROS production, activating HIF1α and contributing to apoptosis resistance in vitro. Mice lacking UCP2 spontaneously develop PHT with distal PA remodeling similar to hypoxic wildtype mice (a standard PHT model). This is the first description of UCP2 influencing oxygen sensing and may open a new window for biomarker or therapeutic strategies. We also show targeting ER-stress is a viable therapeutic strategy in PHT. 4-phenylbutyric acid (PBA), a FDA approved chemical chaperone that facilitates protein folding and attenuates ER-stress. PBA prevented and reversed pulmonary vascular remodeling and PHT in chronic hypoxia and monocrotaline

rodents. In isolated PASMCs, PBA, and a second chemical chaperone tauroursodeoxycholate maintained Ca^{2+}_{m}, normalizing PDH activity and mROS/αKG, reducing proliferation and inducing apoptosis in hypoxia (an ER-stress inducer). Thus, pathobiology linked with the functional dysregulation between mitochondria and other organelles can be therapeutically targeted. Finally, we show that mitochondrial activation with thiazolidinediones can impair HIF1α signaling in a hindlimb ischemia model, potentially explaining some of the adverse cardiovascular events in some patients with these drugs.

Table of Contents

Chapter Four

Chapter Five

Chapter One

Mitochondria in Vascular Health and Disease

Introduction

Adaptation is a foundation of life, and responsive sensing systems (RSS), which can both sense altered conditions and respond appropriately, are its most critical tools. An ideal cellular system must sense the supply and demand of fuel, including oxygen, and respond with fine-tuning signals that reach throughout the cell, or even with the induction of death if severe or permanent damage is unavoidable to protect the remaining cells. Such an RSS is critical for normal cellular function but could also be exploited by disease and even by evolution itself.

Possibly the most sophisticated RSS known is the cell's mitochondrial network. Mitochondria are recognized sensors of oxygen and fuel (carbohydrates, fatty acids), producers of heat and the "molecule of life" ATP, signaling hubs with their redox-based signals reaching the cell membrane and the nucleus, and effective inducers of cell death (apoptosis). They can also sense danger signals and induce inflammation in an effort to defend and repair. Mitochondria constantly move using cytoskeletal motors, connect with each other to form continuous networks, and change the network size and shape through dynamic processes such as fission and fusion. The mitochondrial network constantly integrates information from multiple sources intracellularly (such as from the nucleus or the endoplasmic reticulum), locally from paracrine signals, or even remotely in response to circulating cytokines or hormones. An intact mitochondrial network can respond by disseminating information with redox and electrical signals or Ca^{2+} waves throughout the cell, to the local environment and beyond, reaching the whole organism with recently discovered mediators called mitokines (Figure 1-1).

Traditional biochemistry taught us that the main function of mitochondria is the production of ATP in the presence of oxygen. We now know that although this is the most energetically efficient way of producing ATP, it is not the only one. ATP can be produced in large amounts outside of the mitochondria in the cytoplasm, enough to support even rapidly proliferating cancer cells. Although mitochondrial ATP production is critical in energy-consuming tissues such as the

myocardium, the importance of mitochondria goes far beyond energy production in other tissues. In the vasculature, a tissue that does not require large amounts of energy, mitochondria function as a sensors, signaling hubs, and regulators of apoptosis.

Another recent concept is that mitochondria have a range of function within which they operate normally, as all RSS should. In other words, their function is not all-or-none, dysfunctional or normal. A prime example is their traditional role in cancer biology in which they were thought to be permanently damaged by the cancerous process. A recent paradigm shift suggests that mitochondrial suppression is perhaps a desirable process for the survival of proliferating cells and a part of an adaptive response for growing cancer cells. In that sense, mitochondria play a causal role in cancer, and their reversible, functional suppression can be a target of therapy. There is evidence that elucidating a similar role in the diseased vasculature can be the target of novel drug discovery approaches.

1.1.0 OVERVIEW

Mitochondria are the remnants of aerobic bacteria that invaded protoeukaryotic cells a billion years ago. The ability to utilize oxygen drove the development and evolution of the cardiovascular system in multicellular organisms, and for this reason mitochondria are linked to the cardiovascular system from ground zero. Mice lacking proteins critical for mitochondrial function typically die at the exact time in development when the cardiovascular system forms. This chapter does not intend to provide a comprehensive review of mitochondrial biology or include all the evidence that implicates mitochondria in vascular disease. Rather, it focuses on three concepts that could potentially provide a different angle from which to look at these intriguing organelles to better understand normal vascular function or treat vascular disease.

1.1.1 Mitochondria and oxygen homeostasis

The primary function of the vasculature is the optimization of the delivery of oxygen and fuels to organs, and mitochondria play a central role in this fundamental function. Although most organs and tissues are oxygen consumers, others (such as the vasculature and lungs) do not consume much oxygen but rather regulate its distribution to the oxygen-consuming tissues. Remarkably, there are key differences between the pulmonary and systemic vascular mitochondria suggesting a coordinated evolution of functional diversity to optimize oxygenation of the whole organism. First, the role of systemic and pulmonary vascular mitochondria in acute hypoxia is discussed, followed by a discussion of recent evidence supporting the view that the role of mitochondria in acute oxygen sensing can extend to chronic hypoxia and the control of the master regulator of angiogenesis: hypoxia-inducible factor 1a (HIF1α).

1.1.2 Mitochondria, oxidative stress, and vascular inflammation

Although not investigated in this dissertation, mitochondria can sense, in addition to oxygen, danger signals such as infectious agents or cholesterol crystals. They respond by inducing an inflammatory response that perhaps stems from their bacterial origin. Mitochondria-derived reactive oxygen species (mROS) are the critical signal for the initiation of this inflammatory response, linking the well-known oxidative stress and aging theory of vascular disease to vascular inflammation. The mitochondria's ability to induce sterile inflammation has shed light on the intriguing association between metabolic syndrome and inflammation.

1.1.3 Mitochondria, apoptosis, and proliferative vascular remodeling:

The observation that mitochondrial function can be reversibly suppressed in cancer cells to block apoptosis and promote proliferation has a vascular parallel. A cancer-like biology leading to metabolic remodeling and apoptosis resistance takes place in another deadly vascular disease: pulmonary arterial hypertension (PAH). The mitochondria/metabolic theory of PAH can explain

several unresolved questions in PAH and could extrapolate to vascular diseases with similar pathology, such as transplant arteriopathy.

1.2.0 A BRIEF OVERVIEW OF SOME ESSENTIAL MITOCHONDRIAL FUNCTIONS

1.2.1 Adenosine Triphosphate Production

Glucose and fatty acids are the two major fuels entering the mitochondria. Glycolysis metabolizes glucose in the cytoplasm to generate pyruvate, which enters the mitochondria and undergoes decarboxylation to acetyl-CoA by pyruvate dehydrogenase (PDH). Fatty acids enter the mitochondria and undergo β-oxidation, also producing acetyl-CoA. Acetyl-CoA enters the Krebs cycle, where it is oxidized, generating reduction of the electron donors nicotinamide adenine dinucleotide (NADH) and flavin adenine dinucleotide ($FADH_2$). Electrons are then transferred to the electron transport chain (ETC), a series of five iron-sulfur-rich protein megacomplexes that span the inner mitochondrial membrane. As electrons flow down the redox gradient of the ETC, hydrogen ions are extruded from the mitochondrial matrix across the inner mitochondrial membrane, contributing to an electrical gradient called the mitochondrial membrane potential ($\Delta\Psi$m). The stored energy of the $\Delta\Psi$m is used to phosphorylate ADP to ATP as protons reenter the mitochondrial matrix through the fifth ETC complex (ATP synthase), whereas the protons, electrons, and molecular oxygen form water. Oxidative phosphorylation efficiently generates ATP, producing 36 ATP/glucose or 105 ATP/palmitate[1]. In the absence of oxygen (or functional mitochondria as discussed later), glycolysis produces two ATP/glucose in the cytoplasm, and pyruvate becomes lactate instead of entering the mitochondria[1]. Under such conditions, the cell upregulates glycolysis in a coordinated approach often involving activation of HIF1α which induces the expression of several glucose transporters and all the glycolytic enzymes [hypoxia (absence of oxygen) induces HIF1α activation, which subsequently upregulates glucose transporters and glycolytic enzymes[2]] to meet basic energetic needs. Yet neither hypoxia nor suppressed mitochondria are abnormal states. For example,

systemic vessels are normally exposed to hypoxia (i.e., $pO_2 \sim 50$ mmHg), compared with pulmonary vessels exposed to $pO_2 \sim 120$ mmHg. The induction of gatekeeping enzymes [such as pyruvate dehydrogenase kinase (PDK), which inhibits PDH] can lead to a functional suppression of glucose oxidation and the Krebs cycle, whereas mitochondria remain otherwise intact. Indeed, glycolysis is the major ATP-producing pathway in most cancers[3], and therefore less efficient energy producing pathways may be sufficient for even the most rapidly proliferating cells. Thus, although the production of ATP is important, life does not always depend on mitochondrial ATP.

1.2.2 mROS Signaling

Although most electrons flowing down the ETC redox gradient ultimately reach complex V, 1-3% of electrons prematurely react with oxygen, at complexes I and III, to form superoxide. The superoxide anion in the matrix is highly reactive and can damage mitochondrial DNA (mtDNA) and proteins, including the high iron-sulfur-containing ETC complexes themselves. As a result, mROS were initially considered toxic molecules; however, this view has now changed. Rather, mROS can be critical signaling molecules that, within a certain range, can support normal or compensatory functions of the cell. This means that mROS can increase even as part of normal signaling in the cell, even though the mitochondria remain normal. Mitochondria-based manganese superoxide dismutase (MnSOD) immediately dismutates superoxide to the more stable and diffusible H_2O_2, which leaves the mitochondria and can reach several critical redox-sensitive targets in the cytoplasm (e.g., HIF1α or p53) or the cell membrane [e.g., the voltage-gated potassium (Kv) channels]. For as long as MnSOD can dismutate superoxide and decrease the potential for mtDNA damage, H_2O_2 can perform its functions in regulating redox-sensitive cellular systems. If superoxide production exceeds the capacity of MnSOD and reaches superphysiological levels, for example with high rates of oxidative phosphorylation, pathological processes ultimately leading to cell dysfunction and death ensue. Likewise,

subphysiological levels of superoxide production, for example in low oxygen, may also contribute to pathological processes (Figure 1-2).

1.2.3 Ca^{2+} Signaling

The very negative ΔΨm allows mitochondria to sequester positive ions such as Ca^{2+} from the cytoplasm. For example, at any given time in endothelial cells, mitochondria hold ~25% of the Ca^{2+} [4]. For a long time, we considered mitochondria passive sinks of Ca^{2+}, but we now know that they play a critical role in the dynamic regulation and propagation of Ca^{2+} signaling throughout the cell[5]. Similar to how ΔΨm relates to mitochondrial function and the influx of fuel, the regulation of Ca^{2+} in the cell can be matched to metabolic signals. At the same time, the function of many key mitochondrial enzymes, including PDH, are very Ca^{2+} dependent, and thus mitochondrial Ca^{2+} levels regulate mitochondrial function[6]. Therefore, mitochondrial networks allow synchronization of metabolism with Ca^{2+} signals throughout the cell[5].

1.2.4 Apoptosis

Given that mitochondria have the intrinsic ability to integrate the availability of fuel and oxygen into redox or Ca^{2+} signals that coordinate fundamental cellular functions, it seems logical that they also possess the ability to induce cell death when conditions become highly unfavorable. Mitochondria induce cell death by releasing proapoptotic mediators, which are normally concealed in the mitochondrial matrix, and thus initiating the intrinsic pathway of apoptosis. This occurs in part via the voltage- and redox-sensitive mitochondrial transition pore (MTP), a megachannel that spans the mitochondrial membranes[7]. Mitochondrial depolarization (low ΔΨm) and/or excessive mROS production promotes apoptosis by favoring MTP opening[8]. In contrast, mitochondrial hyperpolarization (high ΔΨm) and suppression of mROS favor MTP closure, locking the cells into an apoptosis-resistant state[7]. As the regulation of ΔΨm and mROS production depends on the supply and processing of fuel, the opening of the MTP, at least within a certain range, can be matched to the fuel

7

supply/demand balance. In terminal conditions of severe cellular stress or mitochondrial dysfunction, additional mechanisms activate to regulate cell death, perhaps in an all-or-none response. However, the threshold of apoptosis within more physiological conditions may be gated according to metabolic signals and needs.

1.2.5 The Endoplasmic Reticulum-Mitochondria Unit

Compatible with their role as RSS, mitochondria are strategically located to process signals from critical cellular structures efficiently and respond effectively. The ER and mitochondria networks are in very close proximity; in fact, the two organelles communicate. The form of communication is still a matter of debate, and research has described many mechanisms. Anchoring proteins and mitochondria-associated ER membranes [MAMs[9]; i.e., specialized contact points] have been identified as critical in the ER-mitochondria unit. The communication between the two organelles is important for the vital exchange of lipids, Ca^{2+}, and ATP. Whereas the ER is amongst the largest consumer of mitochondrial ATP, mitochondria critically depend on ER-derived Ca^{2+} [10,11]. Because the mitochondrial Ca^{2+} uniporter has a low Ca^{2+} affinity, optimized Ca^{2+} influx depends on microdomains faciliated organelle proximity[12]. In addition to the direct effects on metabolic enzyme activity, a decrease in Ca^{2+} influx (less of a positive charge) will hyperpolarize mitochondria. Therefore, a functional or structural disruption of this unit could have multiple effects on cell signaling, metabolism, and apoptosis. *This will be explored in chapters 2 and 3 of this dissertation.*

1.3.0 VASCULAR MITOCHONDRIA AND OXYGEN HOMEOSTASIS
1.3.1 Dynamically Suppressed Oxidative Phosphorylation in Systemic Microvessels and Oxygen Gradients

Given the integration of metabolic substrates on cell signaling and apoptosis, mitochondria with suppressed oxidative phosphorylation are not necessarily dysfunctional. In systemic microvessels, endothelial cells (ECs)[13-15]

and smooth muscle cells (SMCs)[16, 17] primarily utilize glycolysis and not mitochondrial metabolism during basal conditions, even when oxygen is present. The use of less efficient ATP-producing pathways is in keeping with the relatively low energy requirements of microvascular cells. Because ATP is adequately derived via oxygen-independent glycolysis, the oxygen consumption in these cells is minimal. Rather than consuming oxygen for ATP unnecessarily, microvessels allow oxygen to diffuse to the underlying oxygen-requiring tissues. Suppression of oxidative phosphorylation is achieved without compromise in the resting vasculature. For example, ECs remain functional even at extreme hypoxia (pO_2 of 0.1 mmHg)[18]. However, the suppression of oxidative phosphorylation is reversible during states of increased energy demand. For example, ATP levels remain constant in microvascular tissue cultures in which glycolysis is inhibited, suggesting that alternative energy pathways, including fatty acid oxidation, can be recruited[19, 20]. Vasoconstriction with either KCl or norepinephrine increases glucose oxidation (GO) or fatty acid oxidation (FAO), respectively[16]. As these vasoconstrictors increase cytosolic Ca^{2+} and often trigger an IP_3-mediated Ca^{2+} release from the ER, they can increase mitochondrial Ca^{2+}, the activity of mitochondrial enzymes, respiration, and oxidative phosphorylation. This ability to rapidly re-engage mitochondrial ATP production during energy-demanding constriction suggests that the oxidative phosphorylation suppression observed under resting conditions is reversible and dynamic.

A recently discovered mechanism could potentially explain aspects of this intriguing plasticity. ECs are primary producers of NO, which has myriads of effects within the vascular wall. NO reversibly binds and inhibits cytochrome c oxidase of the ETC[21, 22] in a manner inversely related to oxygen levels. NO-mediated ETC inhibition suppresses mitochondrial function and thus allows oxygen to diffuse to the surrounding tissues[22]. This concentration gradient between the blood and the perfused tissues becomes greater in ischemic states in which the need for oxygen increases further. NO secretion decreases vascular mitochondria oxygen consumption and causes vasodilation, increasing the delivery of oxygen and fuels to the ischemic tissues.

Although the rapid effects of NO allow for the acute fine-tuning of oxidative phosphorylation, another potential mechanism to minimize oxygen consumption is to decrease the number of mitochondria by decreasing mitochondria biogenesis or increase their removal with mitophagy. Thus, it is not surprising that mitochondria compose 5% of the cell volume in ECs as opposed to 28% in hepatocytes[23]. However, if the number of mitochondria decreases below the normal levels in ECs and microvessels, the flexibility to increase their engagement based on demand will diminish. The observation that mitochondrial biogenesis is significantly suppressed in aging vascular ECs and SMCs[24, 25] is important, particularly because systemic vascular diseases such as atherosclerosis or hypertension are often diseases of the aging population.

1.3.2 Hypoxic Pulmonary Vasoconstriction

A fundamental difference between pulmonary and systemic circulation is that the former is designed to regulate the supply of blood/oxygen to the body whereas the latter is designed to regulate the consumption of blood/oxygen by the tissues. This explains the different regulatory mechanisms in response to hypoxia. When a lung lobe has reduced alveolar oxygen, for example during pneumonia, the resistance pulmonary arteries (PAs) in that lobe immediately constrict. This vasoconstriction -hypoxic pulmonary vasoconstriction (HPV)- reduces perfusion to lung tissues with suboptimal gas exchange to avoid systemic hypoxia due to ventilation-perfusion mismatch. In contrast, hypoxia causes systemic arterial dilation, which enhances oxygen supply to the underlying hypoxic tissues.

Recent work has identified a sophisticated mitochondria-based O_2-sensing system in resistance pulmonary but not resistance systemic arteries[26, 27] where mitochondria tend to be suppressed as discussed above. This difference in mitochondrial function is reflected by the decreased $\Delta\Psi m$ in isolated PASMCs compared with systemic SMCs, even at baseline[28] (Figure 1-3A). Under hypoxia, the decrease in pO_2 is sensed in the ETC, which alters the production of a diffusible mediator (mROS-derived H_2O_2) that regulates effector mechanisms [plasmalemmal Kv channels], ultimately increasing cytosolic Ca^{2+} and causing

vasoconstriction[26, 27]. This system is intrinsic to the PASMCs as hypoxia increases cytosolic Ca^{2+} and causes contraction, whereas in systemic SMCs it decreases cytosolic Ca^{2+} [29]. Moreover, vascular rings of resistance PAs denuded of endothelium can exhibit HPV[28, 30]. ECs produce vasoactive substances (such as NO) that can modulate the constrictive response, but this is not essential for HPV. Although several mechanisms intrinsic to the PASMCs have been proposed[31], evidence widely supports a mitochondrial-mROS-Kv-channel axis[27].

In keeping with this, $\Delta\Psi m$ disruption with chemical uncouplers mimics hypoxia, constricting pulmonary while dilating systemic arteries[32]; ETC complex I and III inhibitors are the only class of drugs that completely mimic the arterial effects of acute hypoxia[32] (Figure 1-3B). This underlies the critical role of mROS because these ETCs are the main sites of mROS production. PASMC exposure to acute, mild, and physiologically relevant degrees of hypoxia (i.e., $pO_2 \sim 40$ mmHg) or to ETC inhibitors results in a rapid decrease in both mitochondria-derived superoxide[28, 33] and cellular H_2O_2[28, 34], Kv-channel inhibition, plasma membrane depolarization, opening of voltage-gated Ca^{2+} channels, Ca^{2+} influx, and contraction. Although some controversy exists as to whether mROS increase or decrease in hypoxia[35], this may be owing to methodological and model differences. However, most agree that mitochondria are critical in oxygen sensing and regulate HPV via production of a redox signal under physiological hypoxia[36].

The importance of mitochondrial metabolism on pulmonary vascular tone and HPV is highlighted in mice deficient in malonyl-CoA decarboxylase (MCD)[33]. MCD catalyzes the conversion of cytosolic malonyl-CoA (a potent inhibitor of the mitochondrial fatty-acid transporter) to acetyl-CoA, resulting in enhanced FAO. In addition to promoting β-oxidation, MCD reduces GO, as β-oxidation produces acetyl-CoA that inhibits pyruvate dehydrogenase (PDH) via the Randle feedback mechanism[37]. The resistance PAs of mice lacking MCD demonstrate reduced FAO and enhanced GO that fails to decrease, even during hypoxia. Thus MCD-knockout PASMC mROS production does not decrease under hypoxia, in contrast to MCD-wild-type PASMCs. PAs from these mice lack HPV (Figure 1-3C), although vasoconstrictive responses to phenylephrine and

endothelin remain[33]. This metabolic animal model is the only known model in which HPV is selectively absent both in vivo and ex vivo.

The main effector in HPV appears to be redox-sensitive Kv channels in the plasma membrane. These channels, including Kv1.5 and 2.1, regulate the resting plasma-membrane potential of PASMCs and thus regulate the opening of voltage-gated Ca^{2+} channels[38]. As Kv channels are oxidized when mROS are elevated, for example in normoxic conditions, they tend to be open, limiting cytosolic Ca^{2+} and promoting vasodilation. In contrast, during hypoxia, as mROS decrease, Kv channels close, opening voltage-gated Ca^{2+} channels and increasing Ca^{2+} levels and vasoconstriction. Although other Ca^{2+} sources may also play a role, particularly beyond the acute phase of HPV[31], the mROS, Kv-channel, and voltage-gated Ca^{2+}-channel axis forms the basis of HPV.

1.3.3 Mitochondria, Hypoxia-Inducible Factor 1α and Angiogenesis

In addition to acute hypoxia, mitochondria are involved in the vascular response to chronic hypoxia. Angiogenesis is regulated by the transcription factor HIF1α, which transcribes many proangiogenic signaling molecules[39]. Hypoxic stabilization of HIF1α is mediated largely by the inhibition of O_2-sensitive HIF-prolyl-hydroxylases (HPHs)[39], which utilize O_2 to hydroxylate HIF, causing its ubiquitination and proteosomal degradation[39, 40]. However, some tissues, such as cancer, have normoxic HIF1α stabilization, suggesting oxygen-independent regulation. New evidence now links suppressed mitochondrial signaling to this pseudohypoxic phenotype[41]. Although some evidence suggests that elevated ROS (such as H_2O_2 and other oxidative signals) directly inhibit the redox-sensitive HPHs and thus stabilize HIF1α[42, 43], ROS inhibits HIF1α via several HPH-independent mechanisms (Figure 1-4A). For example, ROS oxidize sulfhydryl groups on HIF1α, reducing its transcriptional activity[44, 45]. ROS also activate other redox-sensitive transcription factors, such as p53[46], promoting HIF1α ubiquitination and degradation[47, 48], and decrease HIF1α transcriptional activity, as p53 and HIF1α compete for the cotranscription factor p300[49]. Whether ROS-

dependent inhibition or activation of HIF1α predominates may vary according to conditions (i.e., normoxia or hypoxia), disease states (cancer), or tissue types.

In addition to oxygen, HPHs are sensitive to Krebs cycle metabolites (Figure 1-4A). For example, a-ketoglutarate (αKG), a product of isocitrate dehydrogenase, is a necessary cofactor for HPH-mediated HIF hydroxylation[50]. Low αKG to succinate-fumarate ratios (Krebs metabolites proximal to αKG) promote HIF1α stability, and mutations in succinate dehydrogenase and fumarate hydratase, which degrade succinate and fumarate, respectively, are linked to highly vascular tumors with enhanced HIF1α stability[51]. Thus, mutations in nuclear-encoded mitochondrial Krebs cycle enzymes influence HPH-mediated HIF1α stability.

Reducing mitochondrial Ca^{2+} could mimic Krebs enzymes' loss-of-function mutations because several Krebs' cycle enzymes are highly Ca^{2+} sensitive. PDH, the gatekeeper enzyme for GO, is also Ca^{2+} sensitive, reducing αKG indirectly by reducing substrate flux into the Krebs cycle. In addition, HIF1α itself suppresses mitochondrial function, closing a positive feedback loop by inducing the expression of less efficient cytochrome c oxidases, decreasing mitochondrial biogenesis[51], and inducing expression of PDH kinase (PDK), which phosphorylates and inhibits PDH[52]. In cancer, the molecular or pharmacological [i.e., with dicholoroacetate (DCA)] inhibition of PDK promotes αKG and mROS production, resulting in HPH-dependent and independent HIF1α inhibition[41]. Moreover, DCA-treated rats have smaller tumors with reduced vascularity and tumor perfusion compared with vehicle-treated controls[41] (Figure 1-4B). Investigators have documented similar antiangiogenic effects in glioblastoma multiforme patients receiving oral DCA in a small clinical trial[53]. *The effects of reducing mitochondrial calcium on oxygen sensing in the pulmonary vasculature will be explored in chapter 2 of this dissertation.*

Although ectopic HIF1α activation is undesirable in hypervascular tissues such as cancer, HIF1α augmentation is desirable in other tissues. For example, in patients with coronary artery occlusion, those with more collateral vessels have smaller infarct size and better survival[54, 55], and augmenting HIF1α results in

better outcomes after coronary ligation[56]. In elderly patients with critical limb ischemia, HIF1α activation is impaired[57]. There is an intriguing association between thiazolidinediones and increased risk of myocardial infarction and revascularization surgery in diabetics[58]. Thiazolidinediones, peroxisome proliferator-activated receptor γ (PPARγ) ligands developed for type II diabetes, stimulate mitochondrial biogenesis, expression of genes involved in fatty acid oxidation, and mitochondrial respiration (mimicking DCA). *Determination of whether the increased risks observed clinically relate to the mitochondria-stimulating effects of these agents is explored in chapter 4 of this dissertation.*

1.4.0 MITOCHONDRIA AND VASCULOPROLIFERATIVE DISEASES: PULMONARY ARTERIAL HYPERTENSION

PAH is an ideal vascular disease to discuss because it reflects all of the functions of mitochondria discussed so far. Its pathogenesis follows the common theme of multiple hits/triggers on a genetically predisposed background, and its pathology (which remains remarkably similar regardless of its diverse triggers) shares intriguing similarities with other common vascular diseases of excessive vascular cell proliferation and inflammatory cell invasion such as coronary restenosis following intervention and transplant vasculopathy. Similar to atherosclerosis, endothelial dysfunction/apoptosis appears to be an early event[59]. However, later stages are characterized by hyperproliferative and apoptosis-resistant ECs and SMCs that exhibit a metabolic profile strikingly similar to cancer[33, 60, 61]. Like cancer, PAH remains lethal[62]. Although available treatments may improve symptoms, all fail to reverse PAH or significantly prolong life[62, 63].

1.4.1 Current Challenges in PAH

There are two major challenges in the treatment of PAH. First, its pathogenesis is complex and incompletely understood. PAH can be idiopathic, familial, or associated with a diverse group of medical conditions, including autoimmune and inflammatory diseases such as scleroderma, congenital heart disease, and HIV infection, among others[63]. Research has described many

molecular abnormalities and environmental factors[64-66] in addition to genetic predispositions, including loss-of-function mutations in the bone morphogenetic protein receptor II (BMPRII)[67] and Kv-channel polymorphisms[68]. This complexity calls for therapeutic targeting of comprehensive and integrative mechanisms rather than individual signaling pathways[66].

Current PAH therapies (endothelin antagonists, phosphodiesterase type V inhibitors, and prostacyclin analogs), originally designed to treat systemic vascular disease, lack pulmonary selectivity and are limited by the fact that systemic vessels are typically intact in PAH. Clinicians applied these therapies to PAH with the hope of reversing pulmonary vasoconstriction and reducing elevated PA pressures and resistance. More recently, many laboratories have focused on identifying PA-specific targets that address the vascular remodeling. One must consider the differences between the pulmonary and systemic circulations, such as HPV, in which mitochondria play a fundamental role. Indeed, mitochondria may be at the core of PAH pathogenesis and thus may be the cornerstones of new therapeutic approaches[60].

1.4.2 Mitochondria Are Suppressed in Pulmonary Arterial Hypertension, Causing a State of Apoptosis Resistance (the Cancer Paradigm)

Mitochondria are central to the metabolic theory of cancer[51, 69-71]. Mitochondria integrate diverse oncogene-driven molecular signals (such as loss of p53 or activation of Akt and c-myc) and respond by suppressing GO and switching cellular metabolism toward glycolysis, even in normoxia [i.e., the Warburg effect]. This metabolic switch favors apoptosis resistance[69, 72, 73]. Most solid tumors have the high mitochondrial membrane potential ($\Delta\Psi m$) typically associated with decreased mROS production[74, 75], which inhibits apoptosis by decreasing MTP opening. To compensate for decreased mitochondrial ATP production, cancer cells upregulate glucose uptake and glycolysis, which is the basis of diagnostic ^{18}fluorodeoxyglucose positron emission tomography (^{18}FDG-PET) imaging. This remodeling provides several advantages to cancer cells, including (*a*) diversion of pyruvate into anabolic pathways[71, 76]; (*b*) suppression of

apoptosis by the hyperpolarized $\Delta\Psi m^7$; (*c*) inhibition of Kv channels due to decreased mROS (see the HPV paradigm), increasing cytosolic Ca^{2+}, which in turn activates the hyperproliferative transcription factor nuclear factor of activated T cells (NFAT), whose activation causes downregulation of Kv channels and upregulation of glycolytic enzymes[77] and; (*d*) activation of HIF1α (see the Mitochondria, HIF1α, and Angiogenesis section), which increases PDK expression[52], thus sustaining mitochondrial suppression in another reinforcing feedback loop.

Intriguingly, the same changes in the mitochondria-mROS-NFAT/HIF1α-Kv-channel axis also characterize PAH-PASMCs (Figure 1-5)[60]. Compared with normal cells, PAH-PASMCs from hypoxia- or monocrotaline-induced PAH (an inflammatory model of PAH) or from PAH patients have suppressed GO, increased $\Delta\Psi m$ and decreased mROS, downregulated Kv channels, activated NFAT and HIF1α even under normoxia, enhanced proliferation, and suppressed apoptosis[60]. PASMCs and PAECs from PAH tissues show evidence of upregulated glycolysis, and both animals and patients with PAH show a cancer-like increased glucose uptake with ^{18}FDG-PET in the lungs[33, 61]. In summary, there is overwhelming evidence that hyperproliferative and anti-apoptotic vascular cells in PAH share a cancer-like mitochondrial suppression. Below I discuss the several potential mechanisms that can lead to reversible mitochondrial suppression in PAH.

1.4.3 Limited Mitochondrial Substrate Influx

Primary mitochondrial suppression can occur via the induction of PDK, which inhibits PDH and GO. The importance of this mechanism in cancer is highlighted by the fact that PDK inhibition enhances mROS production and reactivates functionally suppressed mitochondrial signaling pathways, including apoptosis. The PDK inhibitor DCA increases PDH activity, depolarizes $\Delta\Psi m$, and increases Krebs cycle intermediates and mROS. Together these effects reduce NFAT (Figure 1-5) and HIF1α activation and increase proapoptotic transcription factors, such as p53, to induce apoptosis and tumor regression in animal models

(Figure 1-3B) [53, 74] and in patients receiving DCA in a small clinical trial[53]. Thus, inhibition of PDK can reactivate functionally suppressed mitochondria in cancer.

In an identical manner in PAH, DCA increases PDH activity, depolarizes $\Delta\Psi m$, increases mROS, decreases NFAT and HIF1α activity, increases Kv-channel expression, suppresses proliferation, and increases mitochondria-dependent apoptosis. The similarity of the molecular effects of DCA in cancer and in PAH vascular cells is intriguing (Figure 1-5). In animal models of PAH, DCA administered in the drinking water reduced mean PA pressure and PA medial wall thickening by inducing apoptosis in the PA wall without significant effects on systemic vessels (Figure 1-6A)[3, 34, 78, 79]. Activation of PDH (and thus GO) can also occur by inhibiting FAO via the Randle cycle (see the Hypoxic Pulmonary Vasoconstriction section). Mice that lack MCD and thus have suppressed FAO are resistant to PAH. Likewise, drugs that reduce FAO, such as trimetazidine (TMZ), reverse established PAH, mimicking DCA (Figure 1-6B)[33].

This metabolic remodeling within the PA vessel wall is also compatible with the emerging view that there is a generalized resistance to insulin and a widespread problem with carbohydrate metabolism in PAH. PAH patients are more likely to have insulin resistance than controls[80]. PPARγ agonists are currently used in type II diabetes, and there is evidence that these may be beneficial in PAH[81].

1.4.4 Decreased Mitochondrial Ca^{2+}

By suppressing GO, PDH inhibition can explain the mitochondrial remodeling in PAH, but how does this relate to the diverse PAH triggers? Pursuing a unifying theory, we were intrigued that many PAH triggers are linked with ER stress. For example, mutations to BMPRII result in the accumulation of unfolded protein and ER stress[82]. Viruses such as HIV[83, 84] and herpes[85, 86], as well as hypoxia and inflammation, also cause ER stress[87]. Recently, studies implicated Notch-3 overexpression in both PAH pathogenesis[88] and ER stress[89]. Thus, diverse PAH triggers may share a converging ER stress pathway.

Researchers described ER stress in PAH as early as the 1970s, but its involvement in the pathogenesis of PAH remained unknown[90]. Recent work suggests that ER stress contributes to PAH pathogenesis by disrupting the ER-mitochondria unit and thus facilitating mitochondrial suppression[91]. PASMCs exposed to hypoxia, an ER-stress stimulus and well-accepted trigger of PAH, show activation of the activating transcription factor 6 (ATF6) arm of ER stress (Figure 1-7A). ATF6 upregulates an ER-resident protein, Nogo, which is critical in maintaining ER morphology[91]. Excessive ER curvature caused by excessive Nogo increases the ER-mitochondria distance (Figure 1-7B), disrupting ER-mitochondrial Ca^{2+} transfer. This decreases PDH activity and causes mitochondrial suppression and apoptosis resistance. Mice lacking Nogo are resistant to chronic hypoxia-induced PAH, and heterozygous mice develop PAH, but less severely than wild-type littermates, suggesting a gene dose-dependent effect. Accordingly, Nogo expression is increased in the remodeled PAs and serum of PAH patients[91]. Perhaps owing to the redox sensitivity of ATF6, induction of Nogo occurs only in the pulmonary circulation and not in the systemic circulation, despite systemic hypoxia, addressing a fundamental feature of PAH (i.e., the pulmonary-restricted pathology)[91]. *Therapies that attenuate the ER-stress response in pulmonary hypertension are explored in chapter 4 of this dissertation.*

1.4.5 Mitochondrial Fragmentation and Mitophagy

Investigators first described mitochondrial fragmentation in the PASMCs of fawn-hooded rats, which develop spontaneous PAH[34]. Markers of mitochondrial fission, including dynamin-related protein 1 (DRP1) are increased in PASMCs from patients and rats with PAH (Figure 1-7C)[92]. However, the exact role of mitochondrial fragmentation on mitochondrial function in PAH requires further studies. For example, destruction of the mitochondrial network quite possibly disrupts the ER-mitochondria unit. As discussed above, mitochondrial fragmentation is a precursor to mitophagy. Intriguingly, markers of authophagy

are also increased in the pulmonary vascular wall of PAH patients[93], but the involvement of mitophagy specifically remains unknown.

In summary, although the defense mechanisms that suppress mitochondrial function to limit oxidative stress may prevent apoptosis in the short term, they may, if sustained, facilitate the pathogenesis of vascular remodeling diseases. Using the rationale of the basic defenses described above, I outline some emerging mitochondria-targeting vascular therapies that have either shown efficacy or appear promising.
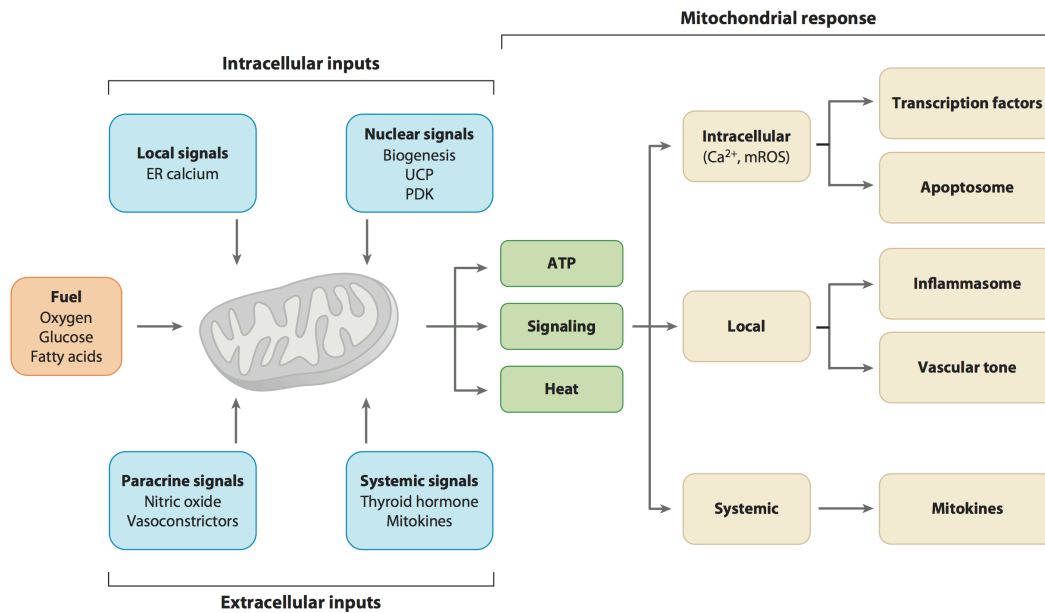
Figure 1-1. The mitochondrion: the ultimate responsive sensing system.
Based on the availability of fuel (oxygen, glucose, and fatty acids), mitochondria generate ATP, heat, and a variety of signals that coordinate the response of the cell, tissue, or entire organism. Mitochondria are also responsive to intracellular signals, for example, inter-organelle inputs such as endoplasmic reticulum (ER) calcium and nuclear-encoded proteins, as well as extracellular signaling molecules, hormones, and inflammatory cytokines. They respond with signals that can reach the whole cell and beyond. As shown, the production of ATP is only a very small part of vascular mitochondria's role in health and disease. Abbreviations: UCP-uncoupling proteins; PDK-pyruvate dehydrogenase kinase; ATP- adenosine triphosphate; mROS- mitochondrial-derived reactive oxygen species.
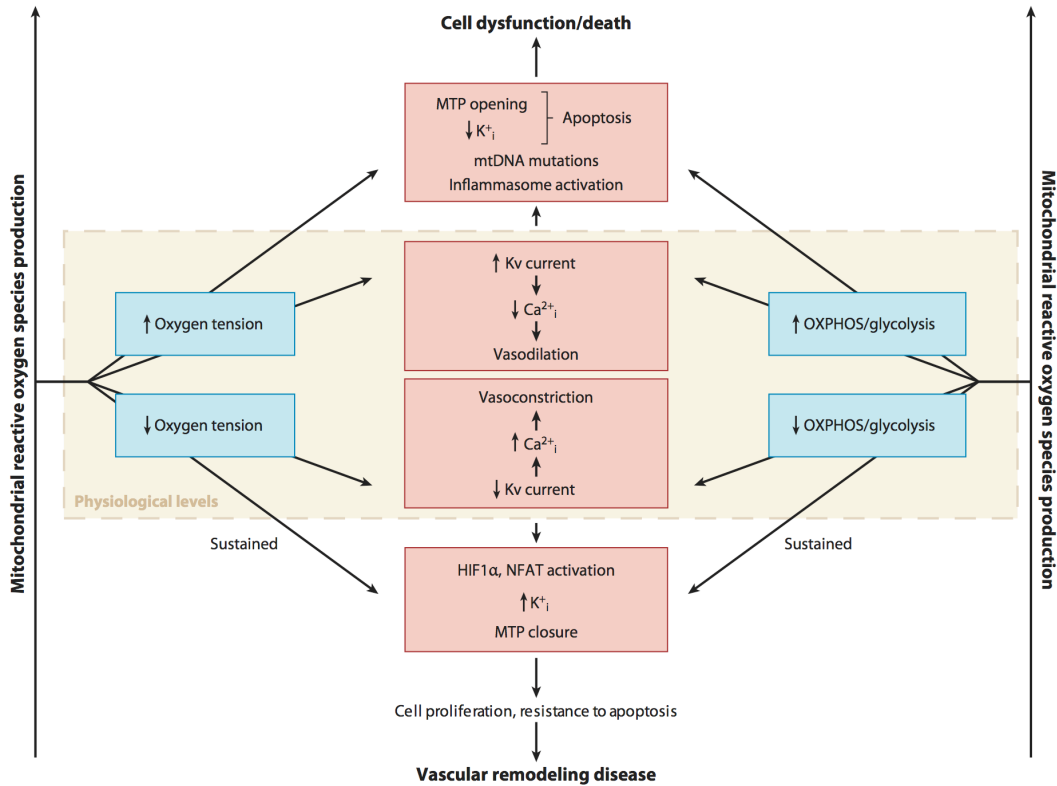
Figure 1-2. Mitochondrial-derived ROS (mROS) in physiology and pathobiology. mROS levels are largerly dependent on two environmental inputs – oxygen and metabolic substrate availability, which influences the rates of oxidative phosphorylation (OXPHOS). Within a specific range, mROS function as important regulators of physiological processes like the vascular tone by modulating the redox status of Kv-channels. However, superphysiological mROS production, which may occur with excessively high OXPHOS, triggers pathological processes like activation of the inflammasome (triggering sterile inflammation), mutations to mitochondrial or nuclear DNA, and opening of the mitochondrial transition pore (MTP), ultimately resulting in cell dysfunction and/or death. Alternatively, supraphysiological mROS production, for example when oxygen levels are reduced, faciliates activation of several transcription factors like hypoxia inducible factor 1α (HIF1α) or nuclear factor of activated T-cells (NFAT) and closure of the MTP, in an attempt to promote proliferation and resistance to apoptosis.
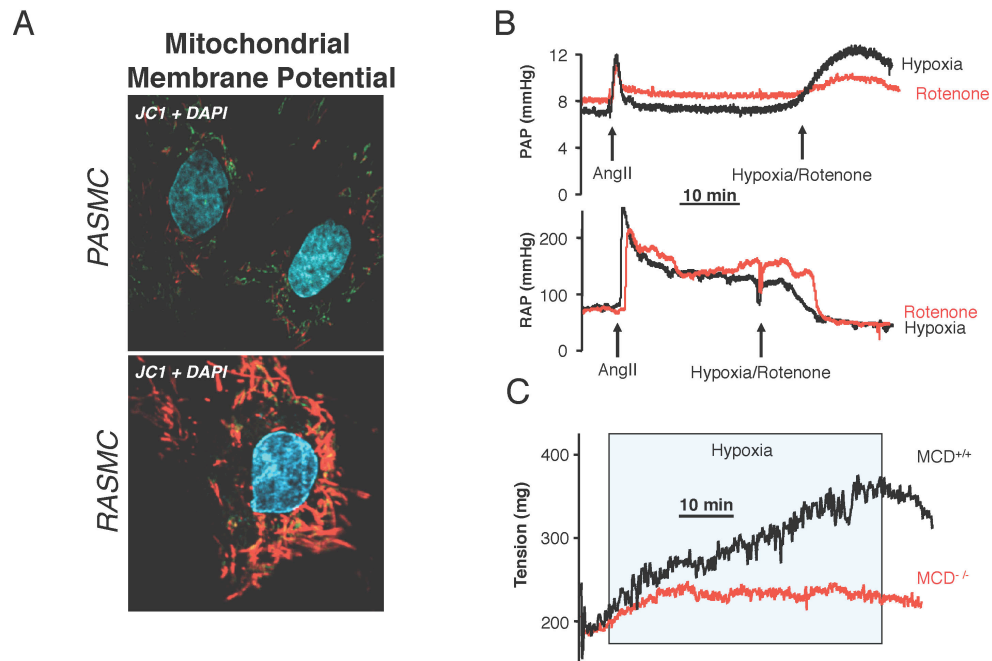
Figure 1-3. Mitochondrial regulation of vascular tone. A. The mitochondria of pulmonary artery smooth muscle cells (PASMCs) are more depolarized than mitochondria of renal artery SMCs (RASMCs), as shown by the greater red:green fluorescence of a $\Delta\Psi$m-sensitive dye, JC1, under identical conditions. Similarly (not shown), PASMC mitochondria produce more mitochondrial-derived reactive oxygen species (mROS) compared with RASMC mitochondria. These findings reflect intrinsic differences in mitochondria, which also persist when mitochondria are isolated. **B.** Continuous renal artery pressure (RAP) and pulmonary artery pressure (PAP) traces in denuded vessels. The mitochondrial electron transport chain (ETC) complex I inhibitor, rotenone (*red*), mimics hypoxia (*black*), dilating PA rings (*top*) and constricting renal artery (*bottom*) rings. In this system, rat lungs and kidneys are perfused in series in a closed system, which exposes the two circulations to exactly the same degree of hypoxia. ETC inhibitors are the only class of drugs that completely mimic the opposite effects of hypoxia in the pulmonary versus systemic arteries, whereas both vessels respond similar to vasoconstrictors like angiotensin II (AngII) Panel B modified from Reference 28. **C.** PA rings from mice lacking malonyl-CoA decarboxylase

(MCD) (*red*), which have enhanced glucose:fatty-acid oxidation ratios and fail to constrict in response to hypoxia, as opposed to MCD wild-type PA rings (*black*), which have intact hypoxic pulmonary vasoconstriction. Panel C modified from Reference 33.
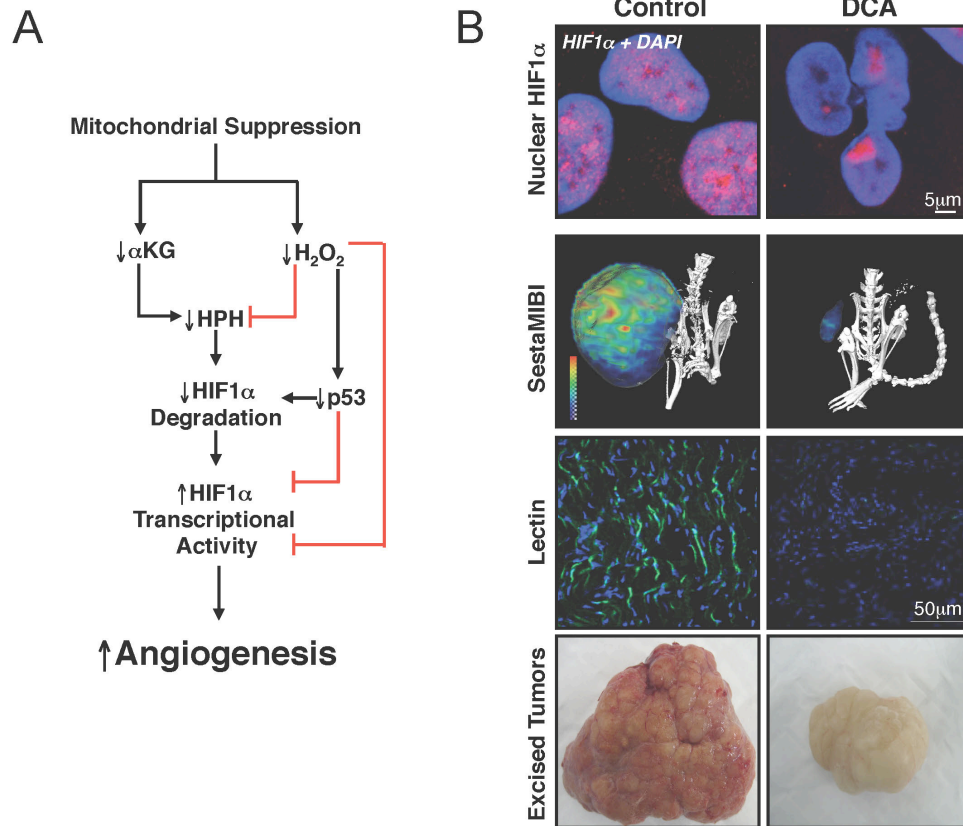
Figure 1-4: Mitochondrial regulation of hypoxia-inducible factor 1α (HIF1α)-driven angiogenesis. **A.** Mitochondrial suppression, which characterizes most cancers, reduces mitochondrial-derived α–ketoglutarate (αKG), a necessary cofactor of HIF-prolyl-hydroxylase (HPH)-mediated HIF1α degradation. Reduced mROS (dismutated to the diffusible H_2O_2) activate HPHs but directly facilitate HIF1α DNA binding and reduce the activity of p53, which inhibits HIF1α at the levels of both transcriptional activity and stability. Thus, reduced mitochondrial activity can activate HIF1α independent of hypoxia. **B.** Activation of mitochondria (glucose oxidation) with dichloroacetate (DCA) reduces normoxic HIF1α in non-small cell lung cancer cells, as seen by the decreased nuclear signal of HIF1α in the treated cells (nuclei stained blue with 4,6-diamidino-2-phenylindole (DAPI)). Animals treated with DCA have smaller tumors with less perfusion indicated by reduced Sestamibi (as shown in these single photon emission computed tomography (SPECT)-CT in vivo images of rat

xenotransplant tumor models) and lectin perfusion (as shown with lectin immunohistochemistry), as well as reduced vasculature, apparent upon gross examination (the treated tumors are both smaller and appear hypoperfused). Panel B modified from Reference 41.
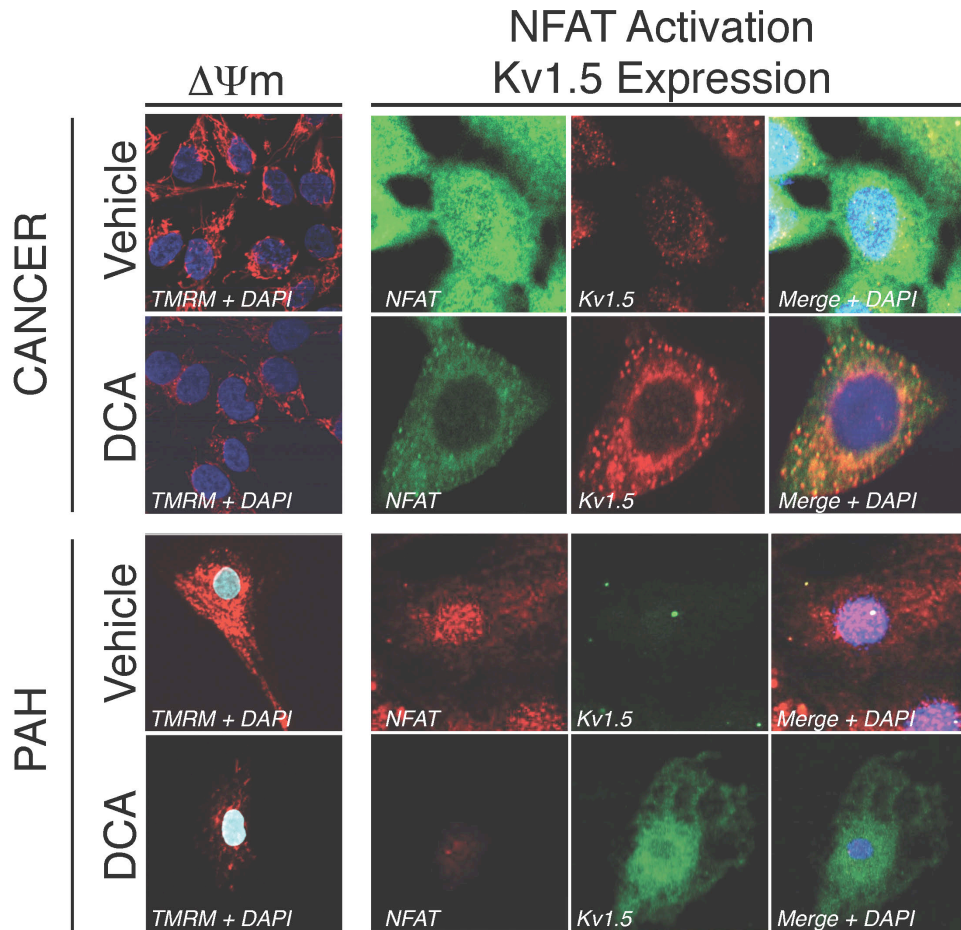
Figure 1-5. A mitochondrial-nuclear factor of activated T cells (NFAT)-Kv1.5 axis in pulmonary arterial hypertension (PAH) and cancer. Similar to cancer, PASMCs have hyperpolarized $\Delta\Psi$m (tetramethylrhodamine methyl ester (TMRM), *red*), an indicator of mitochondrial function. NFAT is activated by increases in cytosolic calcium, which are caused by a reduction in mROS and Kv-channel function. Activation of NFAT reduces the expression of Kv-channels, closing a powerful feedback loop. Stimulation of glucose oxidation with DCA disrupts this feedback, depolarizing $\Delta\Psi$m, suppressing NFAT, and increasing Kv-channel expression in both PAH (PASMC from a rat with PAH shown) and cancer (non-small cell lung cancer cells shown). This impressive similarity in the cellular response to a single drug in two very different tissues and diseases is intriguing and explains the induction of apoptosis in both tissues by DCA. Nuclei

are stained blue with 4,6-diamidino-2-phenylindole (DAPI). Figure modified from References 33, 74, and 78.
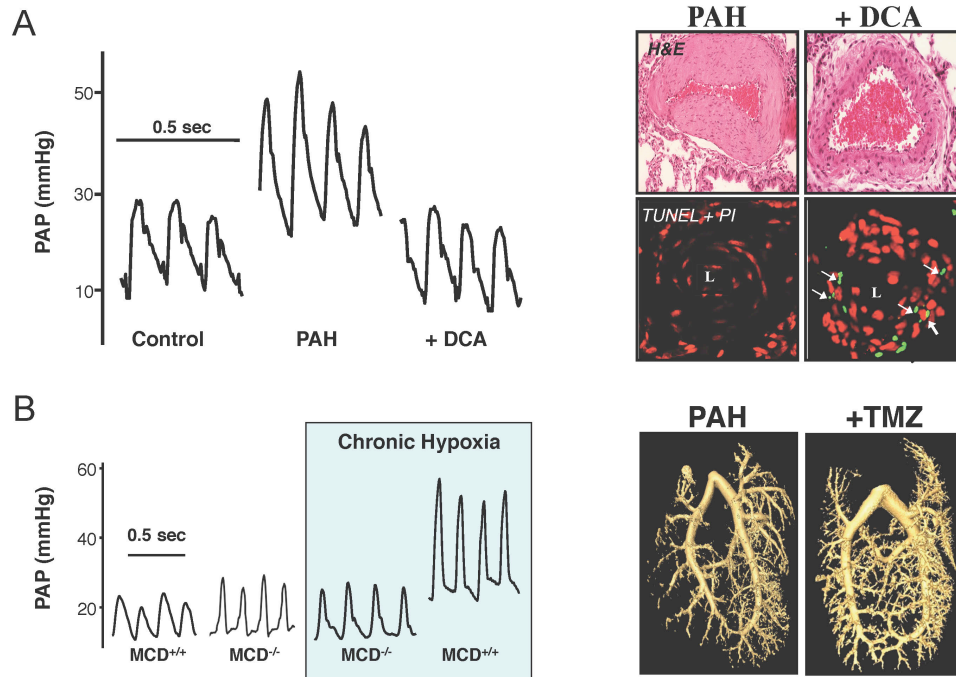
Figure 1-6. Mitochondrial activating drugs as therapies in PAH. A. Direct stimulation of glucose oxidation with DCA in vivo (oral delivery for 2-3 weeks) lowers PA pressures to normal levels in a rat with monocrotaline-induced pulmonary hypertension. The traces are taken by catheters advanced into the PA through the jugular vein in anesthetized rats. This normalization of pressures is the result of the reversal of vascular remodeling due to induction of apoptosis, as shown by terminal deoxynucleotidyl transferase dUTP nick end labeling (TUNEL)-positive (*green*) nuclei (*red*), leading to reduced wall thickness (hematoxylin and eosin (H&E) stain) in the distal PAs. Panel A modified from Reference 79. **B.** Mice lacking MCD fail to develop elevated pulmonary pressures in chronic hypoxia (*left*). Treatment with trimetazidine (TMZ), which pharmacologically suppresses fatty acid oxidation and indirectly augments glucose oxidation, mimicking knockdown of MCD, restores perfusion to the distal PAs, as shown by the micro-CT angiogram (*right*). As in panel *a*, the traces show PA pressure recordings from catheters advanced in the PA through the jugular vein in anesthetized mice. Panel B modified from Reference 33.
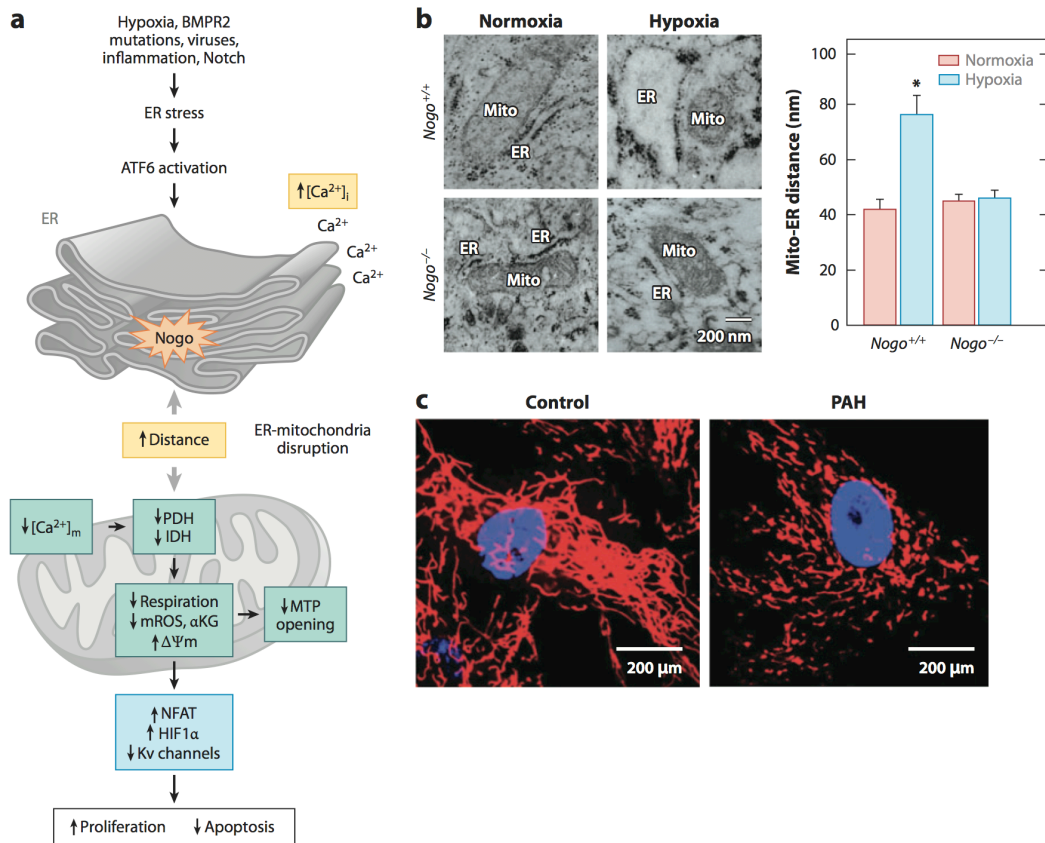
Figure 1-7. Disruption of the ER-mitochondria unit in PAH. A. A schematic linking ER-mitochondria unit disruption in PAH and its consequences. ER stress is a response common to several PAH triggers and activates ATF6, which drives the expression of the ER-resident protein Nogo. Nogo upregulation alters ER morphology, disrupting the association with mitochondria and reducing mitochondrial calcium. Reducing mitochondrial calcium hyperpolarizes $\Delta\Psi$m and reduces glucose oxidation and Krebs' cycle activity, suppressing mROS. This ultimately results in activation of proproliferative/anti-apoptotic transcription factors such as NFAT and HIF1α and suppresses opening of the mitochondrial transition pore (MTP), leading to vascular remodeling. Panel A obtained from Reference 91. **B.** PASMCs from mice lacking Nogo are resistant to hypoxia-induced changes in ER morphology and physical disruption of the ER-mitochondrial unit. Whereas the distance between ER and mitochondria increases in PASMC from wild-type mice exposed to chronic hypoxia, the distance remains

unaltered in PASMC from mice lacking Nogo exposed to the same degree of hypoxia. Panel B modified from Reference 91. **C.** PAH-PASMCs have disrupted mitochondrial networking, as shown by a punctate mitochondrial pattern (*red, right*) compared with a filamentous network in the healthy PASMC (*left*), a change that may also contribute to the disruption of the ER-mitochondria unit. Panel C provided by Dr. Stephen Archer (University of Chicago); also see Reference 92.

References

1.   Lopaschuk GD, Ussher JR, Folmes CD, Jaswal JS, Stanley WC. Myocardial fatty acid metabolism in health and disease. *Physiol Rev.* 2010; 90:207-258.

2.   Semenza GL. Hypoxia-inducible factors in physiology and medicine. *Cell.* 2012; 148:399-408.

3.   Vander Heiden MG, Locasale JW, Swanson KD, Sharfi H, Heffron GJ, Amador-Noguez D, Christofk HR, Wagner G, Rabinowitz JD, Asara JM, Cantley LC. Evidence for an alternative glycolytic pathway in rapidly proliferating cells. *Science.* 2010; 329:1492-1499.

4.   Wood PG, Gillespie JI. Evidence for mitochondrial Ca(2+)-induced Ca2+ release in permeabilised endothelial cells. *Biochem Biophys Res Commun.* 1998; 246:543-548.

5.   Duchen MR. Contributions of mitochondria to animal physiology: from homeostatic sensor to calcium signalling and cell death. *J Physiol.* 1999; 516 (Pt 1):1-17.

6.   Denton RM. Regulation of mitochondrial dehydrogenases by calcium ions. *Biochim Biophys Acta.* 2009; 1787:1309-1316.

7.   Zamzami N, Kroemer G. The mitochondrion in apoptosis: how Pandora's box opens. *Nat Rev Mol Cell Biol.* 2001; 2:67-71.

8.   Halestrap AP, Woodfield KY, Connern CP. Oxidative stress, thiol reagents, and membrane potential modulate the mitochondrial permeability transition by affecting nucleotide binding to the adenine nucleotide translocase. *J Biol Chem.* 1997; 272:3346-3354.

9.   Vance JE. Phospholipid synthesis in a membrane fraction associated with mitochondria. *J Biol Chem.* 1990; 265:7248-7256.

10.   Szabadkai G, Duchen MR. Mitochondria: the hub of cellular Ca2+ signaling. *Physiology (Bethesda).* 2008; 23:84-94.

11.   Rizzuto R, Duchen MR, Pozzan T. Flirting in little space: the ER/mitochondria Ca2+ liaison. *Sci STKE.* 2004; 2004:re1.

12.   Szanda G, Koncz P, Varnai P, Spat A. Mitochondrial Ca2+ uptake with and without the formation of high-Ca2+ microdomains. *Cell Calcium.* 2006; 40:527-537.

13.   Krutzfeldt A, Spahr R, Mertens S, Siegmund B, Piper HM. Metabolism of exogenous substrates by coronary endothelial cells in culture. *J Mol Cell Cardiol.* 1990; 22:1393-1404.

14.   Quintero M, Colombo SL, Godfrey A, Moncada S. Mitochondria as signaling organelles in the vascular endothelium. *Proc Natl Acad Sci U S A.* 2006; 103:5379-5384.

15.   Culic O, Gruwel ML, Schrader J. Energy turnover of vascular endothelial cells. *Am J Physiol.* 1997; 273:C205-213.

16.   Barron JT, Barany M, Gu L, Parrillo JE. Metabolic fate of glucose in vascular smooth muscle during contraction induced by norepinephrine. *J Mol Cell Cardiol.* 1998; 30:709-719.

17.   Lynch RM, Paul RJ. Compartmentation of glycolytic and glycogenolytic metabolism in vascular smooth muscle. *Science.* 1983; 222:1344-1346.

18.   Mertens S, Noll T, Spahr R, Krutzfeldt A, Piper HM. Energetic response of coronary endothelial cells to hypoxia. *Am J Physiol.* 1990; 258:H689-694.

19.   Barron JT, Kopp SJ, Tow JP, Messer JV. Effects of altering carbohydrate metabolism on energy status and contractile function of vascular smooth muscle. *Biochim Biophys Acta.* 1989; 976:42-52.

20.   Barron JT, Kopp SJ, Tow J, Parrillo JE. Fatty acid, tricarboxylic acid cycle metabolites, and energy metabolism in vascular smooth muscle. *Am J Physiol.* 1994; 267:H764-769.

21.   Cleeter MW, Cooper JM, Darley-Usmar VM, Moncada S, Schapira AH. Reversible inhibition of cytochrome c oxidase, the terminal enzyme of the mitochondrial respiratory chain, by nitric oxide. Implications for neurodegenerative diseases. *FEBS Lett.* 1994; 345:50-54.

22.   Clementi E, Brown GC, Foxwell N, Moncada S. On the mechanism by which vascular endothelial cells regulate their oxygen consumption. *Proc Natl Acad Sci U S A.* 1999; 96:1559-1562.

23.   Blouin A, Bolender RP, Weibel ER. Distribution of organelles and membranes between hepatocytes and nonhepatocytes in the rat liver parenchyma. A stereological study. *J Cell Biol.* 1977; 72:441-455.

24.   Ungvari Z, Labinskyy N, Gupte S, Chander PN, Edwards JG, Csiszar A. Dysregulation of mitochondrial biogenesis in vascular endothelial and smooth muscle cells of aged rats. *Am J Physiol Heart Circ Physiol.* 2008; 294:H2121-2128.

25.   Burns EM, Kruckeberg TW, Comerford LE, Buschmann MT. Thinning of capillary walls and declining numbers of endothelial mitochondria in the cerebral cortex of the aging primate, Macaca nemestrina. *J Gerontol.* 1979; 34:642-650.

26.   Michelakis ED, Thebaud B, Weir EK, Archer SL. Hypoxic pulmonary vasoconstriction: redox regulation of O2-sensitive K+ channels by a mitochondrial O2-sensor in resistance artery smooth muscle cells. *J Mol Cell Cardiol.* 2004; 37:1119-1136.

27.   Weir EK, Lopez-Barneo J, Buckler KJ, Archer SL. Acute oxygen-sensing mechanisms. *N Engl J Med.* 2005; 353:2042-2055.

28.   Michelakis ED, Hampl V, Nsair A, Wu X, Harry G, Haromy A, Gurtu R, Archer SL. Diversity in mitochondrial function explains differences in vascular oxygen sensing. *Circ Res.* 2002; 90:1307-1315.

29.   Vadula MS, Kleinman JG, Madden JA. Effect of hypoxia and norepinephrine on cytoplasmic free Ca2+ in pulmonary and cerebral arterial myocytes. *Am J Physiol.* 1993; 265:L591-597.

30.   Archer SL, Wu XC, Thebaud B, Nsair A, Bonnet S, Tyrrell B, McMurtry MS, Hashimoto K, Harry G, Michelakis ED. Preferential expression and function of voltage-gated, O2-sensitive K+ channels in resistance pulmonary arteries explains regional heterogeneity in hypoxic pulmonary vasoconstriction: ionic diversity in smooth muscle cells. *Circ Res.* 2004; 95:308-318.

31.   Sylvester JT, Shimoda LA, Aaronson PI, Ward JP. Hypoxic pulmonary vasoconstriction. *Physiol Rev.* 2012; 92:367-520.

32.   Rounds S, McMurtry IF. Inhibitors of oxidative ATP production cause transient vasoconstriction and block subsequent pressor responses in rat lungs. *Circ Res.* 1981; 48:393-400.

33.   Sutendra G, Bonnet S, Rochefort G, Haromy A, Folmes KD, Lopaschuk GD, Dyck JR, Michelakis ED. Fatty acid oxidation and malonyl-CoA decarboxylase in the vascular remodeling of pulmonary hypertension. *Sci Transl Med.* 2010; 2:44ra58.

34.   Bonnet S, Michelakis ED, Porter CJ, Andrade-Navarro MA, Thebaud B, Haromy A, Harry G, Moudgil R, McMurtry MS, Weir EK, Archer SL. An abnormal mitochondrial-hypoxia inducible factor-1alpha-Kv channel pathway disrupts oxygen sensing and triggers pulmonary arterial hypertension in fawn hooded rats: similarities to human pulmonary arterial hypertension. *Circulation.* 2006; 113:2630-2641.

35.   Weir EK, Archer SL. Counterpoint: Hypoxic pulmonary vasoconstriction is not mediated by increased production of reactive oxygen species. *J Appl Physiol.* 2006; 101:995-998; discussion 998.

36.   Waypa GB, Marks JD, Guzy R, Mungai PT, Schriewer J, Dokic D, Schumacker PT. Hypoxia triggers subcellular compartmental redox signaling in vascular smooth muscle cells. *Circ Res.* 2010; 106:526-535.

37.   Randle PJ. Regulatory interactions between lipids and carbohydrates: the glucose fatty acid cycle after 35 years. *Diabetes Metab Rev.* 1998; 14:263-283.

38.   Archer SL, Souil E, Dinh-Xuan AT, Schremmer B, Mercier JC, El Yaagoubi A, Nguyen-Huu L, Reeve HL, Hampl V. Molecular identification of the role of voltage-gated K+ channels, Kv1.5 and Kv2.1, in hypoxic pulmonary vasoconstriction and control of resting membrane potential in rat pulmonary artery myocytes. *J Clin Invest.* 1998; 101:2319-2330.

39.   Semenza GL. Oxygen sensing, homeostasis, and disease. *N Engl J Med.* 2011; 365:537-547.

40.   Bruick RK, McKnight SL. A conserved family of prolyl-4-hydroxylases that modify HIF. *Science.* 2001; 294:1337-1340.

41.   Sutendra G, Dromparis P, Kinnaird A, Stenson TH, Haromy A, Parker JM, McMurtry MS, Michelakis ED. Mitochondrial activation by inhibition of PDKII suppresses HIF1α signaling and angiogenesis in cancer. *Oncogene.* 2012.

42.   Brunelle JK, Bell EL, Quesada NM, Vercauteren K, Tiranti V, Zeviani M, Scarpulla RC, Chandel NS. Oxygen sensing requires mitochondrial ROS but not oxidative phosphorylation. *Cell Metab.* 2005; 1:409-414.

43.   Mansfield KD, Guzy RD, Pan Y, Young RM, Cash TP, Schumacker PT, Simon MC. Mitochondrial dysfunction resulting from loss of cytochrome c impairs cellular oxygen sensing and hypoxic HIF-alpha activation. *Cell Metab.* 2005; 1:393-399.

44.   Huang LE, Arany Z, Livingston DM, Bunn HF. Activation of hypoxia-inducible transcription factor depends primarily upon redox-sensitive stabilization of its alpha subunit. *J Biol Chem.* 1996; 271:32253-32259.

45.   Wang GL, Jiang BH, Rue EA, Semenza GL. Hypoxia-inducible factor 1 is a basic-helix-loop-helix-PAS heterodimer regulated by cellular O2 tension. *Proc Natl Acad Sci U S A.* 1995; 92:5510-5514.

46.   Huang C, Zhang Z, Ding M, Li J, Ye J, Leonard SS, Shen HM, Butterworth L, Lu Y, Costa M, Rojanasakul Y, Castranova V, Vallyathan V, Shi X. Vanadate induces p53 transactivation through hydrogen peroxide and causes apoptosis. *J Biol Chem.* 2000; 275:32516-32522.

47.   Kaluzova M, Kaluz S, Lerman MI, Stanbridge EJ. DNA damage is a prerequisite for p53-mediated proteasomal degradation of HIF-1alpha in hypoxic cells and downregulation of the hypoxia marker carbonic anhydrase IX. *Mol Cell Biol.* 2004; 24:5757-5766.

48.   Ravi R, Mookerjee B, Bhujwalla ZM, Sutter CH, Artemov D, Zeng Q, Dillehay LE, Madan A, Semenza GL, Bedi A. Regulation of tumor angiogenesis by p53-induced degradation of hypoxia-inducible factor 1alpha. *Genes Dev.* 2000; 14:34-44.

49.   Schmid T, Zhou J, Kohl R, Brune B. p300 relieves p53-evoked transcriptional repression of hypoxia-inducible factor-1 (HIF-1). *Biochem J.* 2004; 380:289-295.

50. MacKenzie ED, Selak MA, Tennant DA, Payne LJ, Crosby S, Frederiksen CM, Watson DG, Gottlieb E. Cell-permeating alpha-ketoglutarate derivatives alleviate pseudohypoxia in succinate dehydrogenase-deficient cells. *Mol Cell Biol.* 2007; 27:3282-3289.

51. Denko NC. Hypoxia, HIF1 and glucose metabolism in the solid tumour. *Nat Rev Cancer.* 2008; 8:705-713.

52. Papandreou I, Cairns RA, Fontana L, Lim AL, Denko NC. HIF-1 mediates adaptation to hypoxia by actively downregulating mitochondrial oxygen consumption. *Cell Metab.* 2006; 3:187-197.

53. Michelakis ED, Sutendra G, Dromparis P, Webster L, Haromy A, Niven E, Maguire C, Gammer TL, Mackey JR, Fulton D, Abdulkarim B, McMurtry MS, Petruk KC. Metabolic modulation of glioblastoma with dichloroacetate. *Sci Transl Med.* 2010; 2:31ra34.

54. Habib GB, Heibig J, Forman SA, Brown BG, Roberts R, Terrin ML, Bolli R. Influence of coronary collateral vessels on myocardial infarct size in humans. Results of phase I thrombolysis in myocardial infarction (TIMI) trial. The TIMI Investigators. *Circulation.* 1991; 83:739-746.

55. Sabia PJ, Powers ER, Ragosta M, Sarembock IJ, Burwell LR, Kaul S. An association between collateral blood flow and myocardial viability in patients with recent myocardial infarction. *N Engl J Med.* 1992; 327:1825-1831.

56. Kido M, Du L, Sullivan CC, Li X, Deutsch R, Jamieson SW, Thistlethwaite PA. Hypoxia-inducible factor 1-alpha reduces infarction and attenuates progression of cardiac dysfunction after myocardial infarction in the mouse. *J Am Coll Cardiol.* 2005; 46:2116-2124.

57. Ho TK, Rajkumar V, Ponticos M, Leoni P, Black DC, Abraham DJ, Baker DM. Increased endogenous angiogenic response and hypoxia-inducible factor-1alpha in human critical limb ischemia. *J Vasc Surg.* 2006; 43:125-133.

58. Kaul S, Bolger AF, Herrington D, Giugliano RP, Eckel RH. Thiazolidinedione drugs and cardiovascular risks: a science advisory from the American Heart Association and American College Of Cardiology Foundation. *J Am Coll Cardiol.* 2010; 55:1885-1894.

59.   Michelakis ED. Spatio-temporal diversity of apoptosis within the vascular wall in pulmonary arterial hypertension: heterogeneous BMP signaling may have therapeutic implications. *Circ Res.* 2006; 98:172-175.

60.   Dromparis P, Sutendra G, Michelakis ED. The role of mitochondria in pulmonary vascular remodeling. *J Mol Med (Berl).* 2010; 88:1003-1010.

61.   Xu W, Koeck T, Lara AR, Neumann D, DiFilippo FP, Koo M, Janocha AJ, Masri FA, Arroliga AC, Jennings C, Dweik RA, Tuder RM, Stuehr DJ, Erzurum SC. Alterations of cellular bioenergetics in pulmonary artery endothelial cells. *Proc Natl Acad Sci U S A.* 2007; 104:1342-1347.

62.   Macchia A, Marchioli R, Marfisi R, Scarano M, Levantesi G, Tavazzi L, Tognoni G. A meta-analysis of trials of pulmonary hypertension: a clinical condition looking for drugs and research methodology. *Am Heart J.* 2007; 153:1037-1047.

63.   McLaughlin VV, Archer SL, Badesch DB, Barst RJ, Farber HW, Lindner JR, Mathier MA, McGoon MD, Park MH, Rosenson RS, Rubin LJ, Tapson VF, Varga J, Harrington RA, Anderson JL, Bates ER, Bridges CR, Eisenberg MJ, Ferrari VA, Grines CL, Hlatky MA, Jacobs AK, Kaul S, Lichtenberg RC, Moliterno DJ, Mukherjee D, Pohost GM, Schofield RS, Shubrooks SJ, Stein JH, Tracy CM, Weitz HH, Wesley DJ. ACCF/AHA 2009 expert consensus document on pulmonary hypertension: a report of the American College of Cardiology Foundation Task Force on Expert Consensus Documents and the American Heart Association: developed in collaboration with the American College of Chest Physicians, American Thoracic Society, Inc., and the Pulmonary Hypertension Association. *Circulation.* 2009; 119:2250-2294.

64.   Humbert M, Morrell NW, Archer SL, Stenmark KR, MacLean MR, Lang IM, Christman BW, Weir EK, Eickelberg O, Voelkel NF, Rabinovitch M. Cellular and molecular pathobiology of pulmonary arterial hypertension. *J Am Coll Cardiol.* 2004; 43:13S-24S.

65.   Archer SL, Weir EK, Wilkins MR. Basic science of pulmonary arterial hypertension for clinicians: new concepts and experimental therapies. *Circulation.* 2010; 121:2045-2066.

66.   Michelakis ED, Wilkins MR, Rabinovitch M. Emerging concepts and translational priorities in pulmonary arterial hypertension. *Circulation.* 2008; 118:1486-1495.

67.   Newman JH, Wheeler L, Lane KB, Loyd E, Gaddipati R, Phillips JA, 3rd, Loyd JE. Mutation in the gene for bone morphogenetic protein receptor II as a cause of primary pulmonary hypertension in a large kindred. *N Engl J Med.* 2001; 345:319-324.

68.   Remillard CV, Tigno DD, Platoshyn O, Burg ED, Brevnova EE, Conger D, Nicholson A, Rana BK, Channick RN, Rubin LJ, O'Connor D T, Yuan JX. Function of Kv1.5 channels and genetic variations of KCNA5 in patients with idiopathic pulmonary arterial hypertension. *Am J Physiol Cell Physiol.* 2007; 292:C1837-1853.

69.   Michelakis ED, Webster L, Mackey JR. Dichloroacetate (DCA) as a potential metabolic-targeting therapy for cancer. *Br J Cancer.* 2008; 99:989-994.

70.   Pan JG, Mak TW. Metabolic targeting as an anticancer strategy: dawn of a new era? *Sci STKE.* 2007; 2007:pe14.

71.   Vander Heiden MG, Cantley LC, Thompson CB. Understanding the Warburg effect: the metabolic requirements of cell proliferation. *Science.* 2009; 324:1029-1033.

72.   Kim JW, Dang CV. Cancer's molecular sweet tooth and the Warburg effect. *Cancer Res.* 2006; 66:8927-8930.

73.   Kim JW, Dang CV. Multifaceted roles of glycolytic enzymes. *Trends Biochem Sci.* 2005; 30:142-150.

74.   Bonnet S, Archer SL, Allalunis-Turner J, Haromy A, Beaulieu C, Thompson R, Lee CT, Lopaschuk GD, Puttagunta L, Harry G, Hashimoto K, Porter CJ, Andrade MA, Thebaud B, Michelakis ED. A mitochondria-K+ channel axis is suppressed in cancer and its normalization promotes apoptosis and inhibits cancer growth. *Cancer Cell.* 2007; 11:37-51.

75.   Chen LB. Mitochondrial membrane potential in living cells. *Annu Rev Cell Biol.* 1988; 4:155-181.

76.   DeBerardinis RJ, Lum JJ, Hatzivassiliou G, Thompson CB. The biology of cancer: metabolic reprogramming fuels cell growth and proliferation. *Cell Metab.* 2008; 7:11-20.

77.   Macian F. NFAT proteins: key regulators of T-cell development and function. *Nat Rev Immunol.* 2005; 5:472-484.

78.   McMurtry MS, Bonnet S, Wu X, Dyck JR, Haromy A, Hashimoto K, Michelakis ED. Dichloroacetate prevents and reverses pulmonary hypertension by inducing pulmonary artery smooth muscle cell apoptosis. *Circ Res.* 2004; 95:830-840.

79.   Michelakis ED, McMurtry MS, Wu XC, Dyck JR, Moudgil R, Hopkins TA, Lopaschuk GD, Puttagunta L, Waite R, Archer SL. Dichloroacetate, a metabolic modulator, prevents and reverses chronic hypoxic pulmonary hypertension in rats: role of increased expression and activity of voltage-gated potassium channels. *Circulation.* 2002; 105:244-250.

80.   Zamanian RT, Hansmann G, Snook S, Lilienfeld D, Rappaport KM, Reaven GM, Rabinovitch M, Doyle RL. Insulin resistance in pulmonary arterial hypertension. *Eur Respir J.* 2009; 33:318-324.

81.   Rabinovitch M. PPARgamma and the pathobiology of pulmonary arterial hypertension. *Adv Exp Med Biol.* 2010; 661:447-458.

82.   Sobolewski A, Rudarakanchana N, Upton PD, Yang J, Crilley TK, Trembath RC, Morrell NW. Failure of bone morphogenetic protein receptor trafficking in pulmonary arterial hypertension: potential for rescue. *Hum Mol Genet.* 2008; 17:3180-3190.

83.   Sitbon O, Lascoux-Combe C, Delfraissy JF, Yeni PG, Raffi F, De Zuttere D, Gressin V, Clerson P, Sereni D, Simonneau G. Prevalence of HIV-related pulmonary arterial hypertension in the current antiretroviral therapy era. *Am J Respir Crit Care Med.* 2008; 177:108-113.

84.   Sehgal PB, Mukhopadhyay S, Patel K, Xu F, Almodovar S, Tuder RM, Flores SC. Golgi dysfunction is a common feature in idiopathic human pulmonary hypertension and vascular lesions in SHIV-nef-infected macaques. *Am J Physiol Lung Cell Mol Physiol.* 2009; 297:L729-737.

85.   Voelkel NF, Cool CD, Flores S. From viral infection to pulmonary arterial hypertension: a role for viral proteins? *AIDS*. 2008; 22 Suppl 3:S49-53.

86.   Cool CD, Rai PR, Yeager ME, Hernandez-Saavedra D, Serls AE, Bull TM, Geraci MW, Brown KK, Routes JM, Tuder RM, Voelkel NF. Expression of human herpesvirus 8 in primary pulmonary hypertension. *N Engl J Med.* 2003; 349:1113-1122.

87.   Hotamisligil GS. Endoplasmic reticulum stress and the inflammatory basis of metabolic disease. *Cell.* 2010; 140:900-917.

88.   Li X, Zhang X, Leathers R, Makino A, Huang C, Parsa P, Macias J, Yuan JX, Jamieson SW, Thistlethwaite PA. Notch3 signaling promotes the development of pulmonary arterial hypertension. *Nat Med.* 2009; 15:1289-1297.

89.   Takahashi K, Adachi K, Yoshizaki K, Kunimoto S, Kalaria RN, Watanabe A. Mutations in NOTCH3 cause the formation and retention of aggregates in the endoplasmic reticulum, leading to impaired cell proliferation. *Hum Mol Genet.* 2009; 19:79-89.

90.   Smith P, Heath D. Electron microscopy of the plexiform lesion. *Thorax.* 1979; 34:177-186.

91.   Sutendra G, Dromparis P, Wright P, Bonnet S, Haromy A, Hao Z, McMurtry MS, Michalak M, Vance JE, Sessa WC, Michelakis ED. The role of Nogo and the mitochondria-endoplasmic reticulum unit in pulmonary hypertension. *Sci Transl Med.* 2011; 3:88ra55.

92.   Marsboom G, Toth PT, Ryan JJ, Hong Z, Wu X, Fang YH, Thenappan T, Piao L, Zhang HJ, Pogoriler J, Chen Y, Morrow E, Weir EK, Rehman J, Archer SL. Dynamin-related protein 1-mediated mitochondrial mitotic fission permits hyperproliferation of vascular smooth muscle cells and offers a novel therapeutic target in pulmonary hypertension. *Circ Res.* 2012; 110:1484-1497.

93.   Lee SJ, Smith A, Guo L, Alastalo TP, Li M, Sawada H, Liu X, Chen ZH, Ifedigbo E, Jin Y, Feghali-Bostwick C, Ryter SW, Kim HP, Rabinovitch M, Choi AM. Autophagic protein LC3B confers resistance against hypoxia-induced pulmonary hypertension. *Am J Respir Crit Care Med.* 2011; 183:649-658.

A version of this chapter has been published. Dromparis P and Michelakis ED 2013. Annual Review of Physiology. 75:95-126.

Chapter Two

Uncoupling protein 2 deficiency mimics hypoxia and endoplasmic reticulum stress in mitochondria and triggers pseudo-hypoxic pulmonary vascular remodeling

Introduction

The role of mitochondria is increasingly being recognized in vascular health and disease[1] and is particularly critical in the pulmonary circulation. As recognized oxygen sensors, mitochondria form the basis of hypoxic pulmonary vasoconstriction (HPV), a feature of all mammals and the most important difference between the pulmonary and systemic circulation (all systemic vessels dilate to hypoxia while pulmonary arteries constrict)[2]. In response to acute decreases in oxygen levels, mitochondria alter the production of mitochondria-derived reactive oxygen species (mROS), which reach the cell membrane and regulate redox-sensitive voltage-gated potassium channels (Kv). The resulting Kv inhibition depolarizes the cell, increases influx of Ca^{2+} and causes contraction of pulmonary artery smooth muscle cells (PASMC) [2]. Mitochondria may also play an important role in the chronic hypoxic response and in pulmonary vascular disease via the regulation of the hypoxia inducible factor (HIF1α) [3]. Several aspects of the HIF1α axis are redox-sensitive and α-ketoglutarate (αKG), a Krebs' cycle product, is an important cofactor in the hydroxylation reaction that destabilizes HIF1α. A primary suppression of mitochondrial glucose oxidation (GO) reduces mROS and αKG, activating HIF1α even in normoxia [3]. Aberrant HIF1α activation has been shown in normoxic animal and human pulmonary arteries in pulmonary hypertension (PHT) [4,5]. In cancer, where suppression of GO is critical for the apoptosis-resistance that characterizes most tumors, there is normoxic HIF1α activation. This "pseudo-hypoxic" HIF1α activation is reversed by activation of GO, decreasing cancer angiogenesis in vitro and in vivo [3]. Like in cancer, GO suppression also leads to apoptosis suppression and a proliferative diathesis that underlies the vascular remodeling in PHT [6-8]. Thus, it is possible that the HIF1α activation in PHT is also a consequence of suppressed mitochondrial signaling.

The basis of GO suppression in PHT is unknown. Hypoxia, particularly if severe and sustained, directly inhibits GO by decreasing oxygen levels in mitochondria. Chronic hypoxia can inhibit GO by an additional, recently described mechanism: several conditions that cause PHT, including chronic

43

hypoxia, are also known to induce endoplasmic reticulum (ER) stress [8, 9]. ER stress can lead to mitochondrial suppression by decreasing the influx of Ca^{2+} from the ER to mitochondria due to an ER structural remodeling, decreasing mitochondrial Ca^{2+} (Ca^{2+}_m). This inhibits many Ca^{2+}-dependent mitochondrial enzymes including pyruvate dehydrogenase (PDH, the gate-keeper of GO) or isocitrate dehydrogenase (IDH) and αKG dehydrogenase (both regulating αKG levels) [8-10].

We hypothesized that UCP2 deficiency could mimic the effects of hypoxia or ER stress on mitochondria in the pulmonary circulation. This is because UCP2 can function as a Ca^{2+} channel in vascular mitochondria, facilitating influx of Ca^{2+} from the ER to mitochondria [11-13]. UCP2, despite its name, does not appear to have uncoupling functions and has little homology to UCP1 [11-13]. Mitochondria deficient in UCP2 may be deficient in Ca^{2+}_m and thus have suppressed GO in the absence of hypoxia or ER stress, inducing a "pseudo-hypoxia" and apoptosis-resistance state and predisposing to proliferative pulmonary vascular remodeling (Figure 2-1). The description of human *UCP2* polymorphisms leading to decreased gene expression, makes this hypothesis more interesting and clinically relevant [14].

Results

2.1 UCP2-deficiency reduces ER-derived mitochondrial calcium in PASMCs

We isolated mitochondria from whole lung, spleen and isolated PASMCs from resistance pulmonary arteries (>4th division) of mice lacking UCP2 (*Ucp2*KO) and their wild-type controls (*Ucp2*WT). The absence of UCP2 in KO mice was confirmed by qRT-PCR (Figure 2-2A) and immunoblots (Figure 2-2B). We then measured Ca^{2+}_m in *Ucp2*WT- and KO-PASMCs in normoxia and sustained hypoxia (48hrs). FRET imaging showed that *Ucp2*KO-PASMCs had lower levels of Ca^{2+}_m than *Ucp2*WT-PASMCs under basal, normoxic conditions (Figure 2-3A). Unlike *Ucp2*WT-PASMCs, which had the expected Ca^{2+}_m reduction in hypoxia [8], hypoxia did not further reduce Ca^{2+}_m in *Ucp2*KO-PASMCs (Figure 2-3A). Similar results were obtained with the Ca^{2+}_m-sensitive

dye Rhodamine-2AM (Figure 2-4). Pharmacological UCP2 inhibition with genipin reduced Ca^{2+}_m in *Ucp2*WT-PASMCs but not *Ucp2*KO-PASMCs (Figure 2-3A). Thus, UCP2 deficiency reduces Ca^{2+}_m in PASMCs mimicking the effects of hypoxi and ER-stress on PASMC as previously published [8, 9]

To determine whether UCP2 facilitates mitochondrial Ca^{2+} uptake specifically from the ER in PASMCs, we analyzed Ca^{2+}_m upon histamine-stimulation, which releases ER-calcium through IP_3 signaling. Experiments were performed in Ca^{2+}-free solution to eliminate extracellular Ca^{2+} sources. The histamine-induced increase in Ca^{2+}_m was blunted in *Ucp2*KO-PASMCs (Figure 2-3B). Inhibition of the mitochondrial Ca^{2+} uniporter (MCU) with ruthenium red (RR) inhibited the responses similarly between cell genotypes, suggesting that the differences were not due to MCU down-regulation.

Chronically hypoxic PASMCs have an ER stress-induced disruption of the normal communication between the ER and mitochondria, including Ca^{2+} exchange, due to an ER structural remodeling and an increase in the minimal distance between the two organelles [8]. Using transmission electron microscopy we showed that the minimal ER-mitochondria distance was similar between *Ucp2*WT- and *Ucp2*KO-PASMCs under normoxia, suggesting that altered baseline Ca^{2+}_m levels in the later were a result of decreased transport, rather than a potential structural remodeling (Figure 2-3C). In contrast, hypoxia increased the ER-mitochondria distance similarly in *Ucp2*WT- and *Ucp2*KO-PASMCs (Figure 2-3C) [8]. Furthermore, spatial ER-mitochondria disruption does not further reduce Ca^{2+}_m in *Ucp2*KO-PASMCs, suggesting that lack of UCP2 in normoxia induces a "pseudo-hypoxia" state in terms of Ca^{2+}_m. In other words, a primary loss of UCP2 or an ER stress-induced disruption of the ER-mitochondria unit may both result in a similar reduction of Ca^{2+}_m and thus GO.

2.2 UCP2-deficiency reduces mitochondrial metabolism and signaling

Several key metabolic enzymes are Ca^{2+}_m-dependent, including PDH and the Krebs' cycle enzymes IDH and α-KG dehydrogenase [10]. PDH drives mitochondrial GO and its inhibition is associated with PHT [15]. In keeping with

45

reduced $Ca^{2+}{}_m$, *Ucp2*KO-PASMCs had lower PDH activity than *Ucp2*WT-PASMCs (Figure 2-5A). PDH inhibition decreases the acetyl-CoA influx into the Krebs' cycle, while Krebs' cycle activity can be further decreased by IDH and αKG dehydrogenase inhibition. Indeed, a metabolomics assessment of Krebs' cycle function showed reduced levels of many metabolites, including αKG, in *Ucp2*KO-PASMCs compared to the *Ucp2*WT-PASMCs under normoxia (Figure 2-5B). Once again, the reduction of Krebs' cycle metabolites in normoxic *Ucp2*KO-PASMCs (compared to wild-type) was similar to the chronic hypoxia-induced reduction in *Ucp2*WT-PASMCs. Thus, lack of *Ucp2* mimics a hypoxic state and hypoxia does not cause a further suppression of mitochondrial function over and above what lack of *Ucp2* does.

A similar pattern was present when we studied two other important indices of mitochondrial function: mROS (which are produced by the electron transport chain in proportion to Krebs' cycle-derived electron donors) and mitochondrial membrane potential (ΔΨm). *Ucp2*KO-PASMCs had lower mROS and increased ΔΨm compared to *Ucp2*WT-PASMCs in normoxia (Figure 2-5C). The increased ΔΨm in *Ucp2*KO-PASMCs which, like the decreased mROS levels, is described in human and animal PHT-PASMC [6], is in keeping with reduced mitochondrial levels of the positively charged Ca^{2+}. Once again, normoxic *Ucp2*KO-PASMCs mimicked hypoxic *Ucp2*WT-PASMCs and hypoxia did not further suppress any tested parameter in *Ucp2*KO-PASMCs (Figure 2-5 A-C).

2.3 UCP2-deficiency promotes apoptosis resistance

The hyperpolarized ΔΨm and the decreased mROS (both of which directly inhibit the opening of the voltage- and redox-gated mitochondrial transition pore, through which pro-apoptotic mediators like cytochrome c and apoptosis inducing factor efflux from the mitochondria [16]) promote an apoptosis-resistance state in both cancer [3, 17, 18] and pulmonary hypertension [1, 7, 8, 15]. To determine whether *Ucp2*KO-PASMCs are resistant to apoptosis, PASMCs were stressed in serum-starved conditions (0.1% FBS). Apoptosis, measured by TUNEL, was increased in *Ucp2*WT-, but not *Ucp2*KO-, PASMCs (Figure 2-5D).

2.4 UCP2-deficiency promotes HIF1α activation

We then determined whether lack of *Ucp2* could explain the activation of two transcription factors that have been shown to be critical in both hypoxic and non-hypoxic PHT: HIF1α [4] and the nuclear factor of activated T-cells (NFATc2) [19]. Upon dismutation, mitochondria-produced superoxide becomes H_2O_2, a more stable and diffusible mROS that reaches several extra-mitochondrial targets, including Kv-channels and transcription factors like HIF1α. *Ucp2*KO-PASMCs had reduced H_2O_2 (Figure 2-6A) and αKG levels (Figure 2-5B), as well as normoxic HIF1α-activation (Figure 2-6B), similar to hypoxic *Ucp2*WT-PASMCs. The activation of HIF1α was confirmed by both the levels of expression in PASMC nuclei and by direct measurement of its transcriptional activity using a dual-luciferase assay. The activation of HIF1α in normoxic PASMC lacking UCP2 was similar to that in hypoxic *Ucp2*WT-PASMCs and was maximal, as it was not increased further by hypoxia (Figure 2-6B).

2.5 UCP2-deficiency promotes NFATc2 activation

Like HIF1α, NFATc2 is influenced (albeit indirectly) by mitochondrial signals [19]. While de-phosphorylation by the Ca^{2+}-sensitive cytoplasmic enzyme calcineurin activates NFATc2 driving it to the nucleus, phosphorylation by the metabolic sensor glycogen synthase kinase-3β [GSK3β, which is inhibited when GO is suppressed in PASMCs [7] and cancer [17]] results in nuclear export and transcriptional inhibition. Consistent with reduced mROS and inhibited Kv-channels, *Ucp2*KO-PASMCs had elevated levels of cytoplasmic Ca^{2+} compared to *Ucp2*WT-PASMCs (Figure 2-7A). Moreover, *Ucp2*KO-PASMCs had elevated phosphorylated (inactive) GSK3β, compared to *Ucp2*WT-PASMCs (Figure 2-7B). The increased cytoplasmic Ca^{2+} and inhibited GSK3β were associated, as expected, with NFATc2 activation (increased nuclear levels) in normoxic *Ucp2*KO-PASMC, similar to hypoxic *Ucp2*WT-PASMCs (Figure 2-7C).

2.6 UCP2-deficiency mimics hypoxia and ER-stress in vivo

The activation of HIF1α, NFATc2 as well as the hyperpolarized $\Delta\Psi$m and the decreased mROS and GO in *Ucp2*KO-PASMCs essentially create the cellular in vitro phenotype as has been shown in several human and animal PHT models [1, 4, 6-9, 15, 19]. They promote proliferation and apoptosis-resistance and thus would be expected to cause PHT in normoxic mice in vivo. We thus measured mean pressure (mPAP) and cardiac output (CO) in close-chest anesthetized mice. *Ucp2KO* mice had elevated mPAP and total pulmonary resistance (TPR=mPAP/CO) compared to *Ucp2*WT controls (Figure 2-8, Figure 2-9A/B), without differences in systemic blood pressure (Figure 2-10). Lack of *Ucp2* did not worsen pulmonary hemodynamic parameters upon exposure to chronic hypoxia, a standard PHT model (Figure 2-9A-B), in keeping with our in vitro findings. To determine whether the hemodynamic changes were due to pulmonary vascular remodeling, we examined the resistance pulmonary arteries of these mice in normoxia and hypoxia. Normoxic *Ucp2*KO mice had increased medial wall thickness of resistance pulmonary arteries (Figure 2-9C). This was associated with increased nuclear levels of NFATc2 (Figure 2-11) and increased proliferation indices (Ki67) in smooth muscle actin-positive cells (Figure 2-9D). There was also increased arterial muscularization in *Ucp2*KO mice in normoxia, which was not exacerbated in hypoxia (Figure 2-9E). Taken together, these results indicated that the pulmonary vasculature in *Ucp2*-deficient mice resembles that of wild-type mice under chronic hypoxia. In addition, normoxic *Ucp2*KO mice have modestly, but significantly elevated hematocrit compared to *Ucp2*WT mice (Figure 2-9F), suggesting that lack of *Ucp2* mimics hypoxia in the kidney as well, where the HIF1α product erythropoietin is produced, inducing perhaps a global pseudo-hypoxia state.

Discussion

Here we show for the first time that the mitochondrial protein UCP2 is involved in both the normoxic activation of HIF1α as well as pulmonary vascular remodeling and PHT. We specifically show that lack of UCP2 causes a decrease

48

in the entry of Ca^{2+} from the ER to the PASMC mitochondria, resulting in decreased Ca^{2+}_{m} and a subsequent suppression of mitochondrial function. This suppression of mitochondrial function, and its associated metabolic switch toward glycolysis, has been previously shown to be critical for the pro-proliferative and anti-apoptotic diathesis that characterizes several animal and human PHT models [1, 4, 6-9, 15, 19]. The effects of UCP2 deficiency in PASMC mitochondria resemble the effects of hypoxia and ER stress as recently described [8, 9]. Overall, lack of UCP2 induces a cellular and an in vivo phenotype that is identical to that caused by hypoxia as measured by several parameters. Our results are in keeping with the work that has shown that UCP2 conducts mitochondrial Ca^{2+} and support the emerging metabolic hypothesis of pulmonary vascular oxygen sensing and PHT [1, 6].

The activity of the Ca^{2+}-sensitive PDH is decreased in normoxic *Ucp*2KO PASMC and this has been shown in many PHT models, where the PDH activator small molecule dichloroacetate has been shown to reverse PHT [4, 7, 20]. Our data suggest that a potential deficiency of UCP2 in humans could explain the PDH inhibition and perhaps the resulting suppression of GO and activation of glycolysis that has been described in patients with idiopathic pulmonary arterial hypertension [21].

In humans, *Ucp*2 expression is influenced by recently described polymorphisms in the *Ucp2* promoter. These polymorphisms, which decrease *Ucp2* expression, are associated with increased incidence of carotid atherosclerosis [22], proliferative diabetic retinopathy [23], and hypertension [24] when animals are exposed to predisposing conditions. For example, mice lacking *Ucp2* develop systemic hypertension only in appropriately stressed conditions [25], and thus do not conflict with the normal systemic hemodynamics observed in our study. It is also intriguing that *Ucp2* polymorphisms are associated with overall metabolic disturbances like obesity and diabetes [14], while an unexplained insulin-resistance state has recently been described in PHT [26]. As the pulmonary vasculature exists in a much more oxidized environment and the PASMC are different than the systemic vascular mitochondria (perhaps explaining why HPV

is restricted to the pulmonary circulation) [27], the threshold for expressing a disease phenotype may be much lower in the pulmonary arteries than in systemic vessels, explaining why PHT but not systemic hypertension is shown in normal conditions in *Ucp2*KO mice.

The lack of UCP2 appears to cause HIF1α activation in PASMC as well as in the kidney, explaining the increased hematocrit in the *Ucp2*KO mice. The activation of HIF1α in rat and human PHT tissues is well described but remains unexplained [4, 5]. Our data suggest that the suppression of downstream mitochondrial signaling in cells lacking UCP2, including the decreased mROS and αKG levels, may explain this "pseudo-hypoxic" HIF1α activation. We have recently shown that in cancer cells (where HIF1α activation is also present even under normoxia) the suppression in mitochondrial function activates HIF1α by a mechanism that includes a prolyl-hydroxylase dependent mechanism (decrease in αKG production) and a prolyl-hydroxylase independent mechanism (that involves mitochondrial H_2O_2-mediated regulation of p53 as well as inhibition of GSK3β) [3]. Lack of UCP2 causes a direct decrease in H_2O_2 and αKG production from mitochondria as well as an indirect inhibition of GSK3β that follows the inhibition of GO, and thus the mechanism described in cancer cells can be applied to the PASMC. Interestingly, HIF1α activation induces the expression of pyruvate dehydrogenase kinase, a major inhibitor of PDH, thus causing inhibition of GO [28]. This has been used to suggest that the metabolic remodeling in cancer is a result, not a cause of HIF1α activation. Our current data, where the primary abnormality is in mitochondria (lack of UCP2), support a mitochondria-driven regulation of HIF1α. It is likely that both pathways are important and mitochondrial PDK and HIF1α activation are a part of positive feedback loop that promotes a sustained inhibition of GO and HIF1α activation even under normoxia.

A limitation of this study is that we focused on PASMC biology and did not address the role of *Ucp2* in pulmonary artery endothelial cells (PAEC). Nevertheless, it is now recognized that PHT PAEC show similar metabolic

remodeling to PHT-PASMCs, characterized by suppressed GO [21]. UCP2 has also been shown to regulate Ca^{2+}_m handling in vascular endothelial cells as well [11-13]. In other words, we speculate that PAEC will have a similar to PASMC metabolism in the *Ucp2*KO mice. We also did not explore the role of inflammation on PHT-development in these mice. Indeed, inflammation may contribute to PHT-pathogenesis and *Ucp2*-deficient macrophages have basal activation of the pro-inflammatory transcription factor NFκB and exaggerated immune responses [29]. In humans, *Ucp2* polymorphisms are associated with autoimmune diseases [30], a well-recognized feature of PHT [15]. While we do not address a potential role of activated macrophages in the development of PHT in *Ucp2*KO mice, our in vitro studies and their agreement with the in vivo data suggest that a primary mechanism for spontaneous PHT is intrinsic to PASMC. It is possible that these mice will have enhanced responses to more inflammatory models of PHT.

Since the *Ucp2*KO mouse model spontaneously develops PHT and also shares many of the mitochondria abnormalities described in many animal models and human PHT, it may be an important tool for future studies in the field. Clinical studies could explore whether *Ucp*2 polymorphisms contribute to PHT in humans, offering new biomarker and potentially therapeutic strategies. Importantly, the fact that *Ucp2*KO mice have what appears to be a pseudo-hypoxic environment (with vascular and generalized HIF1α activation) in normoxia, makes them an attractive model for oxygen sensing studies as well.

Materials and Methods

All experiments were performed with approval by the University of Alberta Committee on Animal Policy and Welfare. Mice were purchased from Jackson Laboratory and previously validated for UCP2 knockout [31]

Cell Culture: PASMCs from five *Ucp*2WT- or *Ucp*2KO-mice were freshly isolated from fourth generation pulmonary arteries, with an enzymatic cocktail containing papain (1mg/ml) (Sigma Aldrich), dithiothreitol (DTT; 0.5mg/ml) (Sigma Aldrich), collagenase (0.6 mg/ml) (Worthington), and bovine serum

albumin (0.6 mg/ml) (Sigma-Aldrich) and pooled as previously described[7, 8]. PASMCs were grown in Dulbecco's modified Eagle's medium (DMEM) (Gibco, Invitrogen) supplemented with 10% fetal bovine serum (FBS) (Sigma-Aldrich) and 1% antibiotic/antimycotic (Gibco, Invitrogen) and placed in a humidified incubator set at 37°C in either normoxic conditions (21% O_2; pO_2~120mmHg) or mild/physiologic hypoxia conditions (4% O_2; pO_2~40mmHg).

FRET analysis: PASMCs were plated on glass dishes and transfected with the 4mtD3CPV cameleon plasmid using a Xfect transfection reagent (Clontech) under normoxic conditions as previously described [8]. After 24 hours, media was replaced with treatment media containing vehicle (DMSO) (Sigma Aldrich) or genipin (50μM, Wako) and placed in normoxia or hypoxia. After 48 hours, media was diluted with 4% paraformaldehyde in a 1:1 ratio and cells were fixed under treatment conditions for 60 minutes. Cells were washed with distilled water and mounted on a slide using Prolong Gold (Invitrogen) and imaged 48 hours later on a Zeiss LSM 510 confocal microscope. Excitation occurred at 458 nm and the emission filters were 480 to 520 nm for cyan (when Ca^{2+} is not bound) and 535 to 590 nm for FRET (yellow when Ca^{2+} is bound). The ratio of yellow/cyan intensities was used to standardize the rate of infection for each cell, as previously described [8].

Histamine stimulation: Media from cells cultured under normoxic or hypoxic conditions was washed and replaced with calcium-free buffer [NaCl (125mM), KCl (5mM), Na_3PO_4 (1mM), $MgSO_4$ (1mM), Glucose (5.5mM), HEPES (20mM)] as previously described[32], containing either vehicle or ruthenium red (10μm, Calbiochem). A series of 60 images (8sec/image) was performed. Histamine (1mM) was added to give a final concentration of 100μM on the 6th image, in order to establish a 5-image baseline fluorescence. The percent increase was determined by the maximum YFP/CFP ratio after histamine minus the average baseline YFP/CFP ratio divided by the average baseline YFP/CFP ratio.

Electron Microscopy: Cells were grown to 80% confluency on 100mm dishes. Media was aspirated and replaced with Karnovsky's fixative [2% paraformaldehyde (Sigma Aldrich) and 2% gluteraldehyde in phosphate buffer]

for 1 hr at room temperature. Cells were then washed with phosphate buffered saline, scraped and centrifuged. Pelleted material was transferred to a scintillation vial and post-fixed with 1% osmium tetroxide in phosphate buffer for 1 hour on ice. After washing in PBS, cells were serially dehydrated in ethanol and rinsed in propylene oxide, before being incubated for 18 hours in 1:1 ratio of propylene oxide and resin. After 24 hours, cells were placed in 100% embedding resin under a vacuum for 6-8 hours before being transferred to a cutting tube and polymerizing at 60 degrees Celsius for 48 hours. Samples were then sliced, mounted on metal gratings and imaged on a Phillips EM 400T/ST transmission electron microscope. Quantifications were performed at 40,000x magnification. Representative images are at 105,000x magnification.

PDH Activity: PDH activity was measured with a commercially available MitoProfile Dipstick assay kit (Mitosciences) as previously described [8, 15]. Briefly, 50μL of protein (1mg/ml) was incubated with a dipstick containing the PDH complex antibody in a 96 well plate, followed by activity buffer. A flat top scanner was used to measure the band intensity.

Metabolite extraction: PASMCs were pelleted and suspended in 800μL of ice-cold 80% methanol and 20% ddH$_2$O. Samples were vigorously vortexed and placed in liquid N$_2$ for 10 minutes to freeze. Samples were then thawed on ice for 10 minutes and the freeze-thaw cycle was repeated two times. Samples were centrifuged at 13,000g to pellet cell debris, lipids and proteins. Supernatant was evaporated and metabolites were re-suspended in HPLC-grade H$_2$O. Metabolites were normalized to protein concentration.

Mass Spectroscopy: Seven microliters of sample was injected using a 4000 QTRAP mass spectrometer (AB Sciex) equipped with a UHPLC 1290 system (Agilent) via SRM for Krebs' cycle intermediates. Samples were delivered to the MS with mobile phases A (20mM NH$_4$OH, 20mM NH$_4$Ac in 95%/5% H$_2$O/CH$_3$CN) and B (98% CH$_3$CN, 2% H$_2$O) via a 2.0mm i.d. x 10cm HILIC Luna NH$_2$ column (Phenomenex) at 250μl/min using negative ion LC/MS/MS analytical run. The dwell time was 5ms per SRM transition, and collision energy was optimized for each SRM transition. Total cycle time was 2.09 s.

HIF1α luciferase: PASMCs (20,000 cells/well) were seeded into a black, clear bottom 96-well plate and allowed to adhere. Cells were transfected with the HIF1α dual luciferase plasmid (SABiosciences) using Xfect transfection reagent (Clontech) under normoxic conditions. After 24 hours, media was replaced with treatment media and cells were placed in normoxia or hypoxia. HIF1α activity was assessed with the dual-luciferase reporter assay system (Promega). After 48 hours, cells were lysed by a freeze-thaw cycle in passive lysis buffer (provided in kit) and luminescence was measured with a luminometer. HIF1α activity was assessed by HIF1α-driven firefly luminescence normalized to a constitutively-driven Renilla luminescence to standardize the transfection as previously described [3, 8].

qRT-PCR: qRT-PCR was performed as previously described [7, 8]. mRNA isolated from PASMCs were added to a microwell plate with TaqMan probes and reagents. qRT-PCR was performed with the ABI Prism 7700 Sequence Detector (Applied Biosystems), and *β2-microglobulin* was used as a housekeeping gene (Applied Biosystems).

Echocardiography and Hemodynamics: Mice were randomized to normobaric hypoxia (10% O_2) or room air as previously described [7, 8]. Cardiac output was assessed on isoflurane-anesthetized animals by echocardiography using the Vevo770 imaging system with a 707B (30MHz) probe. The cardiac output was calculated after determining the left ventricular outflow tract diameter (LVOT), aortic velocity time integral (AoVTI), and heart rate (HR) using the formula:

$$CO = 7.85 \times LVOT^2 \times AoVTI \times HR / 10000$$

Mean pulmonary artery pressures (mPAP) were assessed in closed-chest animals with a Millar catheter (microtip, 1.4F, Millar Instruments Inc., Houston, TX) as previously described [7, 8]. Animals were placed in a supine position on a heated table under inhaled isoflurane anesthesia and the right jugular vein was cannulated and the catheter advanced into the pulmonary arteries. Pressures from the right atrium, right ventricle and pulmonary arteries were also recorded continuously and mean PAP was calculated electronically (Power Lab, with Chart

software 5.4, ADInstruments). Total pulmonary resistance was calculated by the mPAP/CO ratio.

Medial Wall Thickness: The percent medial wall thickness was determined as previously described [7, 8]. Briefly, 5μm-thick lung sections were stained using hematoxylin and eosin (H&E) stain. Vessels >50μm were identified and measured at the two ends of the shortest external diameter of the distal PAs, and the average was taken [(2 x wall thickness/external diameter) x 100].

Muscularization: Lung sections (5μm) were stained for smooth muscle actin and von Willebrand Factor (endothelial cell marker). Vessels (<50μm) were classified as fully (100%), partially, or non-muscularized (0%), based on the percentage of vWF surrounded by SMA in each vessel as previously described [7].

Hematocrit: Blood was collected from isoflurane-anesthetized mice via cardiac puncture and injected into a RapidLab 348 blood gas analyzer (Bayer Healthcare).

Systemic blood pressure: Systemic systolic and diastolic blood pressures were measured in non-anesthetized mice with the CODA2 (Kent Scientific Corp.) mousetail cuff system as previously described [15]. Animals were restrained in a holding chamber and an occlusion cuff was placed at the base of the tail. A volume pressure cuff was placed distally. Systolic and diastolic blood pressures were obtained by averaging at least five volume-pressure recordings per animal.

Immunoblots: Tissues were collected and immunoblotting was performed as previously described [7, 8, 15, 18]. The films were digitized and quantified with 1D Image Analysis Software (Kodak, Rochester, NY). Expression was normalized to α-actin to correct for loading differences. Antibodies: UCP2 1:1000; COXIV 1:1000 (both Santa Cruz Biotechnologies).

Statistics: All values were expressed as mean±SEM. For in vitro analysis, differences were assessed by Student's t-test. Normality of our in vivo data was confirmed by the Shapiro-Wilk test. Inter-group differences were assessed by ANOVA using Fisher's least square differences post-hoc analysis. All analyses were performed using SPSS 19. Significance was considered at $p < 0.05$.
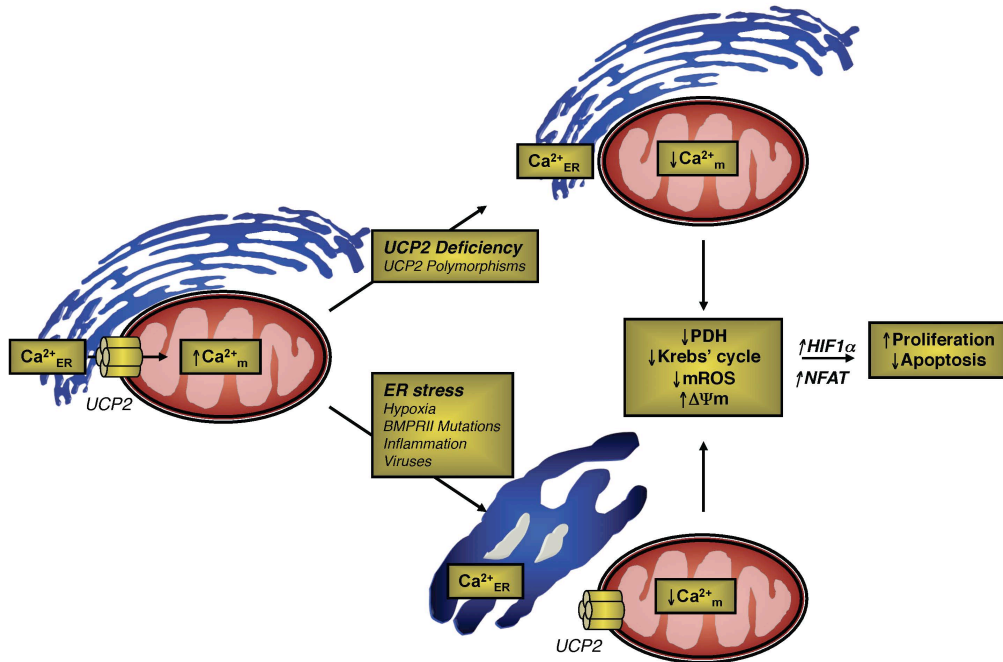
Figure 2-1: A model of how UCP2-deficiency can mimic hypoxia-induced ER stress. UCP2-deficiency reduces calcium transfer from the ER into the mitochondria, which mimics the effects of physical disruption of the ER-mitochondria unit caused by PHT-associated ER-stress inducers like hypoxia, bone-morphogenic receptor II mutations, inflammation, or viruses on Ca^{2+}_{m}. The mechanism and the consequences of such a hypoxia and ER stress induced-disruption of the ER-mitochondria unit was recently described in [8,9]. Reduced Ca^{2+}_{m} inhibits mitochondrial metabolic enzymes like PDH and some Krebs' cycle enzymes, lowers mROS, and hyperpolarizes $\Delta\Psi m$, suppressing apoptosis. Altered mitochondrial-derived signals activate transcription factors like HIF1α and NFAT, potentiating the pro-proliferative and anti-apoptotic signaling.
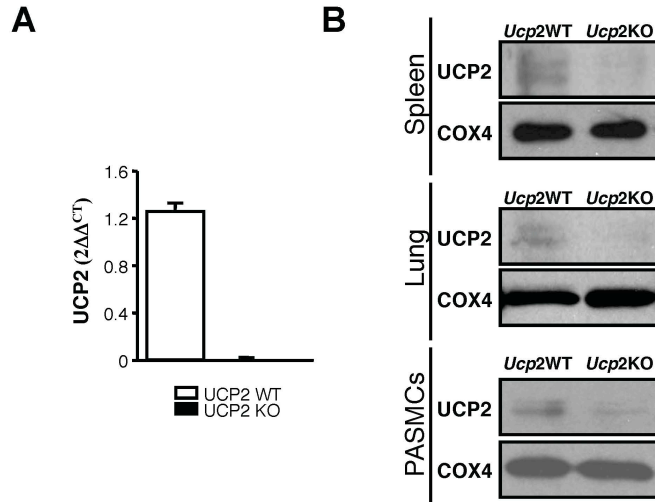
Figure 2-2: UCP2 expression in *Ucp2*KO and *Ucp2*WT mice.
(A) *Ucp2* mRNA expression in UCP2WT- and KO- PASMCs. **(B)** Immunoblot on isolated mitochondria showing presence and absence of UCP2 in spleen (top), lung (middle) and in isolated PASMCs (bottom) from *Ucp2*WT and *Ucp2*KO mice, respectively. Very faint bands can be seen in the UCP2KO samples, likely because UCP2 and 3 have a >70% homology, creating a recognized problem of UCP2 antibodies [33,34]. Even though the faint band can represent UCP3 in these otherwise well-validated and studied Ucp2KO mice [31] (where we also show complete absence of Ucp2 mRNA), it is important to document that UCP2 levels are quite low and compatible with the cellular phenotype that we describe in this work. It is also important that UCP3 has been shown to mostly be expressed in skeletal muscle and brown fat tissues [33].
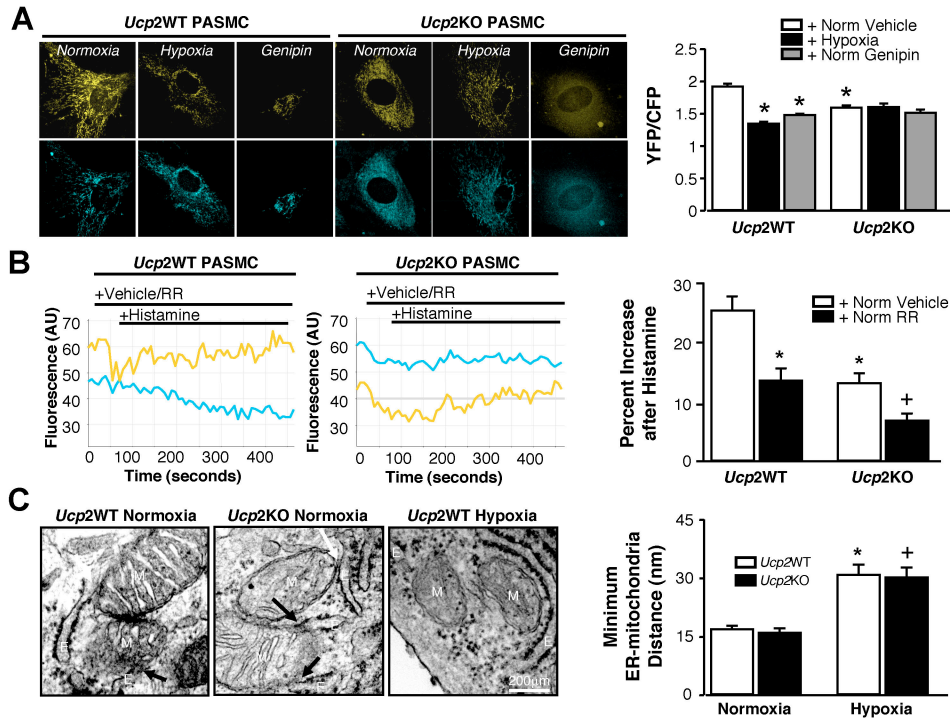
Figure 2-3: *Ucp2*-deficiency reduces ER-mitochondrial calcium transport
(A) FRET analysis of Ca^{2+}_m in *Ucp2*WT- and *Ucp2*KO-PASMCs at basal normoxic conditions, hypoxia, and with the UCP2 inhibitor genipin. Lack of UCP2 causes a decrease in Ca^{2+}_m similar to that caused by either hypoxia or genipin in *Ucp2*WT-PASMCs. Hypoxia or genipin do not have any additional effects on *Ucp2*KO-PASMCs (n>50 cells/group; *p<0.05 compared to normoxic vehicle). **(B)** Representative traces of YFP and CFP fluorescence after histamine addition on PASMCs treated with either vehicle or ruthenium red (RR) (left). Percent increase in Ca^{2+}_m in response to histamine is calculated by the YFP/CFP ratio (right). The response to histamine is blunted in *Ucp2*KO-PASMC, whereas the RR inhibits the response to histamine by a similar degree in *Ucp2*WT- and *Ucp2*KO-PASMC (n>15 cells/group, *p<0.05 compared to WT normoxic vehicle, [+]p<0.05 compared to KO normoxic vehicle). **(C)** Transmission electron microscopy of *Ucp2*WT- and *Ucp2*KO-PASMCs (left) and minimum ER-mitochondrial distance (right) (n=50 ER-mitochondria contact points/group, * and [+] p<0.05 compared to normoxic controls). E=endoplasmic reticulum, M=mitochondria.
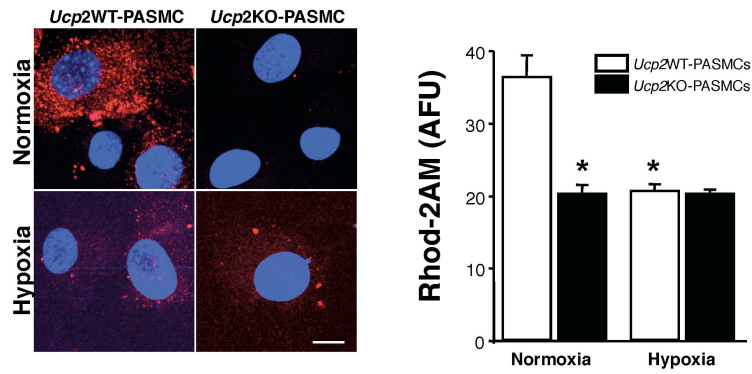
Figure 2-4: Rhodamine-2AM staining for Ca$^{2+}_m$ in *Ucp2*WT- and *Ucp2*KO-PASMCs in normoxia and hypoxia. Representative confocal microscopy images show Representative confocal microscopy images show Rhodamine-2AM (red) and the nuclear stain Hoechst 33342 (blue). Normoxic *Ucp2*KO-PASMCs have Ca$^{2+}_m$ levels similar to hypoxic *Ucp2*WT-PASMCs. Hypoxia does not further reduce Ca$^{2+}_m$ in *Ucp2*KO-PASMCs (n~100 cells/group). *p<0.05 vs. normoxic *Ucp2*WT-PASMCs. Bar = 20μm.
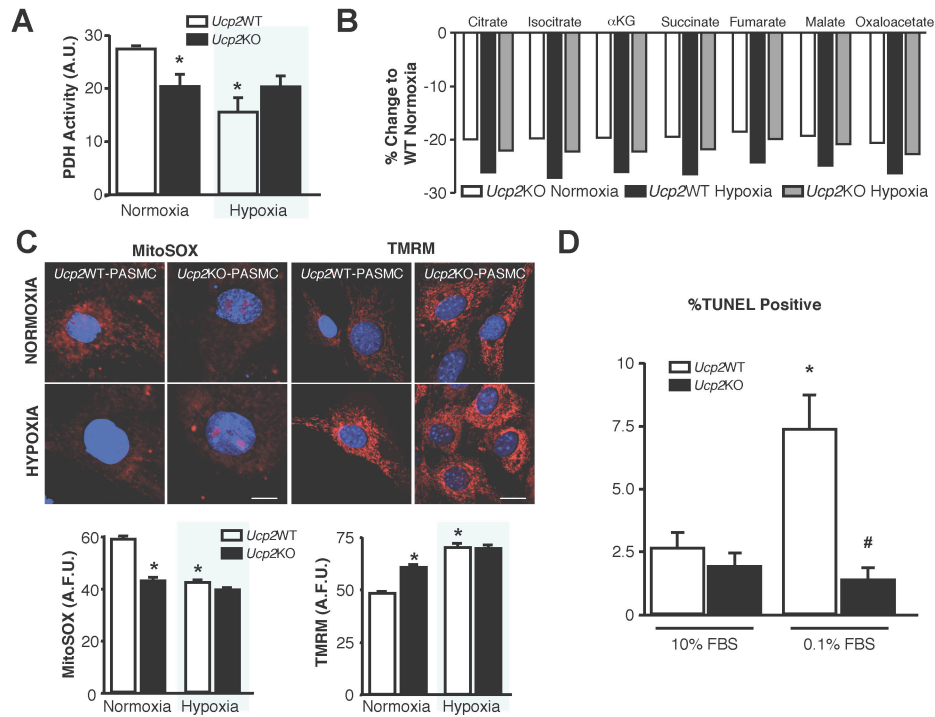
Figure 2-5: ***Ucp*2-deficiency mimics a hypoxia-induced suppression of mitochondrial function and apoptosis**
(A) Lack of UCP2 in *Ucp2*KO-PASMCs decreases PDH activity similar to hypoxia in the *Ucp2*WT-PASMCs. Hypoxia does not have additional effects on *Ucp2*KO-PASMCs (n=3 experiments; *p<0.05 compared to normoxic vehicle). **(B)** Percent decrease in Krebs' cycle metabolites of hypoxic *Ucp2*WT-PASMCs and normoxic and hypoxic *Ucp2*KO-PASMCs compared to normoxic *Ucp2*WT-PASMCs. Lack of UCP2 decreases all Krebs' metabolites, similar to hypoxia in *Ucp2*WT-PASMCs. Hypoxia does not have any additional effects on *UCP2*KO-PASMCs (n=3 merged samples/group). **(C)** Representative confocal images of mROS (Mitosox; red, left panels) and ΔΨm (TMRM; red, right panels) in *Ucp2*WT-PASMC and *Ucp2*KO-PASMCs in normoxia and hypoxia. Nuclei are stained with DAPI (blue) Lack of UCP2 decreases mROS and increases ΔΨm similar to hypoxia in *Ucp2*WT-PASMCs. Hypoxia does not have any additional effects on *Ucp2*KO-PASMCs (n>150 cells/group, *p<0.05 compared to normoxic vehicle). Bar = 20μm. **(D)** Serum-starvation induces apoptosis in *Ucp2*WT-PASMC, but not *Ucp2*KO-PASMCs (n>25 fields/group, * p<0.05 compared to 10%FBS *Ucp2*WT-PASMCs; # p<0.05 vs and 0.1%FBS *Ucp2*WT-PASMCs).
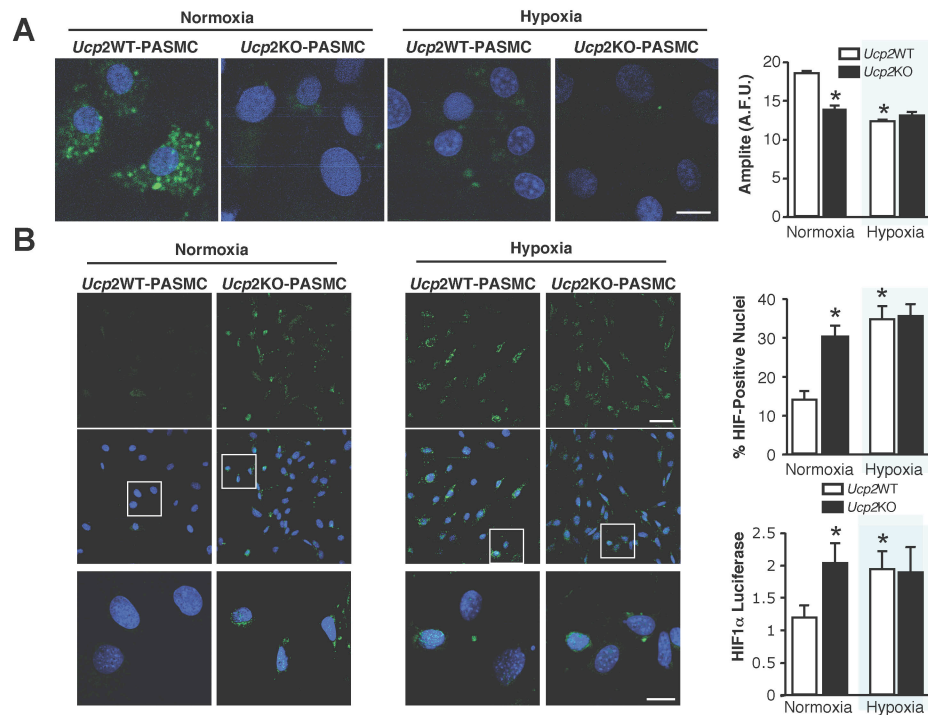
Figure 2-6: *Ucp2*KO-PASMCs have normoxic HIF1α activation.
(A) Representative confocal microscopy images show the H_2O_2-sensitive dye
Amplite (green) and the nuclear stain Hoechst 33342 (blue). Normoxic *Ucp2*KO-
PASMCs have lower H_2O_2 levels than normoxic *Ucp2*WT-PASMCs, but similar
H_2O_2 to hypoxic *Ucp2*WT-PASMCs. Hypoxia does not further reduce Amplite in
*Ucp2*KO-PASMCs (n~150 cells/group). *p<0.05 vs. normoxic *Ucp2*WT-
PASMCs. Bar = 20μm. **(B)** Representative confocal microscopy images show
HIF1α (green) co-localizing with the nuclear stain DAPI (blue). Bar=20μm. Top:
Normoxic *Ucp2*KO-PASMCs a have similar percentage of HIF1α-positive nuclei
compared to hypoxic *Ucp2*WT-PASMCs and this is not increased by hypoxia
(n~30 fields/group from 3 separate experiments). Bottom: Normoxic *Ucp2*KO-
PASMCs have similar HIF1α-driven luciferase signal compared to hypoxic
*Ucp2*WT-PASMCs. Hypoxia does not further increase the HIF1α-driven
luciferase signal in hypoxic *Ucp2*KO-PASMCs (n=15-18 wells/group). *p<0.05
vs. normoxic *Ucp2*WT-PASMCs.
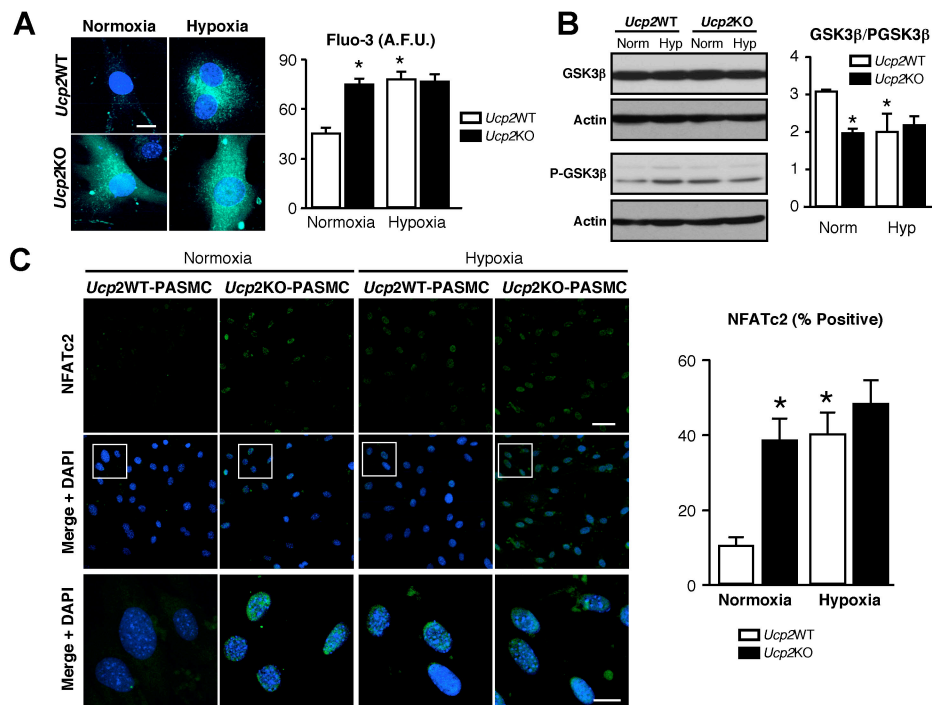
Figure 2-7: *Ucp2*KO-PASMCs have normoxic NFATc2 activation.
A) Representative confocal microscopy images show the cytosolic Ca^{2+}-sensitive dye Fluo3 (green) and the nuclear stain Hoechst 33342 (blue). Normoxic *Ucp2*KO-PASMCs have cytoplasmic Ca^{2+} levels higher than normoxic *Ucp2*WT-PASMCs, but similar to hypoxic *Ucp2*WT-PASMCs. Hypoxia does not further increase cytoplasmic Ca^{2+} in *Ucp2*KO-PASMCs (n=30-80 cells/group; *$p<0.05$ vs. normoxic *Ucp2*WT-PASMCs). Bar = 20μm.
(B) Representative immunoblots showing total and inactive (i.e. phosphorylated) GSK3β (P-GSK3β). Data are presented as a ratio of active to inactive enzyme. Normoxic *Ucp2*KO-PASMCs have similar GSK3β inhibition compared to hypoxic *Ucp2*WT-PASMCs. Hypoxia does not further inhibit GSK3β in *Ucp2*KO-PASMCs (n=3 experiments, *$p<0.05$ vs. normoxic *Ucp2*WT-PASMCs).
(C) Representative confocal microscopy images show the expression of NFATc2 (green) and the nuclear stain DAPI (blue). Normoxic *Ucp2*KO-PASMCs have a similar percentage of NFATc2-positive nuclei compared to hypoxic *Ucp2*WT-PASMCs. Hypoxia does not further increase the percentage of NFATc2-postive nuclei in *Ucp2*KO-PASMCs (n~30 fields/group; *$p<0.05$ vs. normoxic *Ucp2*WT-PASMCs). Top panel: Bar = 50μm; Bottom panel: Bar = 20μm.
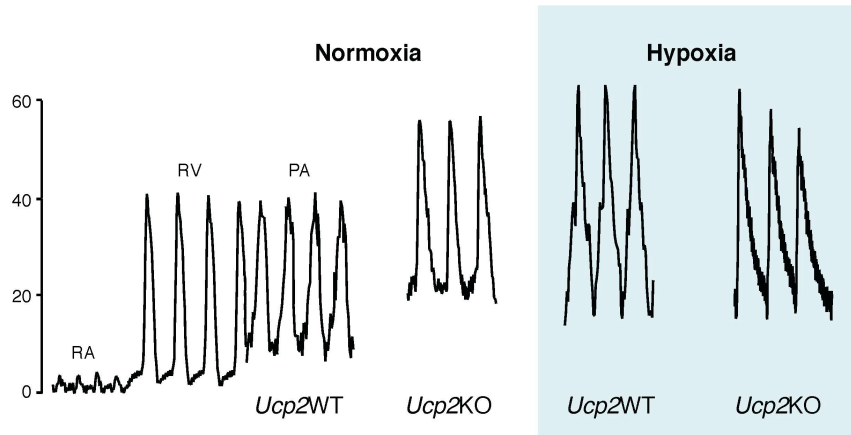
Supplement Figure 2-8: In vivo hemodynamic traces.
Representative traces of the right atrium (RA), right ventricle (RV) and pulmonary arteries (PAs) for *Ucp2*WT- and KO- mice in normoxia and hypoxia. Normoxic *Ucp2*KO mice have higher PA pressures compared to normoxic *Ucp2*WT mice. Hypoxia does not increase PA pressures in *Ucp2*KO-mice more than in *Ucp2*WT mice.
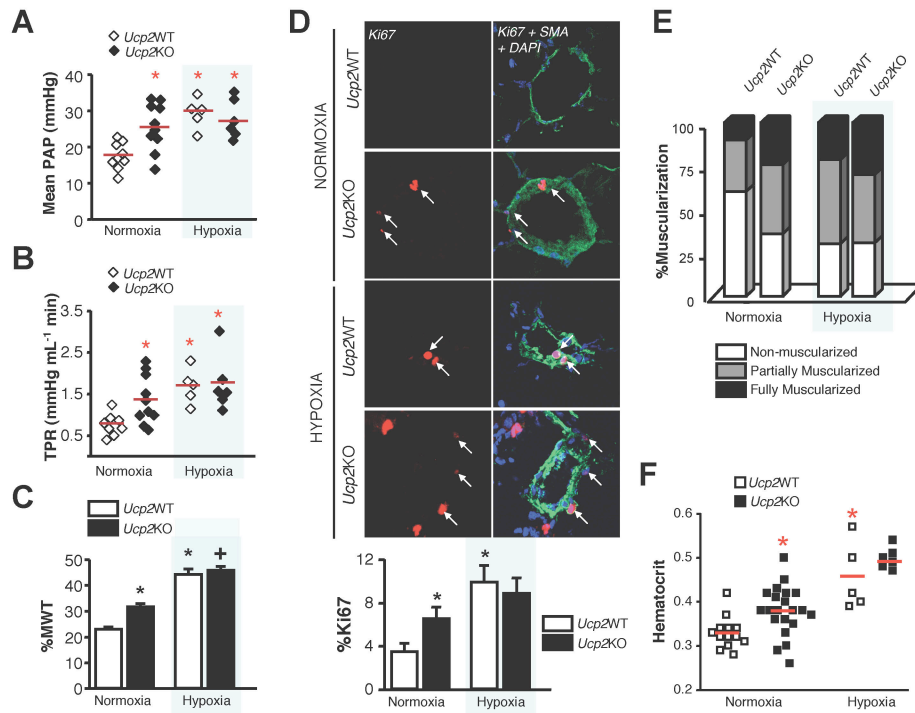
Figure 2-9: *Ucp2*-deficient mice develop spontaneous PHT
(A-B) *Ucp2KO mice* have elevated mean pulmonary artery pressure (mPAP) and total pulmonary resistance (TPR) compared to *Ucp2*WT controls in normoxia, similar hemodynamic changes to hypoxic *Ucp2*WT mice. Hypoxia does not cause further changes in hemodynamics in *UCP2*KO mice (Each point represents one animal, *p<0.05 compared to normoxic *Ucp2*WT mice). **(C)** *Ucp2*KO mice have greater medial wall thickness compared to *Ucp2*WT mice in normoxia (n>50 vessels/group, *p<0.05 vs. normoxic *Ucp2*WT mice.) **(D)** *Ucp2*KO mice have higher proliferation rates (%Ki67-positive) in lung smooth muscle actin (SMA)-positive cells compared to *Ucp2*WT controls in normoxia, but similar proliferation to hypoxic *Ucp2*WT mice (n>35 vessels/group, *p<0.05 compared to normoxic *Ucp2*WT mice). **(E)** *Ucp2*KO mice have greater vessel musclarization compared to *Ucp2*WT controls in normoxia, but muscularization similar to hypoxic *Ucp2*WT mice (n>70 vessels/group). **(F)** *Ucp2*KO mice have higher hematocrit compared to *Ucp2*WT controls in normoxia, but hematocrit similar to hypoxic *Ucp2*WT mice (Each point represents one animal, *p<0.05 vs. normoxic *Ucp2*WT-mice).

64
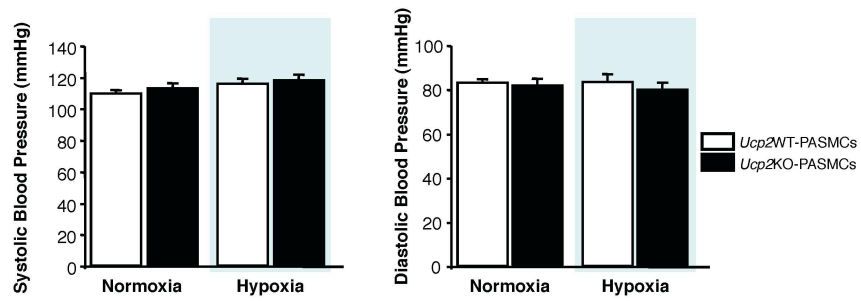
Figure 2-10: Systemic blood pressures in *Ucp2*WT and KO-mice.
There were no statistically significant differences in systolic (left) and diastolic (right) blood pressures of *Ucp2*WT- and KO- mice in normoxia and hypoxia (n=5 animals/group). p>0.05.
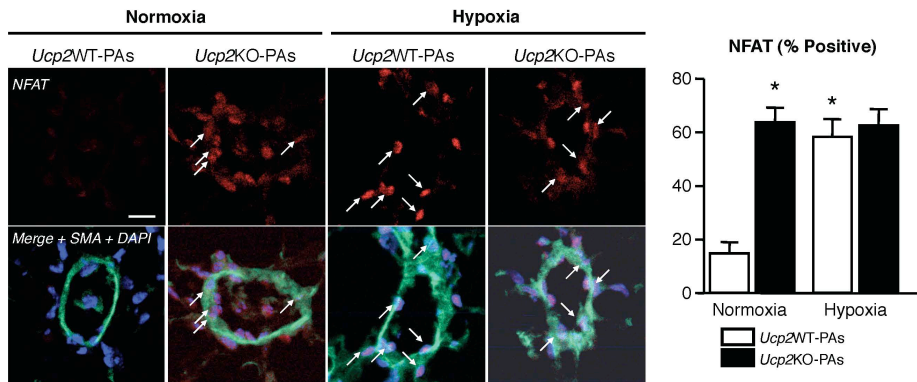
Supplement Figure 2-11: *Ucp2*KO-mice have normoxic NFATc2 activation in SMA-positive cells in the distal pulmonary arteries.
Representative confocal microscopy images show NFATc2 (red), SMA (green) and the nuclear stain DAPI (blue). Arrows represent SMA-positive/NFAT-positive nuclei. SMA-positive cells in the distal PAs of normoxic *Ucp2*KO-mice have similar number of NFATc2-positive nuclei compared to SMA-positive cells in the distal PAs of hypoxic *Ucp2*WT-mice. Hypoxia does not further increase the NFATc2-postive nuclei in SMA-positive cells in the distal PAs of normoxic *Ucp2*KO-mice. (n~30 vessels/group) *p<0.05 vs. normoxic *Ucp2*WT-mice. Bar = 50μm.

References

1.   Dromparis P, Michelakis ED. Mitochondria in Vascular Health and Disease. *Annu Rev Physiol.* 2012; ; Epub ahead of print, Nov 16 2012.

2.   Weir EK, Lopez-Barneo J, Buckler KJ, Archer SL. Acute oxygen-sensing mechanisms. *N Engl J Med.* 2005; 353:2042-2055.

3.   Sutendra G, Dromparis P, Kinnaird A, Stenson TH, Haromy A, Parker JM, McMurtry MS, Michelakis ED. Mitochondrial activation by inhibition of PDKII suppresses HIF1a signaling and angiogenesis in cancer. *Oncogene.* 2012.

4.   Bonnet S, Michelakis ED, Porter CJ, Andrade-Navarro MA, Thebaud B, Haromy A, Harry G, Moudgil R, McMurtry MS, Weir EK, Archer SL. An abnormal mitochondrial-hypoxia inducible factor-1alpha-Kv channel pathway disrupts oxygen sensing and triggers pulmonary arterial hypertension in fawn hooded rats: similarities to human pulmonary arterial hypertension. *Circulation.* 2006; 113:2630-2641.

5.   Tuder RM, Chacon M, Alger L, Wang J, Taraseviciene-Stewart L, Kasahara Y, Cool CD, Bishop AE, Geraci M, Semenza GL, Yacoub M, Polak JM, Voelkel NF. Expression of angiogenesis-related molecules in plexiform lesions in severe pulmonary hypertension: evidence for a process of disordered angiogenesis. *J Pathol.* 2001; 195:367-374.

6.   Dromparis P, Sutendra G, Michelakis ED. The role of mitochondria in pulmonary vascular remodeling. *J Mol Med (Berl).* 2010; 88:1003-1010.

7.   Sutendra G, Bonnet S, Rochefort G, Haromy A, Folmes KD, Lopaschuk GD, Dyck JR, Michelakis ED. Fatty acid oxidation and malonyl-CoA decarboxylase in the vascular remodeling of pulmonary hypertension. *Sci Transl Med.* 2010; 2:44ra58.

8.   Sutendra G, Dromparis P, Wright P, Bonnet S, Haromy A, Hao Z, McMurtry MS, Michalak M, Vance JE, Sessa WC, Michelakis ED. The role of Nogo and the mitochondria-endoplasmic reticulum unit in pulmonary hypertension. *Sci Transl Med.* 2011; 3:88ra55.

9.   Dromparis P, Paulin R, Stenson TH, Haromy A, Sutendra G, Michelakis ED. Attenuating Endoplasmic Reticulum Stress as a Novel Therapeutic Strategy in Pulmonary Hypertension. *Circulation.* 2012.

10.   Denton RM. Regulation of mitochondrial dehydrogenases by calcium ions. *Biochim Biophys Acta.* 2009; 1787:1309-1316.

11.   Graier WF, Trenker M, Malli R. Mitochondrial Ca2+, the secret behind the function of uncoupling proteins 2 and 3? *Cell Calcium.* 2008; 44:36-50.

12.   Trenker M, Malli R, Fertschai I, Levak-Frank S, Graier WF. Uncoupling proteins 2 and 3 are fundamental for mitochondrial Ca2+ uniport. *Nat Cell Biol.* 2007; 9:445-452.

13.   Waldeck-Weiermair M, Malli R, Naghdi S, Trenker M, Kahn MJ, Graier WF. The contribution of UCP2 and UCP3 to mitochondrial Ca(2+) uptake is differentially determined by the source of supplied Ca(2+). *Cell Calcium.* 2010; 47:433-440.

14.   Jia JJ, Zhang X, Ge CR, Jois M. The polymorphisms of UCP2 and UCP3 genes associated with fat metabolism, obesity and diabetes. *Obes Rev.* 2009; 10:519-526.

15.   Sutendra G, Dromparis P, Bonnet S, Haromy A, McMurtry MS, Bleackley RC, Michelakis ED. Pyruvate dehydrogenase inhibition by the inflammatory cytokine TNFalpha contributes to the pathogenesis of pulmonary arterial hypertension. *J Mol Med (Berl).* 2011; 89:771-783.

16.   Zamzami N, Kroemer G. The mitochondrion in apoptosis: how Pandora's box opens. *Nat Rev Mol Cell Biol.* 2001; 2:67-71.

17.   Bonnet S, Archer SL, Allalunis-Turner J, Haromy A, Beaulieu C, Thompson R, Lee CT, Lopaschuk GD, Puttagunta L, Harry G, Hashimoto K, Porter CJ, Andrade MA, Thebaud B, Michelakis ED. A mitochondria-K+ channel axis is suppressed in cancer and its normalization promotes apoptosis and inhibits cancer growth. *Cancer Cell.* 2007; 11:37-51.

18.   Michelakis ED, Sutendra G, Dromparis P, Webster L, Haromy A, Niven E, Maguire C, Gammer TL, Mackey JR, Fulton D, Abdulkarim B,

McMurtry MS, Petruk KC. Metabolic modulation of glioblastoma with dichloroacetate. *Sci Transl Med.* 2010; 2:31ra34.

19. Bonnet S, Rochefort G, Sutendra G, Archer SL, Haromy A, Webster L, Hashimoto K, Bonnet SN, Michelakis ED. The nuclear factor of activated T cells in pulmonary arterial hypertension can be therapeutically targeted. *Proc Natl Acad Sci U S A.* 2007; 104:11418-11423.

20. McMurtry MS, Bonnet S, Wu X, Dyck JR, Haromy A, Hashimoto K, Michelakis ED. Dichloroacetate prevents and reverses pulmonary hypertension by inducing pulmonary artery smooth muscle cell apoptosis. *Circ Res.* 2004; 95:830-840.

21. Xu W, Koeck T, Lara AR, Neumann D, DiFilippo FP, Koo M, Janocha AJ, Masri FA, Arroliga AC, Jennings C, Dweik RA, Tuder RM, Stuehr DJ, Erzurum SC. Alterations of cellular bioenergetics in pulmonary artery endothelial cells. *Proc Natl Acad Sci U S A.* 2007; 104:1342-1347.

22. Oberkofler H, Iglseder B, Klein K, Unger J, Haltmayer M, Krempler F, Paulweber B, Patsch W. Associations of the UCP2 gene locus with asymptomatic carotid atherosclerosis in middle-aged women. *Arterioscler Thromb Vasc Biol.* 2005; 25:604-610.

23. Crispim D, Fagundes NJ, dos Santos KG, Rheinheimer J, Boucas AP, de Souza BM, Macedo GS, Leiria LB, Gross JL, Canani LH. Polymorphisms of the UCP2 gene are associated with proliferative diabetic retinopathy in patients with diabetes mellitus. *Clin Endocrinol (Oxf).* 2010; 72:612-619.

24. Ji Q, Ikegami H, Fujisawa T, Kawabata Y, Ono M, Nishino M, Ohishi M, Katsuya T, Rakugi H, Ogihara T. A common polymorphism of uncoupling protein 2 gene is associated with hypertension. *J Hypertens.* 2004; 22:97-102.

25. Ma S, Ma L, Yang D, Luo Z, Hao X, Liu D, Zhu Z. Uncoupling protein 2 ablation exacerbates high-salt intake-induced vascular dysfunction. *Am J Hypertens.* 2010; 23:822-828.

26.   Zamanian RT, Hansmann G, Snook S, Lilienfeld D, Rappaport KM, Reaven GM, Rabinovitch M, Doyle RL. Insulin resistance in pulmonary arterial hypertension. *Eur Respir J.* 2009; 33:318-324.

27.   Michelakis ED, Hampl V, Nsair A, Wu X, Harry G, Haromy A, Gurtu R, Archer SL. Diversity in mitochondrial function explains differences in vascular oxygen sensing. *Circ Res.* 2002; 90:1307-1315.

28.   Papandreou I, Cairns RA, Fontana L, Lim AL, Denko NC. HIF-1 mediates adaptation to hypoxia by actively downregulating mitochondrial oxygen consumption. *Cell Metab.* 2006; 3:187-197.

29.   Bai Y, Onuma H, Bai X, Medvedev AV, Misukonis M, Weinberg JB, Cao W, Robidoux J, Floering LM, Daniel KW, Collins S. Persistent nuclear factor-kappa B activation in Ucp2-/- mice leads to enhanced nitric oxide and inflammatory cytokine production. *J Biol Chem.* 2005; 280:19062-19069.

30.   Yu X, Wieczorek S, Franke A, Yin H, Pierer M, Sina C, Karlsen TH, Boberg KM, Bergquist A, Kunz M, Witte T, Gross WL, Epplen JT, Alarcon-Riquelme ME, Schreiber S, Ibrahim SM. Association of UCP2 -866 G/A polymorphism with chronic inflammatory diseases. *Genes Immun.* 2009; 10:601-605.

31.   Zhang CY, Baffy G, Perret P, Krauss S, Peroni O, Grujic D, Hagen T, Vidal-Puig AJ, Boss O, Kim YB, Zheng XX, Wheeler MB, Shulman GI, Chan CB, Lowell BB. Uncoupling protein-2 negatively regulates insulin secretion and is a major link between obesity, beta cell dysfunction, and type 2 diabetes. *Cell.* 2001; 105:745-755.

32.   Rizzuto R, Pinton P, Carrington W, Fay FS, Fogarty KE, Lifshitz LM, Tuft RA, Pozzan T. Close contacts with the endoplasmic reticulum as determinants of mitochondrial Ca2+ responses. *Science.* 1998; 280:1763-1766.

33.   Garvey WT. The role of uncoupling protein 3 in human physiology. *J Clin Invest.* 2003;111(4):438-441.

34.   Pecqueur C, Alves-Guerra MC, Gelly C, Levi-Meyrueis C, Couplan E,

Collins S, Ricquier D, Bouillaud F, Miroux B. Uncoupling protein 2, in vivo distribution, induction upon oxidative stress, and evidence for translational regulation. *J Biol Chem.* 2001;276(12):8705-8712.

A version of this chapter has been submitted for publication. Dromparis P, Paulin R, Sutendra G, Qi AC, Bonnet S, and Michelakis ED. 2013.

Chapter Three

Attenuating Endoplasmic Reticulum Stress as a Novel Therapeutic Strategy in Pulmonary Hypertension

Introduction

Pulmonary arterial hypertension (PAH) is a pulmonary-selective vascular remodeling disease in which cells within the vessel wall, including pulmonary artery smooth muscle cells (PASMCs), are characterized by a pro-proliferative and anti-apoptotic diathesis. Pulmonary arterial remodeling occludes the vessel lumen which leads to Right Ventricular (RV) failure and premature death, with the median survival of untreated patients limited to 3 years[1]. However, even in those receiving standard therapies, prognosis remains poor[2].

Although the pathology is restricted to the pulmonary vasculature, sparing the systemic vessels, all approved PAH therapies were originally developed as systemic vasodilators[3]. Moreover, in contrast to the earlier belief that vasoconstriction plays a central role in PAH pathogenesis, it is now accepted that PAH is a result of proliferative remodeling with vasoconstriction playing a limited role[4].

An additional challenge is that, despite the recent groupings of several conditions that share similar lung histology to idiopathic PAH (iPAH) under a 'PAH umbrella', the pathogenesis of PAH is multifactorial, suggesting that therapies that target one molecular abnormality in one form of PAH may not be as effective in other forms of the disease. For example, PAH is associated with inflammatory conditions like scleroderma, viral infections with HIV or HSV, hypoxia, or loss-of-function mutations in the bone morphogenetic protein receptor 2 (BMPR2)[4-6]. In PAH, like in cancer, many different molecular abnormalities can be active in a patient. Thus, an ideal PAH therapy should target common features of all these diverse biological processes in a manner that remains relatively selective to the pulmonary circulation and is effective in reversing pulmonary vascular remodeling[7].

An intriguing common feature of many known PAH-triggering or facilitating processes is endoplasmic reticulum (ER) stress. For example, both viral infections and hypoxia are well known causes of ER stress[8]. More recently, the loss-of-function mutations in BMPR2 and the resultant protein trafficking

dysfunction have been shown to induce ER stress as well[9]. Despite the emerging evidence for protein trafficking dysregulation[10] and the fact that ER abnormalities compatible with ER stress (for example dysmorphic and swollen ER) have been clearly described in the classic description of PAH pathology by Dr. Heath 30 years ago[11], ER stress has not been considered a therapeutic target.

Very recently, we published evidence that ER stress in the pulmonary circulation leads to the activation of the ER stress sensor *activating transcription factor 6* (ATF6), causing upregulation of neurite outgrowth inhibitor (Nogo), a member of the reticulin family of proteins that regulate ER shape[12]. Nogo induction causes disruption of a functional ER-mitochondrial unit, resulting in decreased mitochondrial calcium and inhibition of several key calcium-sensitive mitochondrial enzymes. We and others have described the resulting metabolic abnormalities as critical in PAH pathogenesis[13-16]. The mitochondrial suppression in PAH, much like in cancer, leads to a switch towards a glycolytic phenotype that promotes proliferation and suppresses apoptosis[7, 15]. Perhaps because of previously described mitochondrial differences between the pulmonary and systemic circulations[17], this metabolic abnormality appears to be restricted to the pulmonary circulation in both animals and patients with PAH. Indeed, mice lacking Nogo are phenotypically normal but completely resistant to the metabolic and vascular remodeling and hypoxia-induced PAH[12]. This work provided strong evidence of the role of Nogo and ER stress in PAH but did not offer a therapeutic tool. Although anti-Nogo therapies are currently in development[18], we hypothesized that inhibition of ER stress-induced ATF6 activation, the original signal for Nogo induction, may offer a therapeutic strategy potentially applicable to diverse PAH pathologies. The fact that we had shown that ATF6 is selectively activated in the pulmonary circulation, and not systemic vessels despite systemic hypoxia, provided some evidence that such a therapy may be relatively pulmonary-selective[12].

ER stress can be attenuated with small molecule chemical chaperones like the fatty acid derivative chemical chaperone 4-phenylbutyric acid (PBA) and the bile acid derivative tauroursodeoxycholic acid (TUDCA). Chemical chaperones

mimic native chaperones, promoting folding, preventing aggregation and restoring trafficking of misfolded proteins[19-21]. They have demonstrated anti-proliferative and pro-apoptotic effects in cancer[22-24], which shares a similar metabolic and mitochondrial remodeling with PAH-PASMCs[7, 15]. Moreover, these therapies are orally administered and are currently used clinically[19].

Here we show that these small molecules limit ER stress-induced mitochondrial suppression, preventing and reversing vascular remodeling, using classic models of pulmonary hypertension in both mice (hypoxia) and rats (monocrotaline) as well as in vitro mechanistic studies.

Results

3.1 PBA prevents and reverses pulmonary hypertension in mice and rats

To determine if chemical chaperones could be a potential PHT therapy, we studied mice exposed to 4 weeks of chronic normobaric hypoxia (CH-PHT) treated with PBA in a prevention (PBA starting the day of CH exposure onward for 4 weeks) or reversal protocol (PBA starting on the third week after onset of CH and for 2 weeks onward). Mice treated with PBA in either protocol had lower mean pulmonary artery pressure (mPAP; 35.8 ± 1.3 mmHg vs. 21.8 ± 0.9 and 19.0 ± 0.7 mmHg in PBA reversal and prevention treatments, respectively) and total pulmonary resistance (TPR; 2.56 ± 0.16 vs. 1.13 ± 0.92 and 0.92 ± 0.04 mmHg.min.ml^{-1} in PBA reversal and prevention protocols, respectively) compared to untreated CH-PHT controls (Figure 3-1A). Pulmonary artery acceleration time (PAAT) measured echocardiographically, which is inversely related to mPAP, was also improved with PBA treatment (Figure 3-2A). The decreased afterload resulted in lower RV hypertrophy (RVH) and improved functional capacity assessed by a treadmill test (Figure 3-1A). These parameters were not affected in normal normoxic mice treated with PBA. Systolic and diastolic blood pressure was not affected by hypoxia or PBA treatment (Figure 3-2B). In a second, more severe and inflammatory model of PHT[25], rats injected with monocrotaline (MCT-PHT) and treated in similar prevention (PBA starting the day of MCT injection, for 4 weeks onward) and reversal protocols (PBA

starting on the third week after MCT injection, for 2 weeks onward). Similar to the CH-PHT mice, the PBA treated MCT-PHT rats had decreased mPAP (50.2±5.1 mmHg vs. 33.7±4.3 and 31.3±4.7 mmHg in PBA reversal and prevention protocols, respectively), TPR (0.71±0.08 vs. 0.45±0.07 and 0.33±0.08 mmHg.min.ml^{-1} in PBA reversal and prevention protocols, respectively) (Figure 3-1B) and RVH (Figure 3-3).

3.2 PBA prevents and reverses pulmonary vascular remodeling in PHT

Consistent with the improved hemodynamics, PBA treated CH-PHT and MCT-PHT animals had reduced medial wall thickening of the resistance PAs (50-100μm diameter) and reduced muscularization (in <50μm diameter PAs) in both the reversal and prevention protocols (Figure 3-4A, Figure 3-5). Resistance vessels in vehicle-treated PHT animals from both models had increased expression of the proliferation marker Ki67 in smooth muscle actin-positive cells (SMA), which was reduced by PBA in both treatment protocols (Figure 3-4B). Furthermore, PBA induced apoptosis in resistance pulmonary artery SMA-positive cells, by ~3.6 and 4.5 fold in the CH-PHT and MCT-PHT animals, respectively (Figure 3-4B). Proliferation and apoptosis indices were not affected in von Willebrand Factor-positive cells (PA endothelial cell marker) (Figure 3-6). No changes in any histology-assessed parameters were observed in the lungs of PBA-treated healthy animals (Figure 3-4, Figure 3-5).

3.3 PBA reduces markers of ER stress in the pulmonary vasculature in PHT

Upon ER stress, ATF6 is cleaved in the ER and translocates to the nucleus[26] where it functions as a transcription factor. To determine if the beneficial effects observed in vivo can be associated with decreased cleavage of ATF6, we assessed nuclear ATF6 expression in resistance pulmonary arteries. Vehicle-treated CH-PHT mice had elevated nuclear ATF6 levels in SMA-positive PA cells compared to vehicle-treated normoxic mice (Figure 3-7A), suggesting ATF6 cleavage in the diseased PA. PBA reduced nuclear ATF6 expression in both the prevention and reversal protocols (Figure 3-7A), which corresponded to

decreased expression of the ATF6 target gene, glucose regulated protein 78 (GRP78)[27] (Figure 3-8). To more appropriately quantify the reduction of ATF6 cleavage, we performed immunoblots on isolated PAs (>4th division). In keeping with the immunofluorescence, CH-PHT PAs had increased levels of cleaved (i.e. active form) ATF6 (~60kDa) and increased expression of its target products GRP78 and Nogo (Figure 3-7B), supporting ATF6 activation in the PAs in vivo. This was blocked by PBA in both the prevention and reversal protocols. In contrast to ATF6, the pro-apoptotic ER stress pathway was not upregulated by hypoxia or PBA treatment, as assessed by CHOP expression (Figure 3-9). Similar effects on the ATF6 axis were observed in whole lung samples in both CH- (Figure 3-10) and MCT-PHT (Figure 3-11).

3.4 Chemical chaperones attenuate hypoxia-induced ATF6 activation in vitro

We then exposed cultured murine PASMCs to 48 hours of physiologic mild hypoxia (normoxia: pO_2=122.1±0.6mmHg, pH=7.38±0.02; hypoxia: pO_2=41.9±0.7mmHg, pH=7.39±0.01), to mimic our in vivo CH-PHT conditions. Similar to our in vivo findings, hypoxia caused an increase in nuclear translocation of ATF6, suggesting hypoxia increases ATF6 cleavage in vitro (Figure 3-12A). Double staining with antibodies against both ATF6 and GRP78 showed that in the same cells in which ATF6 was activated, GRP78 expression increased. Both PBA, and a structurally distinct chemical chaperone TUDCA, blocked hypoxia-induced increases in ATF6 nuclear localization (Figure 3-12A) and GRP78 expression (Figure 3-13). Similar to the PAs in vivo, hypoxia did not activate the pro-apoptotic CHOP pathway. In contrast, thapsigargin, an inducer of severe and non-physiological ER stress[26], substantially upregulated both GRP78 and CHOP in PASMCs (Figure 3-13).

To better assess ATF6 transcriptional activity, we performed a dual luciferase ATF6 reporter assay. In keeping with our immunofluorescence data, hypoxia caused a ~113% increase in ATF6 luciferase signal compared to normoxia, but not to the same extent as thapsigargin (~216% increase) (Figure 3-12B). Hypoxia-induced ATF6 activation was blocked by PBA, which had no

78

effects under normoxic conditions (Figure 3-12B). In addition, PBA reduced mRNA levels of GRP78 and Nogo by ~50%, further supporting effective ATF6 inhibition in hypoxic PASMCs (Figure 3-12C).

3.5 Chemical chaperones inhibit the decrease in mitochondrial calcium and function in hypoxic PASMCs

We have previously shown that in PASMCs, hypoxia-induced ATF6 activation triggers an increase in Nogo expression, which disrupts the ER-mitochondrial unit[12]. Spatial disruption of this unit dissociates mitochondria from ER-associated calcium microdomains, reducing intra-mitochondrial calcium[28]. Hypoxia predictably reduced levels of mitochondrial calcium as determined by Forster resonance energy transfer (FRET) imaging (Figure 3-14A). Both PBA and TUDCA inhibited the reduction in mitochondrial calcium despite ongoing hypoxia. Ruthenium red, a mitochondrial calcium uniporter inhibitor, reduced the FRET signal (YFP/CFP ratio) confirming the sensitivity of this technique to measure mitochondrial calcium in our model (Figure 3-14A). These results were also replicated with Rhodamine-2AM, a mitochondrial-specific, calcium-sensitive dye (Figure 3-15).

In keeping with increased mitochondrial calcium, PBA and TUDCA inhibited the hypoxia-induced decrease in the calcium-sensitive[29] mitochondrial enzyme pyruvate dehydrogenase (PDH) (Figure 3-14B). PBA and TUDCA also increased the activity of another calcium-dependent mitochondrial enzyme, isocitrate dehydrogenase (IDH)[29] as assessed by its product, alpha-ketoglutarate ($0.60\pm0.1\mu$g/well vs. 0.80 ± 0.04 and 0.75 ± 0.04 μg/well for PBA and TUDCA treated hypoxic PASMCs respectively, $p<0.05$). Both PDH and IDH produce NADH that feeds into the electron transport chain, proportionally generating mitochondrial reactive oxygen species (mROS). In keeping with restored activity of these enzymes, PBA and TUDCA inhibited the hypoxia-induced decrease in mROS (Figure 3-16A). Finally, since calcium is positively charged, it also influences the mitochondrial membrane potential ($\Delta\Psi$m). Consistent with decreased mitochondrial calcium and as previously described[12, 13, 30], hypoxic

79

PASMCs had increased ΔΨm, which was blocked by both PBA and TUDCA (Figure 3-16A). Taken together, these results suggest that PBA and TUDCA prevent ER-stress induced mitochondrial suppression, a cellular hallmark of PAH[12, 13, 30].

3.6 Chemical chaperones induce apoptosis and normalize proliferation in hypoxic PASMCs

Mitochondrial driven apoptosis is largely mediated by the release of pro-apoptotic factors through the mitochondrial transition pore (MTP)[31]. Since both mROS and ΔΨm depolarization facilitate the opening of the voltage- and redox-sensitive MTP, we explored the effects of chemical chaperones on PASMC apoptosis under hypoxic conditions. PBA and TUDCA increased apoptosis measured by the percentage of TUNEL-positive PASMCs by ~3.93 and ~3.05 fold, respectively (Figure 3-16B). Furthermore, PBA and TUDCA both reduced proliferation measured by the percentage of PASMCs expressing Ki67, in keeping with the effects of these chaperones in vivo (Figure 3-16B).

Discussion

We show that the small molecule chemical chaperone PBA prevents and reverses PAH in two standard rodent models, CH-PHT in mice and MCT-PHT in rats. In vitro, PBA and TUDCA inhibit the ATF6 ER-stress pathway in PASMCs exposed to physiologic hypoxia. The downstream effects of this inhibition include decreased expression of Nogo, increased mitochondrial calcium levels, restoration of the activity of critical metabolic enzymes, decreased ΔΨm and increased mROS, mimicking the genetic deletion of Nogo[12] (Figure 3-17). These agents reduced proliferation and induced apoptosis, in vivo and in vitro, reversing and preventing the pulmonary vascular remodeling of PHT.

Hypoxia, viruses or loss-of-function mutations can cause ER stress and can activate the unfolded protein response (UPR)[8]. There are three arms of the UPR: inositol requiring enzyme-1 (IRE1), protein kinase ER-like kinase (PERK) and ATF6[32]. While the PERK pathway is generally pro-apoptotic, activating

transcription factors like CHOP, the ATF6 response is typically associated with anti-apoptotic and pro-survival signaling[33-35]. The pro-survival response is designed to transiently suppress apoptosis to allow cellular repair and normalization of protein trafficking during stress. We had previously postulated that a very fast and efficient manner to achieve this would be to inactivate mitochondria, major inducers of apoptosis[12]. Since mitochondria are dependent on ER for calcium supply, disruption of the strategically arranged "mitochondria-ER unit" by reshaping the ER upon Nogo induction can achieve this goal. Indeed, PASMCs from *Nogo*^{-/-} mice fail to show ER-mitochondrial disruption, any tested indices of mitochondrial suppression, or a proliferative/anti-apoptotic phenotype upon hypoxic exposure and *Nogo*^{+/-} and [-/-] mice are resistant to CH-PHT in a gene-dose-dependent manner. Moreover, adenoviral delivery of *Nogo* results in hyperpolarized $\Delta\Psi$m and decreased mROS[12]. Thus, although in the short term this ER-stress-induced mitochondrial suppression can protect from apoptosis, the signaling changes that follow downstream promote a state of proliferation and apoptosis resistance that, if sustained, may lead to vascular remodeling and PAH.

The relative contribution of the pro-apoptosis versus pro-survival ER stress pathway is complex, incompletely understood and may depend on the degree and duration of ER-stress as well as be cell-type specific[32]. In keeping with this, exposure of PASMCs to a severe and non-physiological ER-stress stimulus, thapsigargin, caused greater ATF6 activation (Figure 4B) and GRP78 upregulation (Supplement Figure 8), but also activated of the pro-apoptotic ER-stress response (Supplement Figure 8), in contrast to hypoxia. Under the mild stress of physiologic hypoxia (i.e. pO_2~40mmHg), the ATF6 activation may be favored in the pulmonary circulation, which is generally under more oxidized conditions (due to exposure to much higher oxygen levels and baseline mROS levels, compared to systemic vessels)[12, 17]. This is because, compared to the other ER stress sensors, ATF6 is redox-sensitive and has a lower activation threshold under a shift toward more reduced conditions (hypoxia, decreased mROS)[26]. Thus, the relatively mild ER-stress caused by hypoxia (CH-PHT) or inflammation (MCT-PHT), coupled with an overall loss of oxidative signals resulting from

mitochondrial suppression may promote ATF6 activation over the other ER-stress pathways in the pulmonary circulation.

The reversal of ER-stress-induced ATF6 signaling with chemical chaperones could be a potentially attractive therapeutic strategy because it satisfies many of the current therapeutic challenges in PAH: a) it inhibits a pathway potentially common to several, but perhaps not all, PAH pathologies; b) it is effective in decreasing proliferation as well as inducing apoptosis; and c) it is relatively specific to the pulmonary circulation. Obviously, such a strategy may logically have short-term adverse effects since it may remove the beneficial survival response designed to protect against a serious stress. Although we did not observe any gross adverse effects in the treated healthy animals, the possibility remains that if these animals were exposed to another stressor, they might be less able to defend to the cellular stress acutely. On the other hand, *Nogo*^{-/-} mice have a normal development and phenotype[12]. Furthermore, there is ample published experience with these types of agents in humans.

Chemical chaperones are currently being explored therapeutically in a variety of ER-stress associated conditions[19]. In humans, they have been investigated in patients with cystic fibrosis[36, 37], β-thalassemia[38], spinal muscular atrophy[39], ornithine transcarbamylase deficiency[40], primary biliary cirrhosis[41, 42], and cancer[43]. Dosing in clinical trials, ranging up to 600mg/kg/day in children[40], is consistent with the ~500 mg/kg/day dose in our studies. At these doses, PBA is well tolerated with minimal toxicities[36-39, 41]. In our in vitro studies, our PBA dose (2mM) is also comparable to the low millimolar PBA plasma concentrations reported in treated humans[36, 43]. In addition to these clinical research trials, PBA and TUDCA are both FDA-approved for urea cycle and cholestatic liver disorders, respectively[19]. The extensive clinical investigations with these agents make a rapid translation to PAH patients possible.

BMPRII receptor mutations occur in 75% of sporadic and 20% of familial PAH cases[1] and restoration of BMPRII signaling remains an intense area of PAH research. These loss-of-function mutations often result in protein misfolding, aggregation, abnormal trafficking and ER stress. PBA, at a dose similar to the one

used here, restores BMPRII trafficking in HeLa cells transfected with a human disease-causing BMPRII mutant (mutated at a cysteine residue, thus affecting sulfide bonding/protein folding, causing ER accumulation)[9]. PBA enhanced plasma membrane transport and Smad signaling in the mutant-expressing cells. The ability of PBA to restore BMPRII signaling resulting from mutation-dependent trafficking deficits further supports the use of these agents as a PAH therapy.

Our study has limitations. While it is believed that the structural features of PBA are conducive to chaperone activity, PBA also has histone deacetylase inhibitor (HDACi) properties[19]. Indeed, HDACi's have demonstrated anti-proliferative and pro-apoptotic characteristics in cancer, and thus may contribute to the beneficial effects reported herein. However, PBA (20mM), a 10-fold higher dose than our in vitro studies, inhibits HDAC activity by only ~25%[44], suggesting that PBA has relatively weak HDACi activity. Moreover, a second chemical chaperone, TUDCA, which to the best of our knowledge lacks HDACi activity, had effects similar to PBA (Figures 5 and 6), further suggesting the beneficial effects are HDACi-independent.

In this study, we focus on the PASMC and do not address potential direct effects of these agents on PA endothelial cells (PAECs), which contribute to plexiform lesions and the vascular remodeling in PAH patients. Nevertheless in our in vivo models, the proliferation and apoptosis indicators were not localized in PAECs suggesting that (at least at the late stage of disease in which we studied these lungs) effects of PAECs do not contribute significantly to the beneficial effects of these drugs. Recent work has suggested that human PAH-PAECs are proliferative and share a very similar mitochondrial suppression with PAH-PASMCs[16]; thus we speculate that a similar mechanisms could be involved but more studies are needed. In addition, our studies did not directly address potential effects of these drugs on the right ventricle. However, PBA-treated animals had improved cardiac output and performance on the treadmill test, consistent with improved cardiac function.

Although ER stress has not been definitively linked with all known triggers of PAH, this work along with our recent published work[12], strengthens the evolving metabolic theory of PAH[13-15] and links two fundamental cellular processes -ER stress and mitochondrial biology- potentially opening new avenues for therapies. The increase in PDH activity with PBA is also compatible with the beneficial pro-apoptotic effects of dichloroacetate, a PDH activator that prevents and reverses several PAH models[13-15, 45]. Like dichloroacetate, PBA promotes mitochondria-dependent apoptosis (marked by $\Delta\Psi$m depolarization and increase in mROS) without activating the ER stress dependent apoptotic pathway, as shown by the fact that PBA does not increase CHOP levels (Supplement Figures 6 and 9). It is intriguing that these chemical chaperones are also considered for the treatment of diabetes[46], while evidence for a generalized insulin-resistant-like abnormality in PAH is accumulating[47]. Lastly, it is satisfying to eventually attempt to translate important observations made by Dr. Heath in his classic description of PAH pathology more than 30 years ago [11].

Materials and Methods

Animals: All experiments were performed with approval by the University of Alberta committee on animal policy and welfare. Male C57BL/6 and Sprague Dawley rats were purchased from Charles River. The mice were randomized to normobaric hypoxia (10% O_2) or room air, and rats were randomized to injection of saline or monocrotaline (60mg/kg) as previously described[15, 30]. Animals were further randomized to receive PBA in either a prevention (PBA starting the day of pulmonary hypertension (PHT) induction, onward for 4 weeks) or a reversal (on the third week of PHT induction, onward for 2 weeks) protocol in their drinking water. By measuring water consumption and animal weights, we determined that mice and rats received an average dose of ~500mg/kg/day.

Echocardiography and Hemodynamics: Cardiac output was assessed on isoflurane-anesthetized animals by echocardiography using the Vevo770 imaging system with the 707B (30MHz) and 716 (15MHz) probes for mice and rats, respectively. The cardiac output was calculated after determining the left

ventricular outflow tract diameter (LVOT), aortic velocity time integral (AoVTI), and heart rate (HR) using the formula:

$$CO = 7.85 \times LVOT^2 \times AoVTI \times HR / 1000$$

Pulmonary Artery Acceleration Time (PAAT) was measured by echocardiograpy as previously described[12, 15, 30]. Total pulmonary resistance was calculated by the mPAP/CO ratio. Mean pulmonary artery pressures were assessed in closed-chest animals with Millar catheters (Millar Instruments Inc., Huston, TX) as previously described[12, 15, 30]. Under inhaled isoflurane anesthesia, the right jugular vein was cannulated and the catheter advanced into the pulmonary arteries. Pressures from the right atrium, right ventricle and pulmonary arteries were recorded continuously and mean PAP was calculated electronically (Power Lab, with Chart software 5.4, ADInstruments).

Treadmill test: Animals were placed on a calibrated, motor-driven treadmill (Treadmill Simplex II, Columbus Instruments) and run once a week (3 times total) on a non-demanding protocol to allow familiarization of the test. Afterwards animals from each therapy group were run until failure with the following protocol: 3 min at 10m/min, 3 min at 12m/min, 20 min at 14m/min, 20 min at 16m/min, and 18m/min until failure. Failure was defined as >5 consecutive seconds on the shocker grid and the test was terminated.

Blood Pressure: Blood pressure was measured using an iiTC blood pressure apparatus (Life sciences, Woodland Hills, CA) for mice and rats. Animals were restrained in warming chambers (34°C) and a tail cuff was placed at the base of the tail. Systolic and Diastolic blood pressures for each animal were obtained in triplicate and averaged.

Medial Wall Thickness: The percent medial wall thickness was determined as previously described[12, 15, 30]. Briefly, 5μm thick lung sections were stained using hematoxylin and eosin (H&E) stain. Vessels >50μm were identified and measured at the two ends of the shortest external diameter of the distal PAs, and the average was taken ([2 x wall thickness/external diameter] x 100).

Muscularization: Lung sections (5μm) were stained for smooth muscle actin and von Willebrand Factor (endothelial cell maker). Vessels (<50μm) were classified as fully (100%), partially, or non-muscularized (0%), based on the percentage of vWF surrounded by SMA in each vessel.

Cell Culture: PASMCs from five C57BL/6 mice were freshly isolated from third generation pulmonary arteries, with an enzymatic cocktail containing papain (1mg/ml), dithiothreitol (0.5mg/ml), collagenase (0.6 mg/ml), and bovine serum albumin (0.6 mg/ml) (Sigma-Aldrich, St. Louis, MO) and pooled as previously described [12, 15]. PASMCs were grown in Dulbecco's modified Eagle's medium (DMEM) supplemented with 10% fetal bovine serum (FBS) and 1% antibiotic/antimycotic (Gibco, Invitrogen, Burlington, ON) and placed in a humidified incubator set at 37°C in either normoxic conditions (21% O_2; pO_2~120mmHg) or hypoxic conditions (4% O_2; pO_2~40mmHg) with 4-phenylbutyric acid (2mM; Sigma-Aldrich, St. Louis, MO), tauroursodeoxycholic acid (1mM; Calbiochem, San Diego, CA) and thapsigargin (400nM; Sigma-Aldrich, St. Louis, MO) for 48 hours. For apoptosis/proliferation experiments, cells were exposed to normoxia/hypoxia for 48 hours prior to drug treatment. Cells of passage ≤6 were used.

Confocal Microscopy: Immunofluorescence imaging was performed on a Ziess LSM 510 confocal microscope (Carl Zeiss, Toronto, ON) as previously described [12, 15, 30]. ApopTag apoptosis detection kit (Serotologicals, Norcross, GA) and Ki67 antibody (1:100, Abcam, Cambridge, MA) were used as previously described [15]. ATF6 and GRP78 (1:100; Santa Cruz Biotechnologies, Santa Cruz, CA), CHOP (1:100, Cell Signaling, Danvers, MA), tetramethylrhodamine methyl ester (TMRM 10nM; Invitrogen, Burlington, ON), MitoSOX (5μM; Invitrogen, Burlington, ON), and Rhodamine 2AM (5μM; Invitrogen, Burlington, ON) were used as previously described [12, 15, 30]. Fluorescein isothiocyanate (FITC 1:1000; Invitrogen, Burlington, ON), tetramethylrhodamine isothiocyanate (TRITC 1:50 Dako, CA), Far Red (1:1000; Invitrogen, Burlington, ON) and Zenon kit (Invitrogen, Burlington, ON) secondary antibodies were used as previously described [12, 15, 30].

PDH Activity: PDH activity was measured with a commercially available MitoProfile Dipstick assay kit (Mitosciences, Eugene, OR) as previously described [12]. Briefly, 50μL of protein (1mg/ml) was incubated with a dipstick containing the PDH complex antibody in a 96 well plate, followed by activity buffer. A flat top scanner was used to measure the band intensity.

Alpha-ketoglutarate assay: αKG levels were measured with a commercially available spectrophotometric αKG assay kit (BioVision, Milpitas, CA), as previously described [12, 48]. PASMCs were grown, harvested, lysed, and a protein concentration was obtained to normalize between wells. Optical density at 570nm was measured after the kit-based reaction occurred.

Immunoblot: Tissues were collected and immunoblotting was performed as previously described [12, 15, 30]. The films were digitized and quantified with 1D Image Analysis Software (Kodak, Rochester, NY). Expression was normalized to α-actin to correct for loading differences. Antibodies: ATF6 (1:1000; Imgenex, San Diego, CA), GRP78 (1:200; Santa Cruz Biotechnologies, Santa Cruz, CA), Nogo (1:10000; previously described and characterized [49]), CHOP (1:1000, Cell Signaling, Danvers, MA) and α-actin (1:400; Abcam, Cambridge, MA).

ATF6 luciferase: PASMCs (20,000 cells/well) were seeded into a 96 well plate and allowed to adhere. Cells were transfected with the ATF6 dual luciferase plasmid (SABiosciences, Mississauga, ON) using a Xfect transfection reagent (Clontech, Mountain View, CA) under normoxic conditions. After 24 hours, media was replaced with treatment media and cells were placed in normoxia or hypoxia. ATF6 activity was assessed with the dual-luciferase reporter assay system (Promega, Madison, WI). After 48 hours, cells were lysed by a freeze-thaw cycle in passive lysis buffer (provided in kit) and luminescence was measured with an illuminometer. ATF6 activity was assessed by ATF6-driven firefly luminescence normalized to a constitutively-driven Renilla luminescence to standardize the transfection as previously described [12].

FRET analysis: PASMCs were plated on glass dishes and transfected with the 4mtD3CPV cameleon plasmid using a Xfect transfection reagent (Clontech, Mountain View, CA) under normoxic conditions. After 24 hours, media was

replaced with treatment media and placed in normoxia or hypoxia. After 48 hours, media was diluted with 4% paraformaldehyde in a 1:1 ratio and cells were fixed under treatment conditions for 60 minutes. The mitochondrial calcium uniporter (MCU) inhibitor ruthenium red (10μM, Calbiochem, San Diego, CA) was incubated in a separate dish for 3 hours prior to fixation to ensure sensitivity. Cells were washed with distilled water and mounted on a slide using Prolong Gold (Invitrogen, Burlington, ON) and imaged 48 hours later on a Zeiss LSM 510 confocal microscope. Excitation occurred at 458 nm and the emission filters were 480 to 520 nm for cyan (when Ca^{2+} is not bound) and 535 to 590 nm for FRET (yellow when Ca^{2+} is bound). The ratio of yellow/cyan intensities was used to standardize the rate of infection for each cell, as previously described [12].

Statistics: All values are expressed as mean±SEM unless otherwise stated. For in vitro analysis, differences between groups were assessed by either student's t-test or one-way analysis of variance (ANOVA) using Tukey's post hoc analysis as a appropriate. Normality of our in vivo data was assessed by the Shapiro-Wilk normality test. Inter-group differences for in vivo experiments were assessed by either ANOVA using Fisher's least significant differences post hoc analysis or Kruskal-Wallis with a Mann-Whitney U test as appropriate. Vessels from the same animal were assumed to be independent for purposes of analysis. All analyses were performed using SPSS 19 (IBM Corp., Armonk, NY). Significance was defined as p≤0.05.
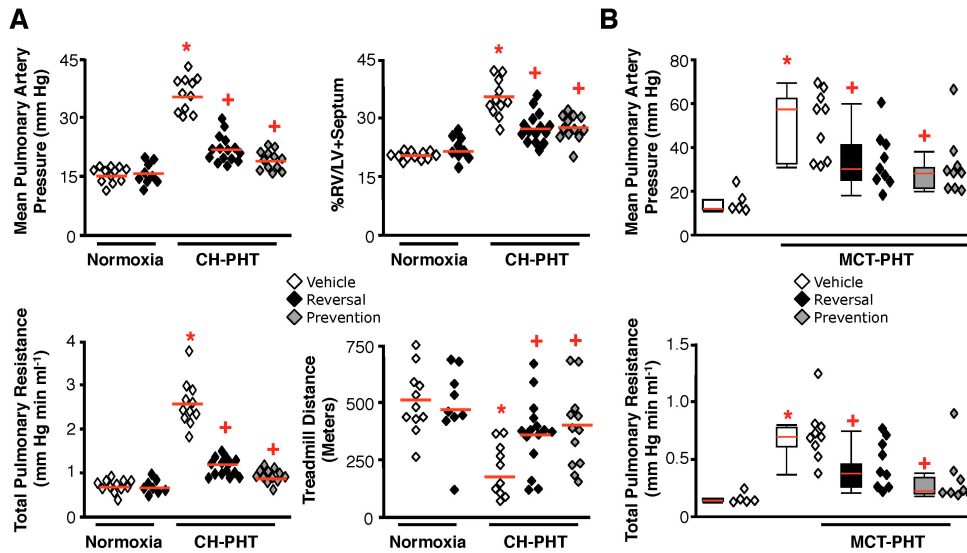
Figure 3-1. PBA prevents and reverses chronic hypoxia- and monocrotaline-induced PHT. A. Chronic hypoxic mice treated with PBA had lower mPAP (top left), total pulmonary resistance (bottom left), decreased RV/LV+septum (top right), and improved treadmill running distance (bottom right) compared to vehicle-treated mice (n=9-15 mice/group; *p<0.05 vs. normoxic vehicle, +p<0.05 vs. hypoxic vehicle. Red lines represent mean values). PBA had no effects on normoxic mice. **B.** Monocrotaline rats treated with PBA had lower mPAP (top) and total pulmonary resistance (bottom) compared to vehicle-treated rats (n=5-12 rats/group; *p<0.05, vs. sham vehicle, +p<0.05 vs. monocrotaline vehicle. In contrast to the CH-PHT, normality was not confirmed, and therefore, the MCT-PHT data are shown with box plots, with red lines representing median values. Each point represents one animal.
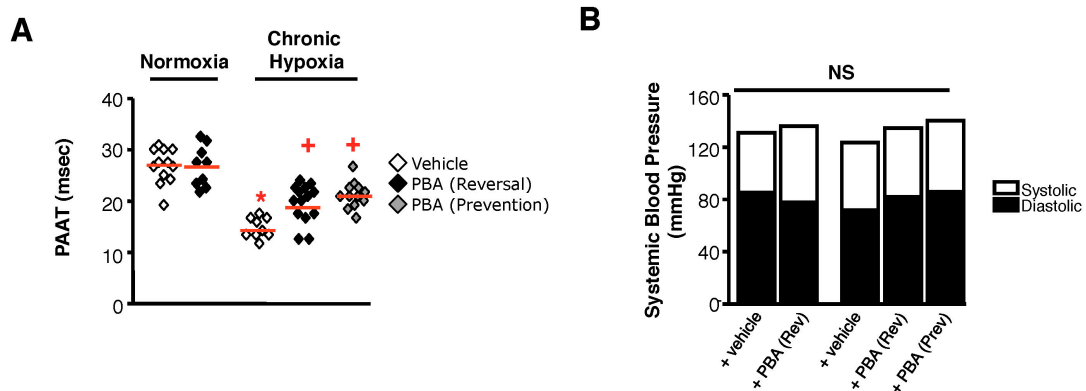
Figure 3-2. PBA prevents and reverses chronic hypoxia-induced reduction in PAAT without affecting systemic hemodynamics. **A.** Chronic hypoxic mice treated with PBA have lower pulmonary artery acceleration time (PAAT) compared to vehicle treated hypoxic mice (n=9-15 mice/group; *p<0.05 vs. normoxia vehicle, +p<0.05 vs. hypoxic vehicle using one-way ANOVA with Fisher's least difference post-hoc. Red lines represent mean values). **B.** Systolic or diastolic systemic blood pressure was not significantly different between any of the groups (p = 0.12 and 0.51 for systolic and diastolic blood pressures, respectively, using one-way ANOVA).

90
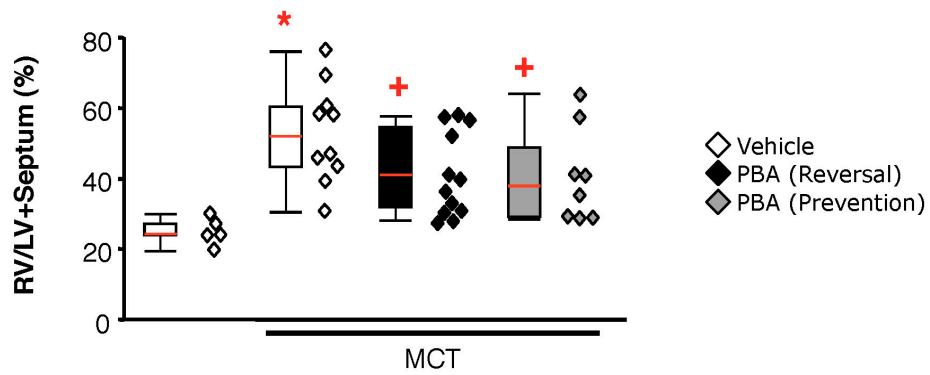
Figure 3-3. **PBA prevents and reverses RV hypertrophy in monocrotaline-induced PHT.** Monocrotaline rats treated with PBA (300-500mg/kg/day) had lower RV/LV+Septum (n=5-12 rats/group; *p≤0.05, vs. sham vehicle, +p≤0.05 vs. monocrotaline vehicle using Kruskal-Wallace with Mann-Whitney U test to compare inter-group differences. Red lines represent the median value). Each point represents one animal.
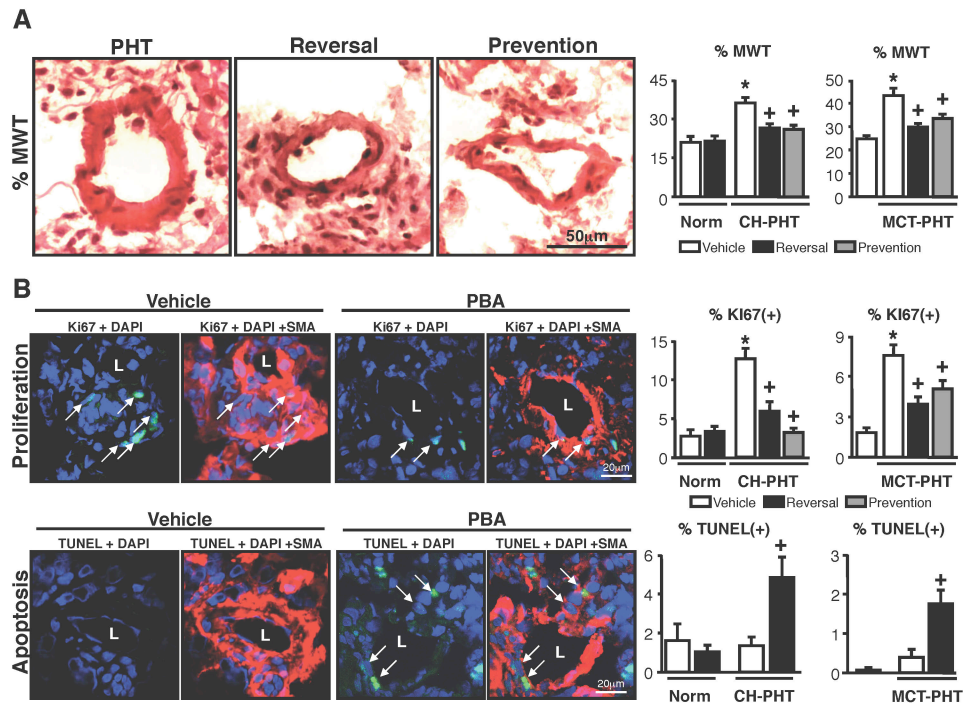
Figure 3-4. PBA prevents and reverses pulmonary vascular remodeling, attenuates proliferation and induces apoptosis in PAs in animal PHT models. **A**. PBA in prevention and reversal protocols reduces the percent medial wall thickness in the resistance PA's (50-100μm diameter) in both the chronic hypoxic (left) and monocrotaline (right) models of PHT. Images show H&E stained resistance PA's from vehicle and PBA treated animals. (n~20 vessels/animal, 5 animals/group; p<0.05). **B.** PBA in prevention and reversal protocols reduces cell proliferation (Ki67+ nuclei) in the resistance SMA+ PASMCs (50-100μm diameter vessels). PBA in a reversal protocol induces apoptosis (TUNEL+ nuclei) in the resistance SMA+ PASMCs. Confocal images show resistance PAs from a vehicle and PBA treated PHT-animal stained with both Ki67 (green, top) and TUNEL (green, bottom) positive nuclei (blue) (left) and merged with SMA (red) (right). (n~10 vessels/mouse and n~20 vessels/rat, 5 animals/group; *p<0.05).
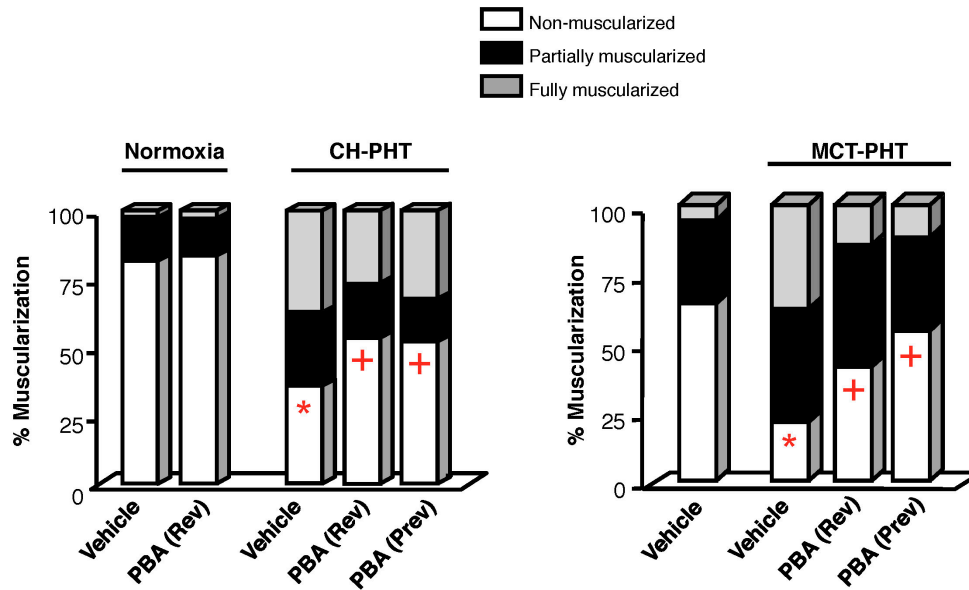
Figure 3-5. **PBA prevents and reverses chronic hypoxia- and monocrotaline-induced muscularization.** PBA in prevention and reversal protocols reduces muscularization of capillary vessels (<50μm diameter) in both the chronic hypoxic (left) and monocrotaline (right) models of PAH (n~20 vessels/animal, 5 animals *p≤0.05, vs. healthy + vehicle, +p≤0.05 vs. PHT + vehicle).
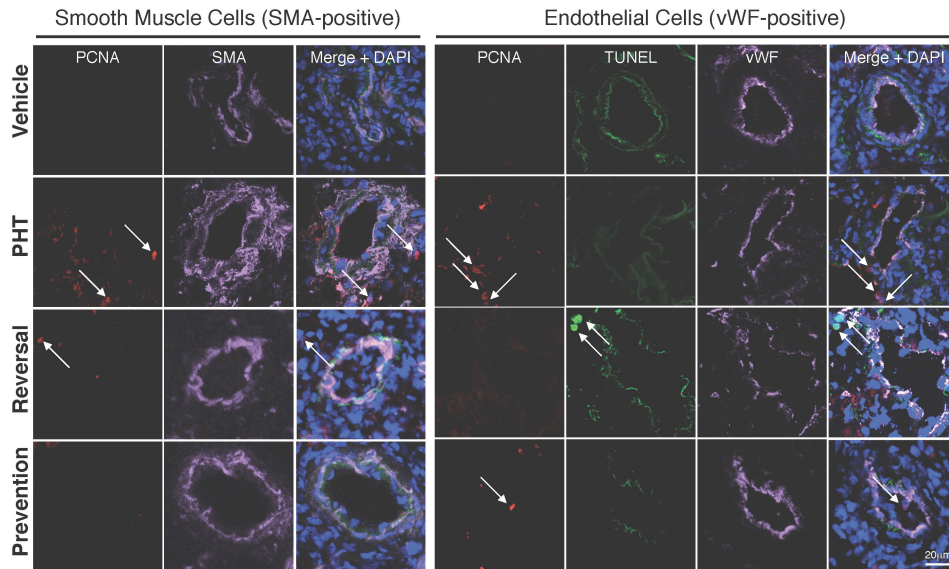
Figure 3-6. **PBA does not influence proliferation or apoptosis in endothelial cells.** Proliferating markers (proliferating cell nuclear antigen; PCNA; red) colocalize with SMA-positive (purple, left), but not vWF-positive (purple, right), cells in PHT distal PAs. PBA does not induce apoptosis (TUNEL, green, right) in vWF-positive cells in either the prevention or reversal protocols.
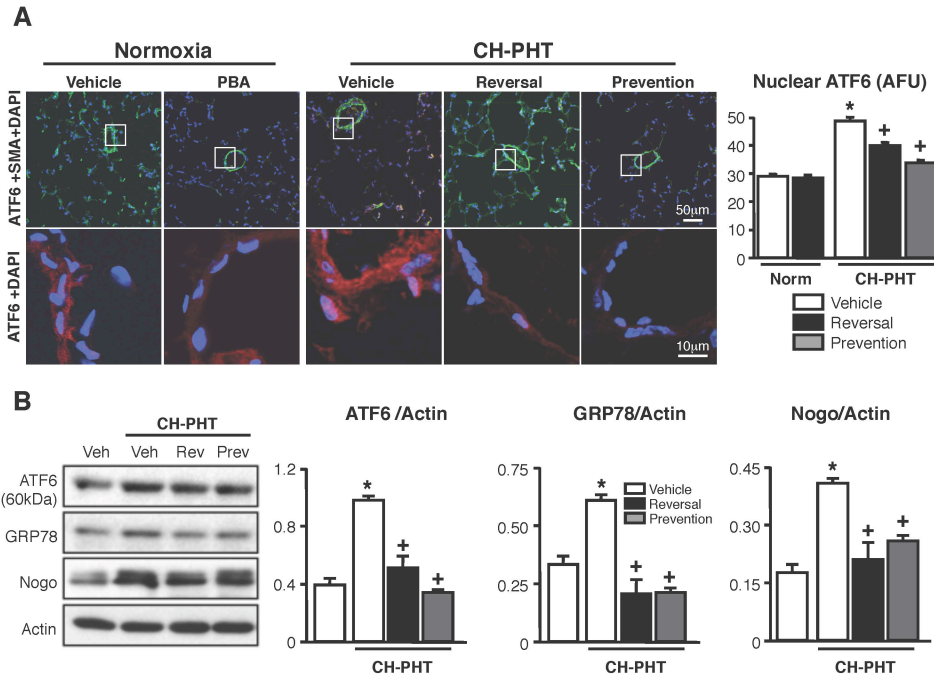
Figure 3-7. PBA reduces ER stress in vivo. A. PBA in prevention and reversal protocols reduces hypoxia-induced ATF6 cleavage in the resistance PA SMA+ cells (50-100µm diameter vessels) as assessed by nuclear ATF6 levels with immunofluorescence and confocal microscopy. Top: low magnification showing SMA (green), ATF6 (red) and nuclei (blue); bottom: high magnification of boxed region showing ATF6 (red) and nuclei (blue) (n~10 vessels/mouse 3-4 mice/group; *p<0.05 vs. normoxia vehicle, +p<0.05 vs. hypoxic vehicle). PBA did not affect ATF6 cleavage in the resistance PA SMA+ cells in normoxic mice. **B.** PBA in prevention and reversal protocols reduces ATF6 cleavage and GRP78 and Nogo protein expression in isolated PAs of CH-PHT mice. (Mean data obtained from blot of n=5 mice per group; *p<0.05 vs. normoxia vehicle, +p<0.05 vs. hypoxic vehicle).
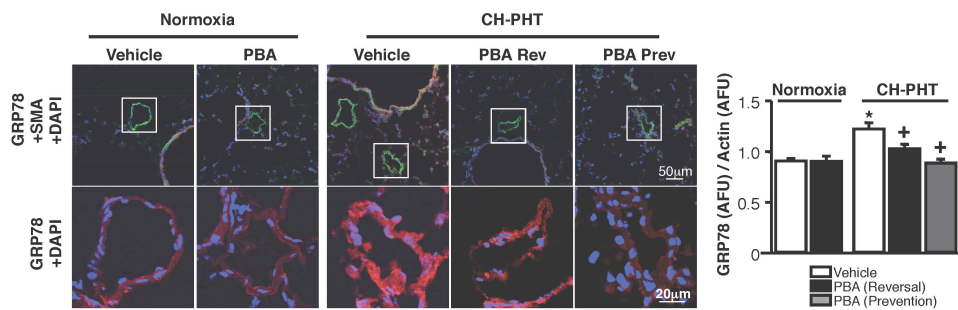
Figure 3-8. PBA reduces GRP78 expression in resistance PAs. PBA in prevention and reversal protocols reduces expression of GRP78 in the resistance SMA+ PASMCs (50-100μm diameter vessels) as assessed by immunofluorescence and confocal microscopy on whole lung tissue. Top: low magnification showing SMA (green), GRP78 (red) and nuclei (blue); bottom: high magnification of boxed region showing GRP78 (red) and nuclei (blue) (n~10 vessels/mouse 4-5 animals/group; *$p<0.05$ vs. normoxia vehicle, +$p<0.05$ vs. hypoxic vehicle). PBA did not effect expression resistance SMA+ PASMCs from normoxic mice.
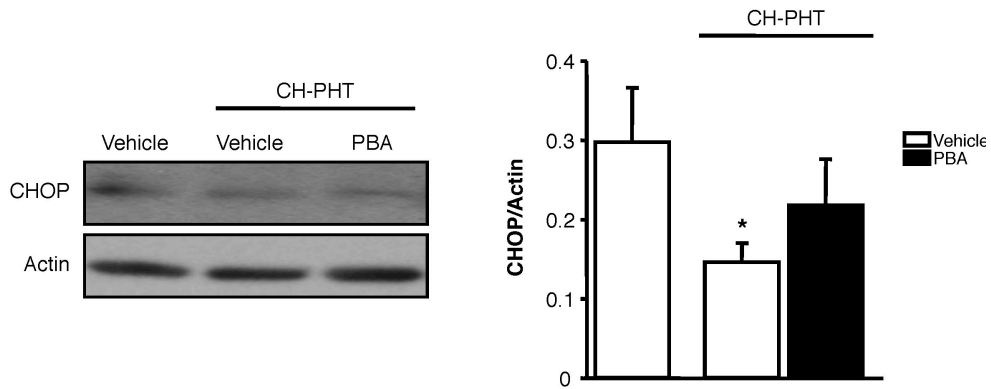
Figure 3-9. PBA does not induce CHOP expression in vivo. CHOP expression is decreased in the PAs of CH-PHT animals. Treatment with PBA does not significantly effect CHOP expression. (*p<0.05 vs. Vehicle using Kruskall-Wallace test with Mann-Whitney U test).
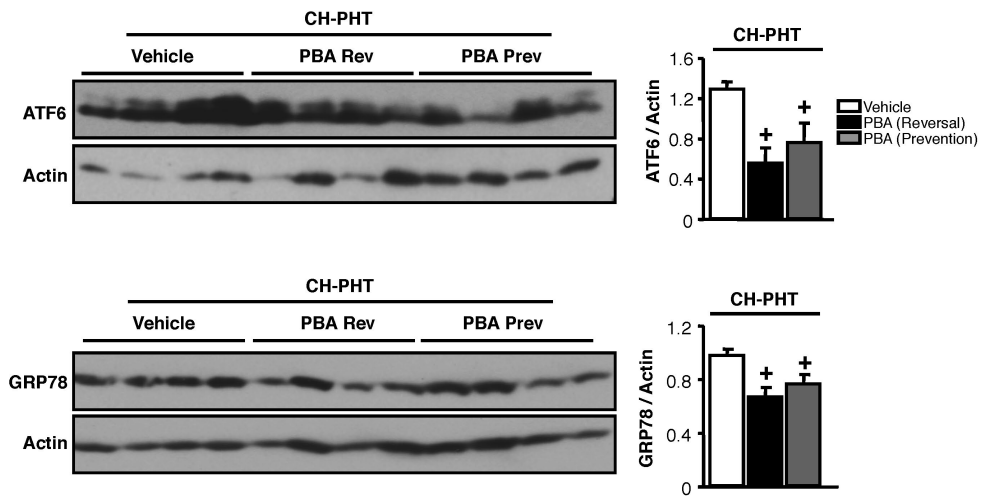
Figure 3-10. PBA reduces ATF6 and GRP78 expression in chronic hypoxia-induced PHT. PBA in prevention and reversal protocols reduces hypoxia-induced ATF6 cleavage (top) and expression of downstream target GRP78 (bottom) as assessed by immunoblot on whole lung tissue. Actin was used as a loading control (each lane represents one animal; $p < 0.05$ using Kruskall-Wallace test with Mann-Whitney U test to compare each treatment to vehicle).
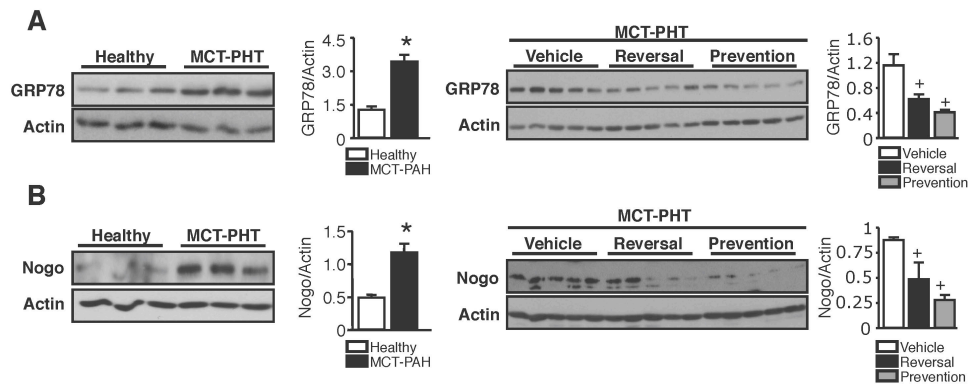
Figure 3-11. PBA reduces GRP78 and Nogo expression in monocrotaline-induced PHT. A. Immunoblot showing increased GRP78 expression in MCT-PHT compared to healthy controls (left) and reduced expression of GRP78 in whole lung tissue in monocrotaline rats treated with PBA in prevention and reversal protocols (right). **B.** Immunoblot showing increased Nogo expression in MCT-PHT compared to healthy controls (left) and reduced expression Nogo in whole lung tissue in monocrotaline rats treated with PBA in prevention and reversal protocols. Actin was used as a loading control (each lane represents one animal; $p<0.05$ using Kruskall-Wallace test with Mann-Whitney U test to compare healthy to MCT-PHT and each treatment to vehicle).
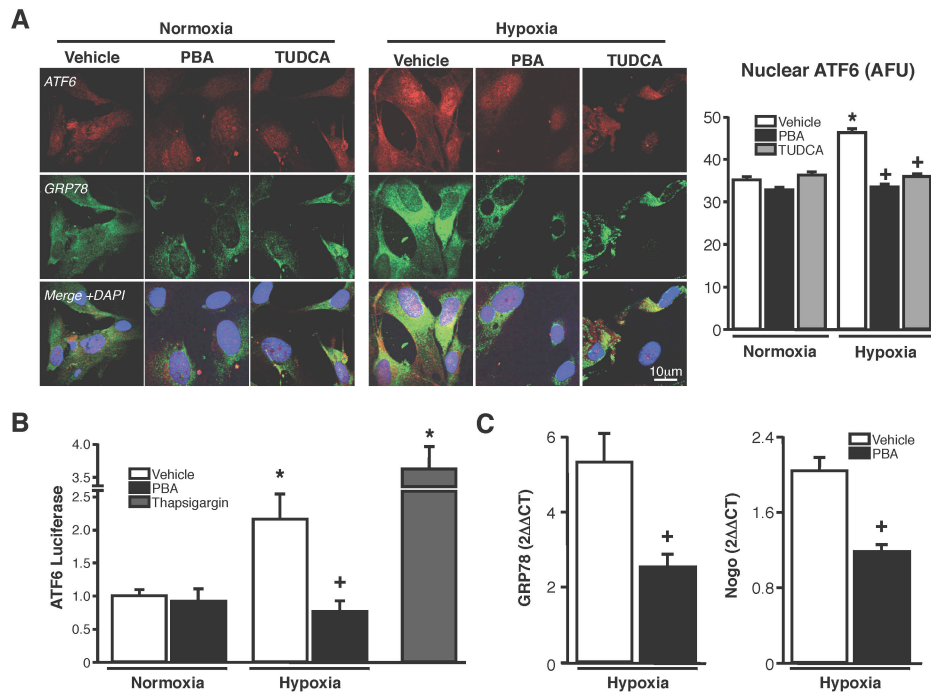
Figure 3-12. PBA reduces ATF6 activation in PASMCs in vitro. A. PBA (2mM) and TUDCA (1mM) block hypoxia-induced ATF6 cleavage assessed by nuclear ATF6 localization (red colocalizing with blue nuclei) without affecting normoxic cells, as assessed by immunofluorescence and confocal microscopy. Cytoplasmic expression of GRP78 (green) was also decreased by PBA or TUDCA in hypoxia, but not normoxia (n=50 cells/experiment, 3 experiments; *$p<0.05$ vs. normoxia vehicle, +$p<0.05$ vs. hypoxia vehicle). **B.** PBA (2mM) blocks hypoxia-induced ATF6 transcriptional activity assessed by an ATF6-driven dual reporter luciferase assay. Hypoxia induced ATF6 activation to a lesser extent than thapsigargin. PBA has no effect on normoxic PASMCs (n=18 wells/group; *$p<0.05$ vs. normoxia vehicle, +$p<0.05$ vs. hypoxia). **C.** PBA (2mM) reduces expression of the ATF6 target genes GRP78 (left) and Nogo (right) in hypoxic PASMCs. (n=5, +$p<0.05$ vs. hypoxia vehicle).

100
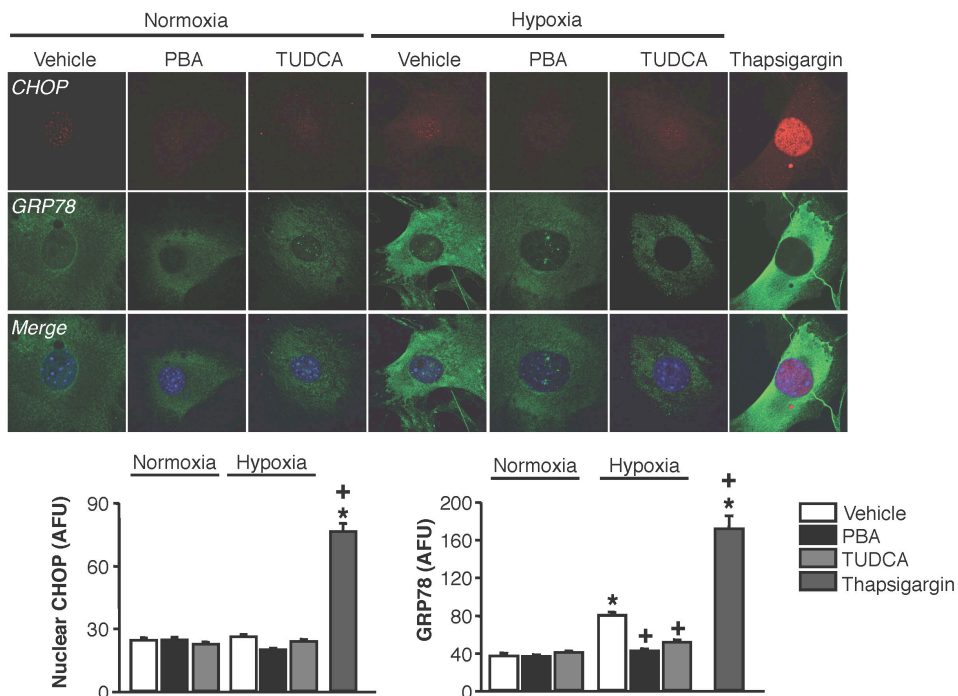
Figure 3-13. Differential regulation of ER-stress pathways by hypoxia.
Hypoxia activates GRP78, but not nuclear (activated) CHOP, in PASMCs
assessed by immunofluorescence and confocal microscopy. PBA and TUDCA
reduce GRP78 in hypoxic PASMCs without affecting CHOP activation (n~50
cells/group; $*p<0.05$ vs. normoxia vehicle, $+p<0.05$ vs. hypoxia vehicle using
one-way ANOVA with Tukey's post hoc analysis).
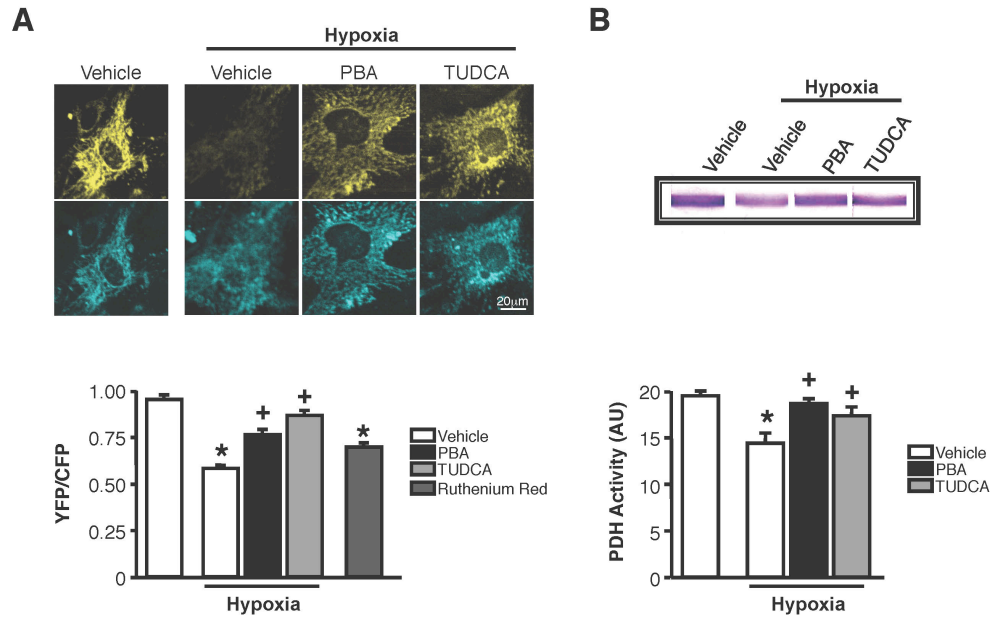
Figure 3-14. PBA prevents the hypoxia-induced decrease in PASMC mitochondrial calcium. **A.** PBA (2mM) and TUDCA (1mM) maintain mitochondrial calcium in hypoxia assessed by the fluorescence ratio of bound mitochondrial Ca^{2+} [yellow fluorescent protein (YFP) signal, yellow] to unbound mitochondrial Ca^{2+} [cyan fluorescent protein (CFP) signal, cyan] measured with fluorescence resonance energy transfer (FRET) imaging and confocal microscopy (n=30 cells/group/experiment, n=3 experiments; *$p<0.05$ vs. normoxia vehicle, +$p<0.05$ vs. hypoxia vehicle). **B.** PBA (2mM) and TUDCA (1mM) maintain activity of the mitochondrial, calcium-sensitive enzyme PDH in hypoxia (n=6/group; *$p<0.05$ vs. normoxia vehicle, +$p<0.05$ vs. hypoxia vehicle).
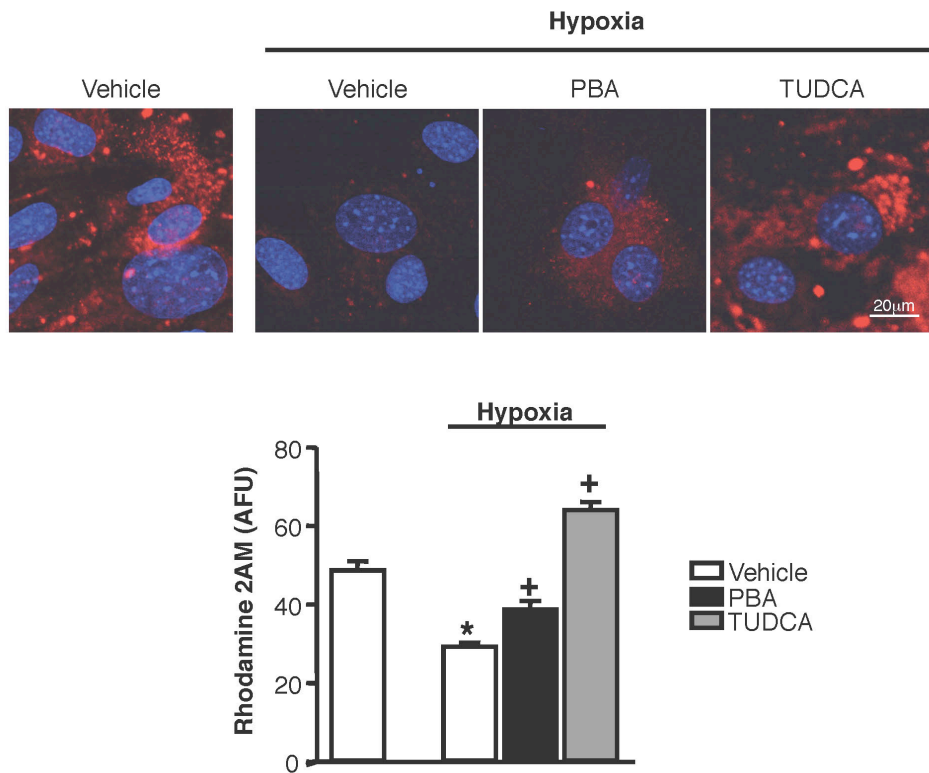
Figure 3-15. **PBA prevents decreases in mitochondrial calcium in hypoxia.** PBA (2mM) and TUDCA (1mM) maintain mitochondrial calcium in hypoxia assessed by Rhodamine 2AM and confocal microscopy (n~50 cells/group/experiment, n=4 experiments; *p<0.05 vs. normoxia vehicle, +p<0.05 vs. hypoxia vehicle using one-way ANOVA with Tukey's post hoc analysis).
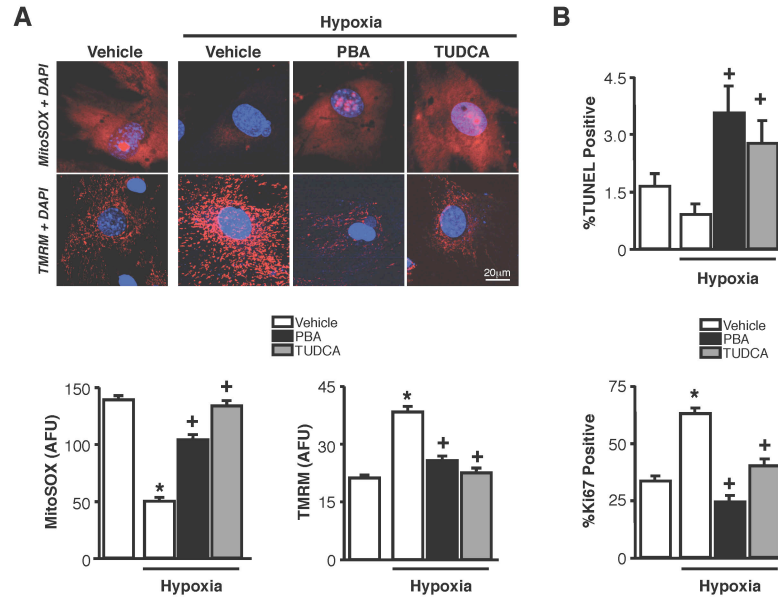
Figure 3-16. PBA prevents the hypoxia-induced decrease in mitochondrial function, induces apoptosis and reduces proliferation in PASMCs. A. PBA (2mM) and TUDCA (1mM) maintain mitochondrial- ROS (top) and ΔΨm (bottom) in hypoxic PASMCs as assessed by MitoSOX (red, top) and TMRM (red, bottom), respectively. Nuclei are shown in blue (n~50 cells/group/experiment, n=3 experiments; *$p<0.05$ vs. normoxia vehicle, +$p<0.05$ vs. hypoxia vehicle). **B.** PBA (2mM) and TUDCA (1mM) increase apoptosis as assessed by percent TUNEL-positive nuclei (top) and reduce proliferation as assessed by percent Ki67-positive nuclei (bottom) in hypoxic PASMCs (n~50 fields/group from 3 experiments; *$p<0.05$ vs. normoxia vehicle, +$p<0.05$ vs. hypoxia vehicle).
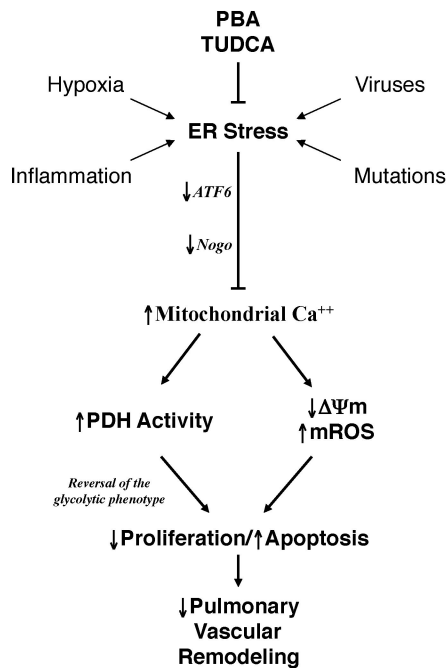
Figure 3-17. Chemical chaperones like PBA and TUDCA reverse pulmonary vascular remodeling by attenuating the ER stress response in PASMCs. PBA and TUDCA block the ER stress response induced by a variety of PAH-associated stimuli including hypoxia, inflammation, viruses and mutations. This results in maintenance of mitochondrial calcium, PDH activity, mitochondrial-derived ROS and ΔΨm, through a mechanism that likely involves inhibition of ATF6 and Nogo upregulation. This inhibits the cancer-like metabolic remodeling in PAH (i.e. suppression of mitochondrial function and a shift toward glycolysis) facilitating apoptosis and inhibiting proliferation. These combined effects contribute to the prevention and reversal of pulmonary vascular remodeling in PAH.

References

1. McLaughlin VV, Archer SL, Badesch DB, Barst RJ, Farber HW, Lindner JR, Mathier MA, McGoon MD, Park MH, Rosenson RS, Rubin LJ, Tapson VF, Varga J, Harrington RA, Anderson JL, Bates ER, Bridges CR, Eisenberg MJ, Ferrari VA, Grines CL, Hlatky MA, Jacobs AK, Kaul S, Lichtenberg RC, Moliterno DJ, Mukherjee D, Pohost GM, Schofield RS, Shubrooks SJ, Stein JH, Tracy CM, Weitz HH, Wesley DJ. ACCF/AHA 2009 expert consensus document on pulmonary hypertension: a report of the American College of Cardiology Foundation Task Force on Expert Consensus Documents and the American Heart Association: developed in collaboration with the American College of Chest Physicians, American Thoracic Society, Inc., and the Pulmonary Hypertension Association. *Circulation.* 2009; 119:2250-2294.

2. Macchia A, Marchioli R, Marfisi R, Scarano M, Levantesi G, Tavazzi L, Tognoni G. A meta-analysis of trials of pulmonary hypertension: a clinical condition looking for drugs and research methodology. *Am Heart J.* 2007; 153:1037-1047.

3. Macchia A, Marchioli R, Tognoni G, Scarano M, Marfisi R, Tavazzi L, Rich S. Systematic review of trials using vasodilators in pulmonary arterial hypertension: why a new approach is needed. *Am Heart J.* 2010; 159:245-257.

4. Michelakis ED, Wilkins MR, Rabinovitch M. Emerging concepts and translational priorities in pulmonary arterial hypertension. *Circulation.* 2008; 118:1486-1495.

5. Archer SL, Weir EK, Wilkins MR. Basic science of pulmonary arterial hypertension for clinicians: new concepts and experimental therapies. *Circulation.* 2010; 121:2045-2066.

6. Newman JH, Wheeler L, Lane KB, Loyd E, Gaddipati R, Phillips JA, 3rd, Loyd JE. Mutation in the gene for bone morphogenetic protein receptor II as a cause of primary pulmonary hypertension in a large kindred. *N Engl J Med.* 2001; 345:319-324.

7.   Dromparis P, Sutendra G, Michelakis ED. The role of mitochondria in pulmonary vascular remodeling. *J Mol Med (Berl).* 2010; 88:1003-1010.

8.   Xu C, Bailly-Maitre B, Reed JC. Endoplasmic reticulum stress: cell life and death decisions. *J Clin Invest.* 2005; 115:2656-2664.

9.   Sobolewski A, Rudarakanchana N, Upton PD, Yang J, Crilley TK, Trembath RC, Morrell NW. Failure of bone morphogenetic protein receptor trafficking in pulmonary arterial hypertension: potential for rescue. *Hum Mol Genet.* 2008; 17:3180-3190.

10.   Sehgal PB, Mukhopadhyay S. Dysfunctional intracellular trafficking in the pathobiology of pulmonary arterial hypertension. *Am J Respir Cell Mol Biol.* 2007; 37:31-37.

11.   Smith P, Heath D. Electron microscopy of the plexiform lesion. *Thorax.* 1979; 34:177-186.

12.   Sutendra G, Dromparis P, Wright P, Bonnet S, Haromy A, Hao Z, McMurtry MS, Michalak M, Vance JE, Sessa WC, Michelakis ED. The role of Nogo and the mitochondria-endoplasmic reticulum unit in pulmonary hypertension. *Sci Transl Med.* 2011; 3:88ra55.

13.   McMurtry MS, Bonnet S, Wu X, Dyck JR, Haromy A, Hashimoto K, Michelakis ED. Dichloroacetate prevents and reverses pulmonary hypertension by inducing pulmonary artery smooth muscle cell apoptosis. *Circ Res.* 2004; 95:830-840.

14.   Michelakis ED, McMurtry MS, Wu XC, Dyck JR, Moudgil R, Hopkins TA, Lopaschuk GD, Puttagunta L, Waite R, Archer SL. Dichloroacetate, a metabolic modulator, prevents and reverses chronic hypoxic pulmonary hypertension in rats: role of increased expression and activity of voltage-gated potassium channels. *Circulation.* 2002; 105:244-250.

15.   Sutendra G, Bonnet S, Rochefort G, Haromy A, Folmes KD, Lopaschuk GD, Dyck JR, Michelakis ED. Fatty acid oxidation and malonyl-CoA decarboxylase in the vascular remodeling of pulmonary hypertension. *Sci Transl Med.* 2010; 2:44ra58.

16. Xu W, Koeck T, Lara AR, Neumann D, DiFilippo FP, Koo M, Janocha AJ, Masri FA, Arroliga AC, Jennings C, Dweik RA, Tuder RM, Stuehr DJ, Erzurum SC. Alterations of cellular bioenergetics in pulmonary artery endothelial cells. *Proc Natl Acad Sci U S A*. 2007; 104:1342-1347.

17. Michelakis ED, Hampl V, Nsair A, Wu X, Harry G, Haromy A, Gurtu R, Archer SL. Diversity in mitochondrial function explains differences in vascular oxygen sensing. *Circ Res*. 2002; 90:1307-1315.

18. Haas MJ. Nogo could go far. *SciBx: Science-Business exchange*. 2011; 4:7-9.

19. Engin F, Hotamisligil GS. Restoring endoplasmic reticulum function by chemical chaperones: an emerging therapeutic approach for metabolic diseases. *Diabetes Obes Metab*. 2010; 12 Suppl 2:108-115.

20. Yam GH, Gaplovska-Kysela K, Zuber C, Roth J. Sodium 4-phenylbutyrate acts as a chemical chaperone on misfolded myocilin to rescue cells from endoplasmic reticulum stress and apoptosis. *Invest Ophthalmol Vis Sci*. 2007; 48:1683-1690.

21. Welch WJ, Brown CR. Influence of molecular and chemical chaperones on protein folding. *Cell Stress Chaperones*. 1996; 1:109-115.

22. DiGiuseppe JA, Weng LJ, Yu KH, Fu S, Kastan MB, Samid D, Gore SD. Phenylbutyrate-induced G1 arrest and apoptosis in myeloid leukemia cells: structure-function analysis. *Leukemia*. 1999; 13:1243-1253.

23. Carducci MA, Nelson JB, Chan-Tack KM, Ayyagari SR, Sweatt WH, Campbell PA, Nelson WG, Simons JW. Phenylbutyrate induces apoptosis in human prostate cancer and is more potent than phenylacetate. *Clin Cancer Res*. 1996; 2:379-387.

24. Melchior SW, Brown LG, Figg WD, Quinn JE, Santucci RA, Brunner J, Thuroff JW, Lange PH, Vessella RL. Effects of phenylbutyrate on proliferation and apoptosis in human prostate cancer cells in vitro and in vivo. *Int J Oncol*. 1999; 14:501-508.

25. Wilson DW, Segall HJ, Pan LC, Dunston SK. Progressive inflammatory and structural changes in the pulmonary vasculature of monocrotaline-treated rats. *Microvasc Res.* 1989; 38:57-80.

26. Nadanaka S, Okada T, Yoshida H, Mori K. Role of disulfide bridges formed in the luminal domain of ATF6 in sensing endoplasmic reticulum stress. *Mol Cell Biol.* 2007; 27:1027-1043.

27. Baumeister P, Luo S, Skarnes WC, Sui G, Seto E, Shi Y, Lee AS. Endoplasmic reticulum stress induction of the Grp78/BiP promoter: activating mechanisms mediated by YY1 and its interactive chromatin modifiers. *Mol Cell Biol.* 2005; 25:4529-4540.

28. Szanda G, Koncz P, Varnai P, Spat A. Mitochondrial Ca2+ uptake with and without the formation of high-Ca2+ microdomains. *Cell Calcium.* 2006; 40:527-537.

29. Denton RM. Regulation of mitochondrial dehydrogenases by calcium ions. *Biochim Biophys Acta.* 2009; 1787:1309-1316.

30. Sutendra G, Dromparis P, Bonnet S, Haromy A, McMurtry MS, Bleackley RC, Michelakis ED. Pyruvate dehydrogenase inhibition by the inflammatory cytokine TNFalpha contributes to the pathogenesis of pulmonary arterial hypertension. *J Mol Med (Berl).* 2010; 89:771-783.

31. Zamzami N, Kroemer G. The mitochondrion in apoptosis: how Pandora's box opens. *Nat Rev Mol Cell Biol.* 2001; 2:67-71.

32. Hotamisligil GS. Endoplasmic reticulum stress and the inflammatory basis of metabolic disease. *Cell.* 2010; 140:900-917.

33. Szegezdi E, Logue SE, Gorman AM, Samali A. Mediators of endoplasmic reticulum stress-induced apoptosis. *EMBO Rep.* 2006; 7:880-885.

34. Schewe DM, Aguirre-Ghiso JA. ATF6alpha-Rheb-mTOR signaling promotes survival of dormant tumor cells in vivo. *Proc Natl Acad Sci U S A.* 2008; 105:10519-10524.

35. Thomas M, Yu Z, Dadgar N, Varambally S, Yu J, Chinnaiyan AM, Lieberman AP. The unfolded protein response modulates toxicity of the

expanded glutamine androgen receptor. *J Biol Chem.* 2005; 280:21264-21271.

36.   Rubenstein RC, Zeitlin PL. A pilot clinical trial of oral sodium 4-phenylbutyrate (Buphenyl) in deltaF508-homozygous cystic fibrosis patients: partial restoration of nasal epithelial CFTR function. *Am J Respir Crit Care Med.* 1998; 157:484-490.

37.   Zeitlin PL, Diener-West M, Rubenstein RC, Boyle MP, Lee CK, Brass-Ernst L. Evidence of CFTR function in cystic fibrosis after systemic administration of 4-phenylbutyrate. *Mol Ther.* 2002; 6:119-126.

38.   Collins AF, Pearson HA, Giardina P, McDonagh KT, Brusilow SW, Dover GJ. Oral sodium phenylbutyrate therapy in homozygous beta thalassemia: a clinical trial. *Blood.* 1995; 85:43-49.

39.   Mercuri E, Bertini E, Messina S, Solari A, D'Amico A, Angelozzi C, Battini R, Berardinelli A, Boffi P, Bruno C, Cini C, Colitto F, Kinali M, Minetti C, Mongini T, Morandi L, Neri G, Orcesi S, Pane M, Pelliccioni M, Pini A, Tiziano FD, Villanova M, Vita G, Brahe C. Randomized, double-blind, placebo-controlled trial of phenylbutyrate in spinal muscular atrophy. *Neurology.* 2007; 68:51-55.

40.   Maestri NE, Brusilow SW, Clissold DB, Bassett SS. Long-term treatment of girls with ornithine transcarbamylase deficiency. *N Engl J Med.* 1996; 335:855-859.

41.   Kaplan MM, Gershwin ME. Primary biliary cirrhosis. *N Engl J Med.* 2005; 353:1261-1273.

42.   Poupon RE, Bonnand AM, Chretien Y, Poupon R. Ten-year survival in ursodeoxycholic acid-treated patients with primary biliary cirrhosis. The UDCA-PBC Study Group. *Hepatology.* 1999; 29:1668-1671.

43.   Phuphanich S, Baker SD, Grossman SA, Carson KA, Gilbert MR, Fisher JD, Carducci MA. Oral sodium phenylbutyrate in patients with recurrent malignant gliomas: a dose escalation and pharmacologic study. *Neuro Oncol.* 2005; 7:177-182.

44. Ooi CC, Good NM, Williams DB, Lewanowitsch T, Cosgrove LJ, Lockett TJ, Head RJ. Structure-activity relationship of butyrate analogues on apoptosis, proliferation and histone deacetylase activity in HCT-116 human colorectal cancer cells. *Clin Exp Pharmacol Physiol.* 2010; 37:905-911.

45. Bonnet S, Rochefort G, Sutendra G, Archer SL, Haromy A, Webster L, Hashimoto K, Bonnet SN, Michelakis ED. The nuclear factor of activated T cells in pulmonary arterial hypertension can be therapeutically targeted. *Proc Natl Acad Sci U S A.* 2007; 104:11418-11423.

46. Ozcan U, Yilmaz E, Ozcan L, Furuhashi M, Vaillancourt E, Smith RO, Gorgun CZ, Hotamisligil GS. Chemical chaperones reduce ER stress and restore glucose homeostasis in a mouse model of type 2 diabetes. *Science.* 2006; 313:1137-1140.

47. Hansmann G, Zamanian RT. PPARgamma activation: a potential treatment for pulmonary hypertension. *Sci Transl Med.* 2009; 1:12ps14.

48. Michelakis ED, Sutendra G, Dromparis P, Webster L, Haromy A, Niven E, Maguire C, Gammer TL, Mackey JR, Fulton D, Abdulkarim B, McMurtry MS, Petruk KC. Metabolic modulation of glioblastoma with dichloroacetate. *Sci Transl Med.* 2010; 2:31ra34.

49. Yu J, Fernandez-Hernando C, Suarez Y, Schleicher M, Hao Z, Wright PL, DiLorenzo A, Kyriakides TR, Sessa WC. Reticulon 4B (Nogo-B) is necessary for macrophage infiltration and tissue repair. *Proc Natl Acad Sci U S A.* 2009; 106:17511-17516.

A version of this chapter has been published. Dromparis P, Paulin R, Sutendra G, Stenson TH, Haromy A, and Michelakis ED 2013. Circulation. 127(1):115-125.

Chapter Four

Pioglitazone inhibits HIF-1α dependent angiogenesis in vivo and in vitro by altering mitochondrial-dependent stabilization of HIF-1α

Introduction

Peripheral arterial disease (PAD) is a common cardiovascular disorder due to obstructive atherosclerosis of the arteries of the lower extremities.[1] Diabetes is a risk factor for PAD,[2] and in patients with diabetes, concomitant PAD is a risk factor for lower extremity amputation.[3] Both diabetes[4, 5] and PAD[6] are associated with adverse cardiovascular outcomes, including death, myocardial infarction, and stroke. The PROactive trial, a randomized trial of pioglitazone versus placebo in 5238 type 2 diabetics with evidence of macrovascular disease,[7] showed paradoxically that pioglitazone was associated with increased rates of lower extremity revascularization in the 1274 subjects with concomitant PAD (hazard ratio 1.69, 95% CI 1.153, 2.484).[8] Moreover, those with PAD did not benefit from pioglitazone with respect to other endpoints like cardiovascular death or acute coronary syndrome.[8] The mechanisms for these findings are not known.

Pioglitazone, along with other thiazolidinediones like rosiglitazone, are peroxisome-proliferator-activated receptor-γ (PPARγ) ligands that were developed as oral hypoglycemic therapies for type 2 diabetes.[9] Their mechanisms of action are incompletely understood, but include PPARγ-dependent tissue specific alterations in fatty acid uptake and storage, with concomitant improvements in peripheral tissue insulin sensitivity and utilization of glucose.[9] In addition to the association between pioglitazone and increased lower extremity revascularization demonstrated in the PROactive trial, exacerbations of heart failure and peripheral edema as well as increased rates of myocardial infarction and stroke have also been linked to these drugs.[9, 10] Dysregulation of angiogenesis has been suggested as a contributor to these adverse effects but the mechanisms remain unclear and at times conflicting [11-13 14-19 20].

Pioglitazone-dependent effects on mitochondria, with subsequent inhibition in hypoxia-inducible factor (HIF)-1α, might explain reduced angiogenesis. Mitochondrial fatty acid oxidation in skeletal muscle is reduced in diabetes,[21, 22] and the thiazolidinediones are known to increase mitochondrial oxygen consumption and mitochondrial biogenesis[22 23 24 25]. Since the Krebs cycle substrate α-ketoglutarate (αKG) can leave mitochondria and is a required co-factor for prolyl-hydroxylation leading to proteolysis of HIF-1α,[26] changes in mitochondrial function could lead to changes in HIF-1α activation. In addition, mitochondria also produce reactive oxygen species (ROS), largely at complex I of the electron transport chain, which can regulate HIF-1 activity and expression.[27] That augmenting αKG and mROS with the mitochondrial activator dichloroacetate impairs cancer-associated angiogenesis in vitro and in vivo[27, 28] supports

114

the concept of mitochondrial-dependent modulation of HIF-1α activation in normal tissues. We therefore hypothesized that pioglitazone-dependent changes in mitochondrial function would inhibit angiogenesis in vitro and in vivo by inhibiting HIF-1α activation. We tested this hypothesis in a set of in vivo and in vitro experiments involving non-insulin resistant (Sprague Dawley) rats, insulin-resistant (JCR:LA-cp) rats, and human skeletal muscle cells (hSkMCs) and human microvascular endothelial cells (hMVECs) in culture.

Results

4.1 Model validation

We found that our hindlimb ischemia model, involving ligating and cutting both the left common iliac and left common femoral arteries, was feasible with no post-operative mortality. Ex vivo CT angiography (Figure 4-1A), Doppler ultrasound (Figure 4-1B), and in vivo CT angiography (Figure 4-2A) all confirmed successful interruption of the large arteries of the left leg with reduced distal arterial flow. This model, in both Sprague Dawley and JCR:LA-cp rats, faithfully mimicked features of human limb ischemia, including superficial lower extremity ulcers (Figure 4-2B). AM blood glucose measurements performed on the JCR:LA-cp rats confirmed an insulin resistant state that was ameliorated in part by pioglitazone treatment (Figure 4-3). In a separate set of Sprague Dawley rats with hindlimb ischemia, we found that the ischemic reserve (ischemic leg perfusion divided by non-ischemic leg perfusion) measured by Tc^{99m}-Sestamibi SPECT-CT imaging significantly correlated with that measured by fluorescent microspheres with a Pearson coefficient 0.798 ($p<0.05$, Figure 4-4), validating Tc^{99m}-Sestamibi SPECT-CT as an assay of perfusion.

4.2 Pioglitazone decreased ischemic limb perfusion of Sprague Dawley and JCR:LA-cp rats

We assessed in vivo limb perfusion bilaterally after two weeks of either pioglitazone or vehicle treatment using two techniques, including Tc^{99m}-Sestamibi SPECT-CT (validated by us) and contrast enhanced ultrasound (previously validated by others[29]). We found significantly reduced perfusion with both techniques in pioglitazone treated Sprague Dawley and JCR:LA-cp rats compared with relevant controls. In Sprague Dawley rats, Tc^{99m}-Sestamibi SPECT-CT ischemic reserve was 0.98 ± 0.12 in vehicle treated rats compared with 0.62 ± 0.09 in pioglitazone treated rats (Figure 4-1C). Similarly, in Sprague Dawley rats, contrast enhanced

115

ultrasound measured ischemic reserve was 0.87 ± 0.02 in vehicle treated rats, compared with 0.65 ± 0.03 in pioglitazone treated rats (Figure 4-1D). In JCR:LA-cp rats, the Tc^{99m}-Sestamibi SPECT-CT measured ischemic reserve was 1.03 ± 0.07 in the vehicle treated rats, compared with 0.69 ± 0.10 in the pioglitazone treated rats (Figure 4-1C). Similarly, in the JCR:LA-cp rats, the contrast enhanced ultrasound measured ischemic reserve was 0.86 ± 0.03 in the vehicle treated rats, compared with 0.64 ± 0.04 in the pioglitazone treated rats (Figure 4-1D).

4.3 Pioglitazone decreased ischemic limb capillary density

We assessed capillary density in gastrocnemius muscles ex vivo by confocal fluorescence microscopy for fluorescent lectin, perfused prior to euthanasia, and by immunohistochemistry for von Willebrand factor. We found reduced capillary density with both endothelial markers in pioglitazone treated Sprague Dawley and JCR:LA-cp rats compared with relevant controls (Figure 4-5 and Figure 4-6A). In Sprague Dawley rats, the ratio of lectin signal in the ligated versus non-ligated limb was 0.86 ± 0.02 in vehicle treated rats compared with 0.60 ± 0.07 in pioglitazone treated rats. In JCR:LA-cp rats, the ratio of lectin signal in the ligated versus non-ligated limb was 0.81 ± 0.03 in the vehicle treated rats, compared with 0.51 ± 0.05 in the pioglitazone treated rats. In addition, we stained muscle tissue with von Willebrand factor and smooth muscle actin, and counted muscularized arterioles in the ischemic limb adductor muscles of the JCR:LA-cp rats as an index of arteriogenesis. We found that there were increased numbers of muscularized arterioles in the ischemic limbs compared with the non-ischemic limbs in both placebo treated (4.0 ± 0.3 versus 2.6 ± 0.2 muscularized arterioles per field) and pioglitazone treated (3.3 ± 0.3 versus 2.2 ± 0.2 muscularized arterioles per field) JCR:LA-cp, consistent with arteriogenesis in the ligated (ischemic) limb (Figure 4-7). However, the number of muscularized arterioles was not reduced in the pioglitazone-treated ischemic limbs compared with the placebo-treated ischemic limbs (3.3 ± 0.3 versus 4.0 ± 0.3, $p = 0.15$).

4.4 Pioglitazone reduced expression of VEGF in ischemic gastrocnemius muscle

We evaluated in vivo expression of VEGF by performing an immunoblot on homogenized ischemic gastrocnemius muscles from placebo and pioglitazone treated JCR:LA-cp rats. We found that VEGF expression was reduced in ischemic muscle tissue in pioglitazone treated rats compared with placebo treated rats (Figure 4-6B).

116

4.5 Pioglitazone inhibits angiogenesis through autocrine and paracrine mechanisms

To specifically address whether pioglitazone inhibits angiogenesis by a paracrine effect via acting on skeletal muscle, we studied the effect on in vitro angiogenesis of hMVECs on matrigel of pretreatment of hSkMCs with pioglitazone or vehicle. The hSkMCs were pre-treated in normoxia with vehicle, hypoxia with vehicle or hypoxia with pioglitazone for 48 hours before the vehicle/drug was washed off to remove any confounding effects of pioglitazone on the hMVECs. The cells were then seeded on the top well of a Boyden chamber, separated from hMVECs by a 0.2μm filter (Figure 4-8A). Normoxic hMVECs exposed to hSkMCs pretreated with hypoxia with vehicle had increased tubule formation (Figure 4-8B), consistent with activation of paracrine angiogenic signaling. To confirm a direct inhibition of angiogenesis by pioglitazone on endothelial cells, we also studied hMVECs exposed directly to hypoxia plus pioglitazone or vehicle. Hypoxia increased in vitro angiogenesis, assessed by both total tubule length and the number of complete tubules per field, and pioglitazone decreased tubule formation in a dose-dependent manner (Figure 4-9).

4.6 Pioglitazone inhibits HIF1α activation in hypoxia hSkMCs

To determine whether the impaired paracrine-mediated angiogenesis involved suppression of the HIF1α axis, we performed immunofluorescence studies to determine the cellular localization of HIF1α in hMVECs. Because HIF1α is a transcription factor, it is only active when nuclear. Hypoxia induced robust increases in HIF1α nuclear localization, which was reversed with pioglitazone (Figure 4-10A). In parallel to changes in HIF1α nuclear expression, there was increased VEGF expression after exposure to hypoxia, which was decreased by pioglitazone. Pioglitazone also reduced overall HIF1α expression and VEGF receptor expression (Figure 4-10B), measured by qRT-PCR.

4.7 Pioglitazone increases mitochondrial signaling in hypoxic hSkMCs

To determine whether pioglitazone-induced inhibition of angiogenesis involved changes in mitochondrial signaling, we measured mitochondrial membrane potential ($\Delta\Psi$m), which links metabolic and oxidative functioning of the mitochondria. In hSkMCs, hypoxia increased $\Delta\Psi$m, indicative of mitochondrial suppression, which was partially reversed by pioglitazone (Figure 4-

11A). Since HIF1α is regulated by α-KG and redox signals, we assessed mitochondrial production of these signaling molecules. Mitochondrial derived ROS production was reduced (Figure 4-11B). Similarly, α-KG was increased in pioglitazone treated hypoxic hSkMCs (Figure 4-11C). Complex I is the major producer of mitochondrial derived ROS, and was suppressed in hypoxic hSkMCs. Pioglitazone reversed a hypoxia induced reduction in complex I activity (Figure 4-11D).

Discussion

Our data support that pioglitazone, a therapy for human patients with type II diabetes, is associated with impaired angiogenesis in vitro and in vivo in Sprague Dawley and JCR:LA-cp insulin resistant rats. Our findings are directly clinically relevant, in that impaired angiogenesis might account for an unexpected finding of The PROactive trial, which evaluated pioglitazone versus placebo in 5238 type 2 diabetics with evidence of macrovascular disease.[7] This trial found that pioglitazone was associated with increased rates of lower extremity revascularization in the 1274 subjects with concomitant PAD (hazard ratio 1.69, 95% CI 1.153, 2.484).[8] Inhibition of angiogenesis in ischemic limbs by pioglitazone, either by direct effects on endothelial cells or by a paracrine mechanism due to effects on skeletal muscle, may explain the increased lower extremity revascularization in the pioglitazone treatment arm. In addition, observational studies of drug safety have also demonstrated an association between pioglitazone and increased rates of bone fractures.[30] Angiogenesis is well established as a key mechanism of bone healing and health,[31] and therefore pioglitazone-related impairments of angiogenesis may explain this treatment complication as well. There is also very good evidence from the cancer literature that inhibition of VEGF-dependent angiogenesis by novel anti-cancer therapies is linked with heart failure.[32] Pioglitazone was also linked to higher rates of exacerbations heart failure than placebo in the PROactive trial,[7] and while some authors have suggested that this mechanism might be that thiazolidinediones stimulated ENaC-mediated renal salt absorption,[33] pioglitazone-induced impaired angiogenesis may be an alternate mechanism.

In addition to demonstrating a direct anti-angiogenic effect of pioglitazone on endothelial cells, we demonstrated that pioglitazone inhibits angiogenesis in a paracrine manner by inducing changes in mitochondrial function within skeletal muscle cells that reduce HIF1α activation (Figure 4-12). These observations are analogous to our groups' novel demonstration of

mitochondrial-dependent stabilization of HIF1α within cancer cells that supports tumor angiogenesis.[28] These findings together suggest that this mitochondrial dependent regulation of HIF1α dependent angiogenesis may be relevant to angiogenesis within many organs and tissues, and that targeting mitochondrial function with metabolic modulating drugs could be a useful therapeutic strategy for many conditions linked with excessive or insufficient angiogenesis. For example, fenofibrate, a peroxisome proliferator-activated receptor alpha agonist known to increase mitochondrial function in humans,[34] is associated with lower risk of diabetic retinopathy, a condition of increased angiogenesis.[35] In addition, thiazolidinediones have demonstrated anti-angiogenic potential in patients with highly vascular tumors[17, 18], in addition to direct effects on cancer cells.[36-39] We have also previously shown that increasing mitochondrial-derived ROS and αKG in cancer with the mitochondrial activator dichloroacetate reduced HIF1α activation, decreases angiogenesis, reduces cell proliferation and induces cell death in tumors from patients with glioblastoma multiforme[27].

More data are required to evaluate the mechanism by which pioglitazone induces changes in mitochondrial function, including increases in αKG and mitochondrial derived ROS. The classical mechanism of action for PPARγ ligands like pioglitazone involves hetero-dimerization of PPARγ with the retinoid X receptor, specific DNA binding to PPAR response elements, and alteration of gene expression.[40] While alterations in gene expression induced in a PPARγ-dependent way could explain our results, direct and PPARγ-independent effects of pioglitazone on mitochondria, such as effects on Complex I,[41] could be responsible. Further work would be required to evaluate this possibility.

Strengths of our work include the use of clinically relevant models and assessments of in vivo physiology. We used two rat models, including non-insulin resistant Sprague Dawley rats and insulin resistant JCR:LA-cp rats in a model system in which each ischemic limb is compared to its non-ischemic contralateral limb, minimizing variability. The insulin resistant JCR:LA-cp rats are a very good model for human type II diabetes,[42] in that they are insulin resistant, obese, and prone to atherosclerosis.[43] We also used commercially available human cell lines for our in vitro studies. While there are limitations with any models of human disease, the use of JCR:LA-cp rats and human cell lines increases the likelihood our findings will accurately reflect biology within human patients. Unlike many studies of hindlimb ischemia, we used two measures of perfusion, including contrast ultrasound and Tc^{99m}-sestamibi SPECT imaging. Using these two

119

measures together, and complementing the in vivo findings with the ex vivo analysis of blood vessel density, supports the veracity of our findings.

Our work is in accord with several studies of the effects of pioglitazone on endothelial cells and angiogenesis[15, 44, 45], as well as studies of pioglitazone in pathological retinal tissue,[46, 47], endometrial tissue,[48] and renal tissue.[12-14]. However, a pro-angiogenic effect of pioglitazone has been reported in adipose tissue,[49] at least raising the possibility that effects of pioglitazone might be in part tissue-specific. Our finding that pioglitazone inhibits angiogenesis in ischemic skeletal muscle tissue is also in conflict with a study performed by Huang et al in a diabetic hindlimb ischemia mouse model [20]. There are several methodological differences between ours and that study, including different species, drug dosing and more limited methods of assessing in vivo vascular perfusion by Huang et al.

Based on our findings, we conclude that pioglitazone is associated with impaired angiogenesis in non-diabetic Sprague Dawley and diabetic JCR:La-cp rats with hindlimb ischemia, due to mitochondrial-dependent reductions in HIF-1α signaling. Reduced angiogenesis in ischemic tissues might explain some clinical reports of adverse effects associated with pioglitazone in humans.

Materials and Methods

Rat Hindlimb Ischemia Model: All experiments were conducted with the approval of the Animal Care and Use Committee of the University of Alberta. Adult male Sprague-Dawley (n=22) and obese JCR:LA-cp insulin resistant (n=20) rats[42] were sequentially numbered, anesthetized with isofluorane anesthesia and placed on a heated surgical table. The abdomen and left groin were shaved and sterilized with 4% chlorhexidine solution. Using sterile technique, the left common iliac artery and left superficial femoral artery were each ligated twice with 3.0 silk suture and cut between the ligatures. The skin was close in one layer with 5.0 prolene suture. After recovery, animals were randomized with allocation concealment to receive either oral pioglitazone (10mg/kg per day; Takeda Pharmaceuticals, Deerfield, IL) or placebo. Only one technician knew the randomization key, and investigators blinded to treatment allocation completed all subsequent experiments. A separate group of Sprague-Dawley rats were used in preliminary experiments to validate the model, including in vivo and ex vivo angiography and Doppler ultrasound, as well as to validate the Tc[99m]-sestamibi perfusion imaging technique. An AM glucose measurement was

120

performed at the end of the protocol in the JCR:LA-cp rats to confirm a hyperglycemic state (Omron Healthcare, Scarborough, ON).

Tc^{99m} Sestamibi SPECT-CT Imaging: Rats were lightly anesthetized, and placed in the bed of a PET-SPECT-CT (Gamma Medica, Northridge, CA). A dose of 2.0 mCu of Tc^{99m} labeled sestamibi was injected via a central venous cannula. After 15 minutes, a CT scan and SPECT images were obtained. Data were fused and analyzed using Amira Software (Visage Imaging Incorporated, San Diego, CA). Signal within the gastrocnemius muscle was identified and quantified based on the CT image.

Contrast Enhanced Ultrasound Perfusion Imaging: Rats were lightly anesthetized with isofluorane and secured on the heated table of a Vevo 770 rodent ultrasound machine (Visualsonics, Toronto, ON). The right and left calves were denuded of hair using a chemical depilatory. Using a 707B probe, a B-mode image of either the right or left calf muscle was obtained. The acquisition was triggered, and after 5 seconds (30 frames) a bolus of 3.5×10^8 microbubbles (Visualsonics, Toronto, ON) was injected into a central venous cannula. A total of 425 frames of data were collected. After 10 minutes of exposing the rodent to an inhaled FiO_2 of 100% (to destroy residual bubbles), the procedure was repeated to image the contralateral limb. Perfusion curves were generated and curve-fit offline using the Vevo analysis software (Visualsonics Toronto, ON).

Fluorescent Microspheres: Ex vivo calf muscle perfusion was measured as previously described.[50] Briefly, a bolus of 3.6×10^6 10μm diameter microspheres were administered to an anesthetized animal via central venous cannula and allowed to circulate for 15 minutes prior to euthanasia. Muscle tissues were excised and digested in ethanolic KOH. Microspheres were sedimented by centrifugation, fluorescent dye was extracted, and fluorescence was measured with a GEMINI-XS fluorimeter (Molecular Devices, Sunnyvale, CA).

Cell Culture: Human microvascular endothelial cells (hMVECs; Cascade Biologics, Portland, OR) and human skeletal muscle cells (hSMCs; Promocell, Heidelberg, Germany) were cultured in M131medium (Invitrogen, Carlsbad, CA) and Promocell C-23060 media (Promocell, Heidelberg, Germany), respectively. Up to passage six cells were used. For the autocrine matrigel studies, hMVECs were cultured in normoxia (pO_2 120 mmHg), hypoxia (pO_2 40 mmHg), or hypoxia plus pioglitazone at 1, 10, or 25 μg/ml for 48 hours.

121

Matrigel Assays: Matrigel was prepared in a 12 well plate per manufacturer's instructions (BDBiosciences, Mississauga, ON), and 50,000 HMVECs/well were applied. HMVECs were then cultured in either normoxia or hypoxia for 4 hours, and images were obtained (5 images/well 40x magnfication). Tubule length and number of completely enclosed structures per image were measured using Image Pro-Plus software version 6.2.0 (Media Cybernetics). Five wells on each of five plates were evaluated per group. In the Paracine Matrigel Assay, a boyden chamber was used. Briefly, hSkMCs were cultured in normoxia (pO$_2$ 120 mmHg), hypoxia (pO$_2$ 40 mmHg), or hypoxia plus pioglitazone (20 μg/ml) for 48 hours and washed to remove all medium and pioglitazone. Matrigel was prepared in a similar manner and hMVECs, previously cultured at pO$_2$ 120 mmHg, were applied to the matrigel. The washed hSkMCs were placed in the top insert of a 12 well 0.4 μm Boyden chamber (Corning, Corning, NY), and placed in contact with medium over the hMVEC cells. The cells were incubated at pO$_2$ 120 mmHg for 4 hours. Images were obtained and data was analyzed as described above.

Confocal Microscopy: All imaging was performed with a Zeiss LSM 510 Confocal microscope (Carl Zeiss, Toronto, ON). Live cell imaging of mitochondrial membrane potential (TMRM; Invitrogen, Burlington, ON) and mitochondrial ROS (Mitosox; Invitrogen, Burlington, ON) were imaged as previously described. Primary antibodies used include VEGF (1:100; Santa Cruz Biotechnologies), HIF1α (1:100; Abcam, San Francisco, CA), vWF (1:200; Abcam, San Francisco, CA, San Francisco, CA), SMA (1:100; Abcam, San Francisco, CA). Lectin fluorescein ricinus communis agglutinin I (5mg) (Vector Laboratories, Inc, Burlingame, CA) was injected via a central venous cannula for 5 minutes prior to sacrifice, gastrocnemius isolation and flash freezing. For semi-quantification, randomly selected fields were evaluated and regions of interest were quantified using the Zeiss LSM Image Examiner software version 3.0.2.70 (Carl Zeiss, Toronto, ON). For HIF-1α, only nuclear signals were included in the regions of interest.

Immunoblot: Tissues were collected and immunoblotting was performed with standard technique using 25 μg protein per sample. The films were digitized and quantified using 1D Image Analysis Software (Kodak, Rochester, NY). Expression was normalized to actin to correct for loading differences.

PDH Assay: hSkMCs were cultured in normoxia, hypoxia or hypoxia + 20ug/ml pioglitazone for 48 hours. PDH activity was measured using the MitoProfile Dipstick Assay Kit (MitoSciences, Eugene, OR). Protein was collected after cells were homogenized. Protein (50mL of 1μg/mL)

was placed in a 96-well dish and incubated with the dipstick containing the PDH complex antibody and then incubated in activity buffer. PDH activity was measured by intensity of band using a flat top scanner as previously described.[27]

α-ketoglutarate Assay: hSkMCs were cultured in normoxia, hypoxia or hypoxia + 20ug/ml pioglitazone for 48 hours. The α-Ketoglutarate levels were measured as described in a commercially available spectro-photometric α-ketoglutarate Assay Kit (BioVision, Mountain View, CA, USA). PASMCs cells were grown to confluency in a T75 flask. Cells were then harvested, lysed and protein concentration was adjusted to equal levels between groups. The α-Ketoglutarate levels were measured by measuring OD at 570nm after the kit-based reaction was completed as previously described.[27]

Complex I Activity Assay: Complex I activity was measured with a complex I activity kit (MitoSciences, Eugene, OR). The hSkMCs were cultured in normoxia, hypoxia or hypoxia + 20ug/ml pioglitazone for 48 hours. Protein was collected after cells were homogenized. Protein (50mL of 1μg/mL) was placed in a 96-well dish and incubated with the dipstick containing an antibody to Complex I and then incubated in activity buffer. Complex I activity was measured by intensity of band using a flat top scanner.

*Statistical Analysis:* Statistics was performed on SPSS 18.0 Software (Somers, NY). Values are expressed as mean±SEM. Comparisons between two groups for in vivo experiments were made using Mann-Whitney U test. For in vitro data, a Mann Whitney U test was used to compare two groups or Kruskal-Wallace test was performed to compare among two or more groups. Significance was considered at $p < 0.05$.
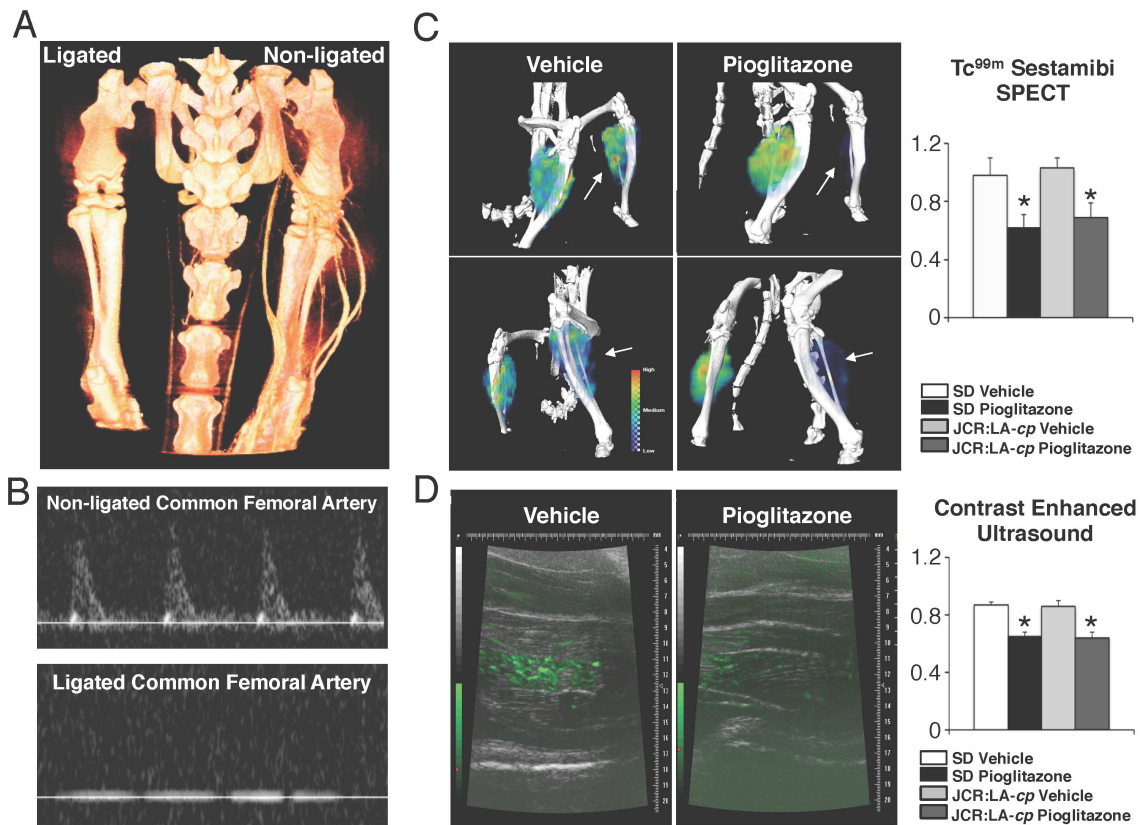
Figure 4-1: Pioglitazone is associated with reduced gastrocnemius perfusion in the hind limb ischemia model. A. Ex vivo contrast enhanced CT-angiogram showing complete vascular occlusion in the ligated gastrocnemius (left) compared to the non-ligated gastrocnemius (right). **B.** Doppler ultrasound showing interruption of femoral artery perfusion in the ligated, but not non-ligated common femoral arteries. **C.** Representative SPECT-CT images of the gastrocnemius muscle after Tc99m-Sestamibi injection. Pioglitazone decreases perfusion in both diabetic and non-diabetic models. Values are represented as mean ± SEM of the ischemic reserve (the ratio of the signal in the ligated/non-ligated leg) (n=20 animals/group. *p<0.05 vs. respective placebo treated control). **D.** Representative contrast-enhanced ultrasound images of the gastrocnemius muscle after micro-bubble injection. Pioglitazone decreases perfusion in both diabetic and non-diabetic models. Values are represented as ischemic reserve mean ± SEM (the ratio of the signal in the ligated/non-ligated leg) (n=20 animals/group. *p<0.05 vs. respective placebo treated control).
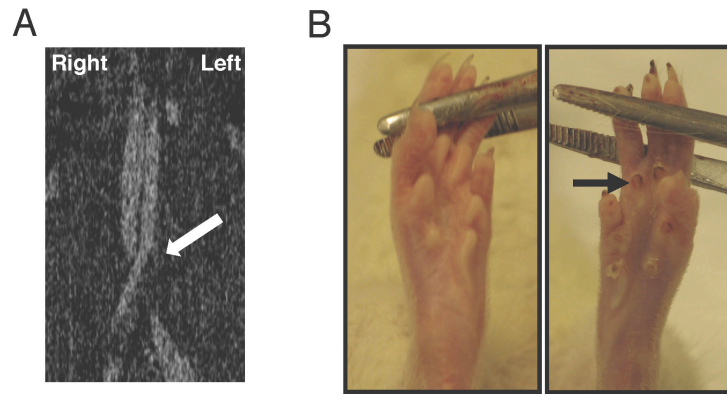
Figure 4-2: Further validation of the hind limb ischemia model. **A.** In vivo contrast enhanced CT-angiogram showing interrupted perfusion (white arrow) of the ligated arteries. **B.** The development of digital ulceration (arrow) on the feet with ligated femoral arteries, mimicking the human clinical presentation.

Blood Glucose (mmol/L)
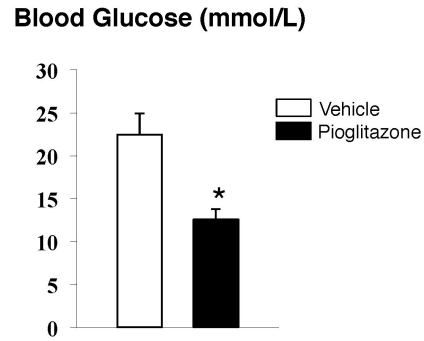
Figure 4-3: Blood glucose in placebo and pioglitazone treated JCR:La-cp insulin resistant rats at time of sacrifice. Pioglitazone treated animals had significantly lower blood glucose compared to vehicle treated controls (n=20 animals/group, *p<0.05 vs placebo).
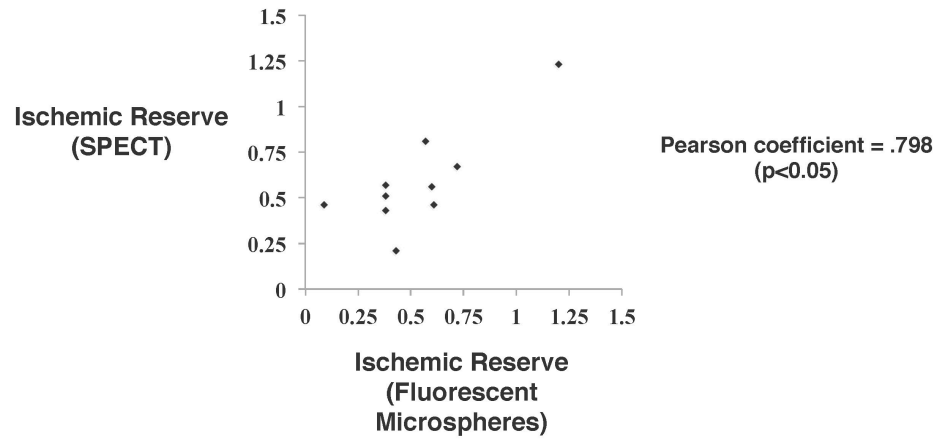
Figure 4-4: SPECT perfusion correlates with fluorescent microsphere perfusion.
Tc^{99m}Sestamibi-SPECT/CT ischemic reserve signal significantly correlates with fluorescent microbubbles ischemic reserve signal. Each dot represents one animal (p<0.05).
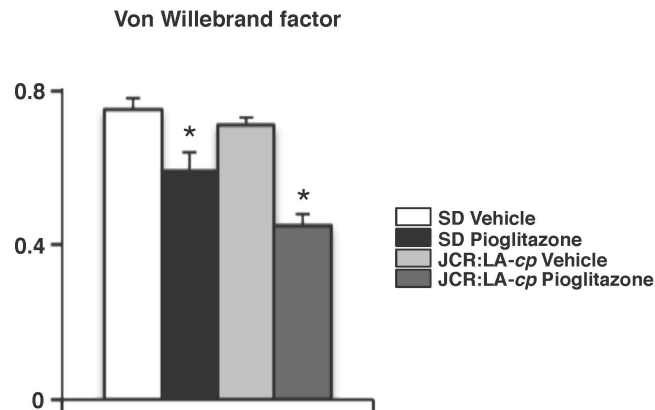
Figure 4-5: Pioglitazone is associated with reduced gastrocnemius vessel density in vivo.
Pioglitazone decreases staining of the endothelial marker von Willebrand Factor in the ischemic gastrocnemius muscle in both diabetic and non-diabetic models. Values are represented as mean ± SEM (the ratio of the signal in the ischemic/non-ischemia leg) (*p<0.05 vs. respective placebo treated control group).
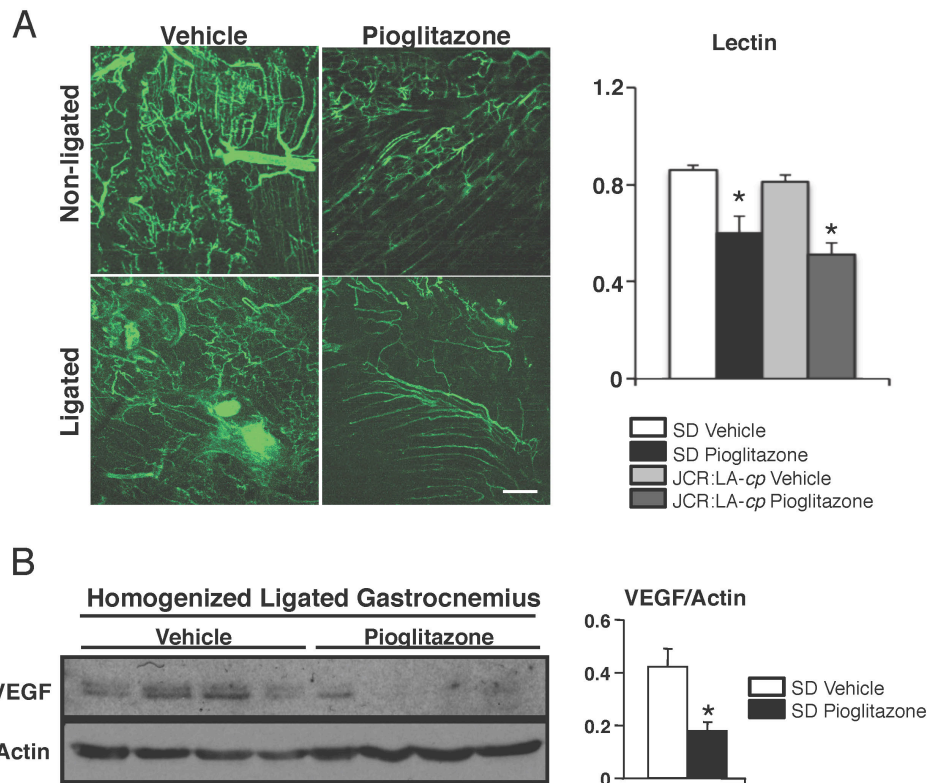
Figure 4-6: Pioglitazone is associated with reduced gastrocnemius lectin perfusion in vivo.
A. Representative confocal images of the gastrocnemius muscle of vehicle (left) and pioglitazone treated rats perfused with lectin (green) immediately prior to sacrifice. Pioglitazone decreases the lectin perfusion (left) in both diabetic and non-diabetic models compared to vehicle controls. Values are represented as mean ± SEM (the ratio of the signal in the ligated/non-ligated leg) (*p<0.05 vs. respective placebo treated control group). Bar = 200μm. **B.** Immunoblot showing reduced VEGF expression in the gastrocnemius muscles with ligated vessels in pioglitazone treated animals compared to vehicle treated animals. Each lane represents muscle tissue from one animal (*p<0.05 vs. vehicle treated group).
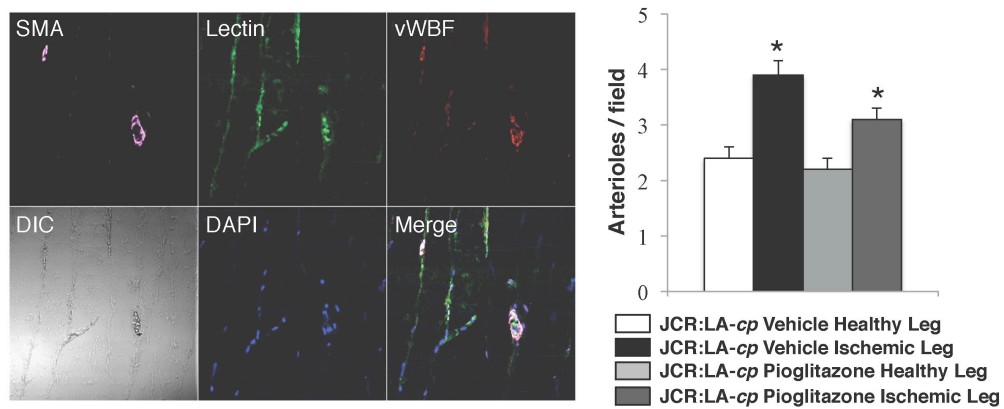
Figure 4-7: Pioglitazone increases arterial density in ischemic limbs. Representative confocal image of muscle tissue stained with the smooth muscle cell marker smooth muscle actin (SMA; purple), the endothelial cell maker von Willebrand factor (red), and lectin (green) marking perfusion. Pioglitazone treatment increases arterial density (SMA enclosed vessels/field) in both diabetic and non-diabetic models (*$p<0.05$ vs. respective placebo treated control group).
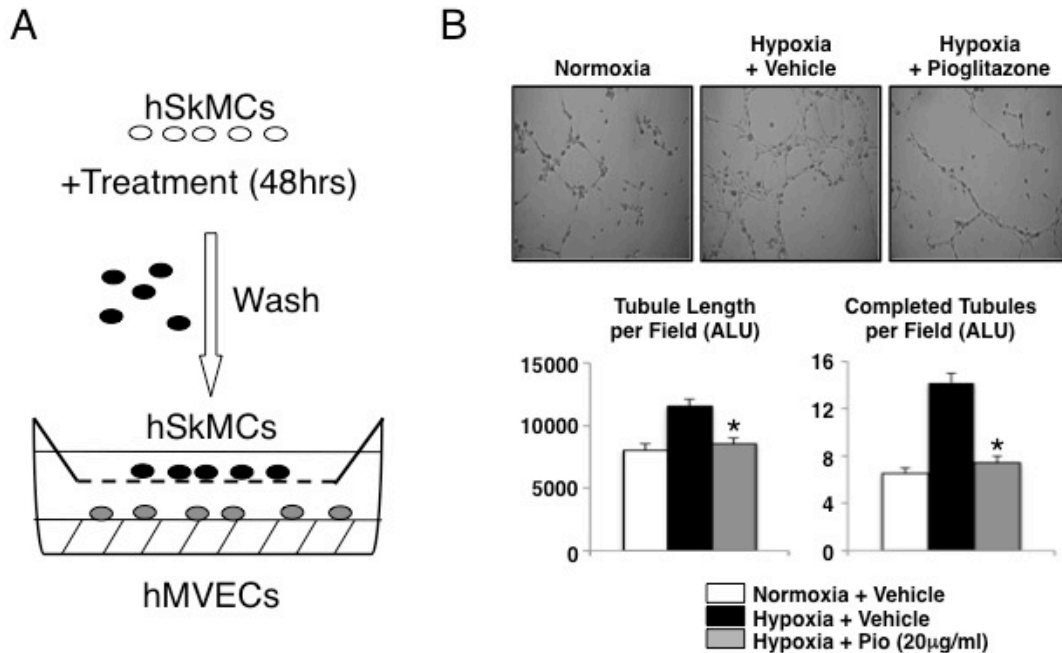
Figure 4-8: Pioglitazone decreases paracrine angiogenic signaling in vitro. A. Schematic of the experimental procedure. hSkMCs were pretreated in normoxic, hypoxic, or hypoxic + pioglitazone conditions for 48 hours. Cells were collected, washed to remove any residual pioglitazone and plated in the top of a Boyden chamber with MVECs on a matrigel assay in normoxic conditions. A porous membrane that only allows diffusion of secreted factors separated the hSKMCs and MVECs. **B.** Representative images hMVECs co-cultured with pretreated hSkMCs on a Boyden chamber matrigel assay. Pioglitazone blocks the hypoxia-induced in both total tubule length per field (left) and completed tubule structures per field (right) in a dose-dependent manner (n=5 images/well, 5 wells/group/experiment, 3 experiments. *p<0.05 vs. hypoxia vehicle).

131
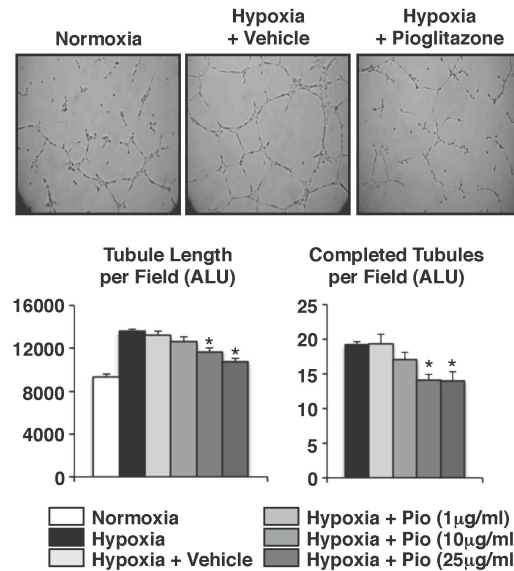
Figure 4-9: Pioglitazone decreases autocrine angiogenic signaling in vitro. Representative images hMVECs on a matrigel assay under normoxic, hypoxic, or hypoxic plus pioglitazone treatments. Pioglitazone blocks the hypoxia-induced increase in both total tubule length per field (left) and completed tubule structures per field (right) in a dose-dependent manner (n=5 images/well, 5 wells/group/experiment, 3 experiments. *p<0.05 vs. hypoxia vehicle).
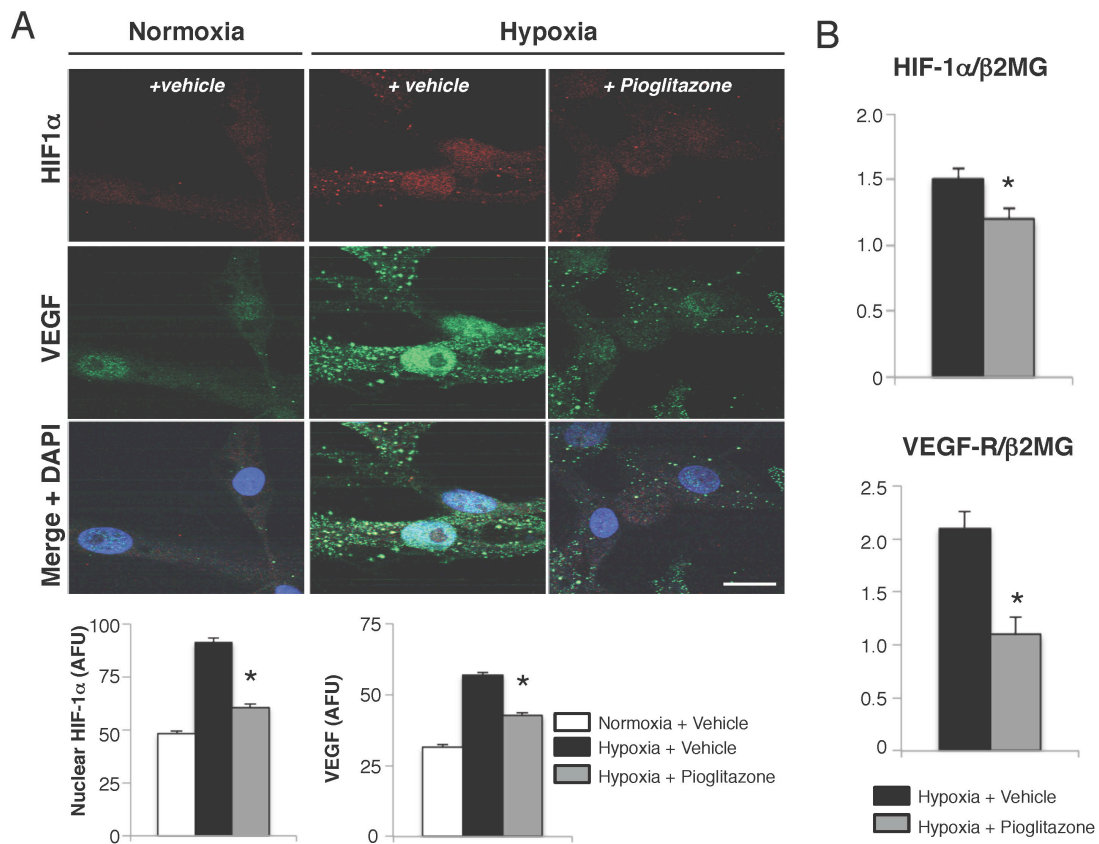
Figure 4-10: Pioglitazone inhibits HIF1α human myoblasts. A. Representative immunofluorescence confocal images of hSkMCs in normoxic, hypoxic, or hypoxic plus pioglitazone conditions and stained with HIF1α (red), VEGF (green) and the nuclear stain DAPI (blue). Pioglitazone reduces nuclear (active) HIF1α and VEGF expression in hypoxic human myoblasts (*p<0.05 vs. hypoxia vehicle). Bar = 20μm. **B.** mRNA expression of HIF1α target genes, HIF1α and VEGF-R, in human myoblasts exposed to hypoxia plus vehicle or pioglitazone. Pioglitazone reduces HIF1α and VEGF-R mRNA (n=3 experiments. *p<0.05 vs. hypoxia vehicle).
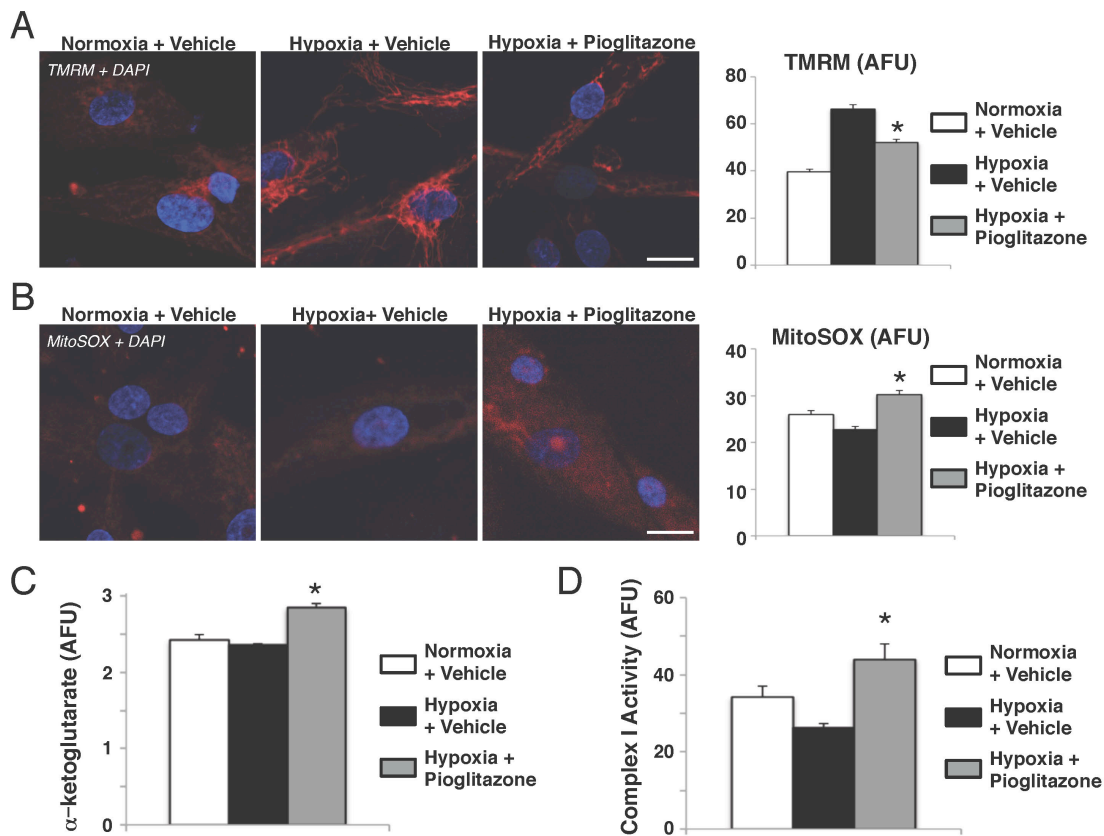
Figure 4-11: Pioglitazone enhances mitochondrial activity human myoblasts. A. Representative confocal images of human myoblasts exposed on normoxia, hypoxia, or hypoxia plus pioglitazone and stained with TMRM (red, ΔΨm marker) and DAPI (blue, nuclear marker). Hypoxia increases ΔΨm, which is partially blocked with pioglitazone (n=40-50 cells/group/experiment, 3 experiments. *$p < 0.05$ vs. hypoxia vehicle)**.** Bar = 20μm. **B.** Representative confocal images of human myoblasts exposed on normoxia, hypoxia, or hypoxia plus pioglitazone and stained with MitoSOX (red, mROS indicator) and DAPI (blue). Hypoxia suppresses mROS, which is restored with pioglitazone (n=40-50 cells/group/experiment, 3 experiments. *$p < 0.05$ vs. hypoxia vehicle)**.** Bar = 20μm. **C.** Complex I activity in human myoblasts exposed on normoxia, hypoxia, or hypoxia plus pioglitazone**.** Hypoxia reduces complex I activity, which is restored with pioglitazone treatment (n=4 wells/group. *$p < 0.05$ vs. hypoxia vehicle)**. D.** αKG levels in human myoblasts exposed on normoxia, hypoxia, or hypoxia plus pioglitazone**.** Pioglitazone treatment increases αKG levels in hypoxia myoblasts (n=5 wells/group. *$p < 0.05$ vs. hypoxia vehicle)**.**
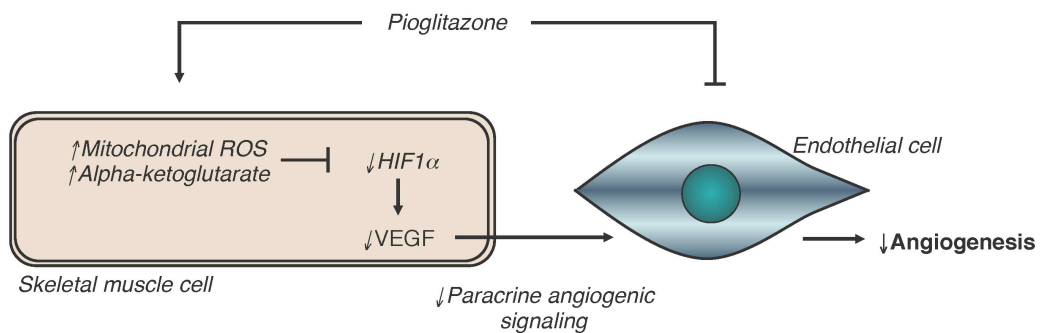
Figure 4-12: A proposed mechanism through which pioglitazone inhibits angiogenesis.
Pioglitazone enhances mitochondrial activity in skeletal muscle tissue. This results in increased mitochondrial derived signals – αKG and mROS- which can inhibit HIF1α signaling. This disrupts skeletal muscle-derived angiogenic signals that act on neighboring endothelial cells, reducing vessel formation. This mechanism may run in parallel with direct anti-angiogenic effects on endothelial cells, inhibiting angiogenesis through two mechanisms.

References

1. Hirsch AT, Haskal ZJ, Hertzer NR, Bakal CW, Creager MA, Halperin JL, Hiratzka LF, Murphy WR, Olin JW, Puschett JB, Rosenfield KA, Sacks D, Stanley JC, Taylor LM, Jr., White CJ, White J, White RA, Antman EM, Smith SC, Jr., Adams CD, Anderson JL, Faxon DP, Fuster V, Gibbons RJ, Hunt SA, Jacobs AK, Nishimura R, Ornato JP, Page RL, Riegel B. ACC/AHA 2005 Practice Guidelines for the management of patients with peripheral arterial disease (lower extremity, renal, mesenteric, and abdominal aortic): a collaborative report from the American Association for Vascular Surgery/Society for Vascular Surgery, Society for Cardiovascular Angiography and Interventions, Society for Vascular Medicine and Biology, Society of Interventional Radiology, and the ACC/AHA Task Force on Practice Guidelines (Writing Committee to Develop Guidelines for the Management of Patients With Peripheral Arterial Disease): endorsed by the American Association of Cardiovascular and Pulmonary Rehabilitation; National Heart, Lung, and Blood Institute; Society for Vascular Nursing; TransAtlantic Inter-Society Consensus; and Vascular Disease Foundation. *Circulation.* 2006;113(11):e463-654.

2. Roger VL, Go AS, Lloyd-Jones DM, Adams RJ, Berry JD, Brown TM, Carnethon MR, Dai S, de Simone G, Ford ES, Fox CS, Fullerton HJ, Gillespie C, Greenlund KJ, Hailpern SM, Heit JA, Ho PM, Howard VJ, Kissela BM, Kittner SJ, Lackland DT, Lichtman JH, Lisabeth LD, Makuc DM, Marcus GM, Marelli A, Matchar DB, McDermott MM, Meigs JB, Moy CS, Mozaffarian D, Mussolino ME, Nichol G, Paynter NP, Rosamond WD, Sorlie PD, Stafford RS, Turan TN, Turner MB, Wong ND, Wylie-Rosett J. Heart disease and stroke statistics--2011 update: a report from the American Heart Association. *Circulation.*123(4):e18-e209.

3. Abou-Zamzam AM, Jr., Gomez NR, Molkara A, Banta JE, Teruya TH, Killeen JD, Bianchi C. A prospective analysis of critical limb ischemia: factors leading to major primary amputation versus revascularization. *Ann Vasc Surg.* 2007;21(4):458-463.

4. Bundo M, Munoz L, Perez C, Montero JJ, Montella N, Toran P, Pera G. Asymptomatic peripheral arterial disease in type 2 diabetes patients: a 10-year follow-up study of the

utility of the ankle brachial index as a prognostic marker of cardiovascular disease. *Ann Vasc Surg.*24(8):985-993.

5. Krempf M, Parhofer KG, Steg PG, Bhatt DL, Ohman EM, Rother J, Goto S, Pasquet B, Wilson PW. Cardiovascular event rates in diabetic and nondiabetic individuals with and without established atherothrombosis (from the REduction of Atherothrombosis for Continued Health [REACH] Registry). *Am J Cardiol.*105(5):667-671.

6. Fowkes FG, Murray GD, Butcher I, Heald CL, Lee RJ, Chambless LE, Folsom AR, Hirsch AT, Dramaix M, deBacker G, Wautrecht JC, Kornitzer M, Newman AB, Cushman M, Sutton-Tyrrell K, Lee AJ, Price JF, d'Agostino RB, Murabito JM, Norman PE, Jamrozik K, Curb JD, Masaki KH, Rodriguez BL, Dekker JM, Bouter LM, Heine RJ, Nijpels G, Stehouwer CD, Ferrucci L, McDermott MM, Stoffers HE, Hooi JD, Knottnerus JA, Ogren M, Hedblad B, Witteman JC, Breteler MM, Hunink MG, Hofman A, Criqui MH, Langer RD, Fronek A, Hiatt WR, Hamman R, Resnick HE, Guralnik J. Ankle brachial index combined with Framingham Risk Score to predict cardiovascular events and mortality: a meta-analysis. *JAMA.* 2008;300(2):197-208.

7. Dormandy JA, Charbonnel B, Eckland DJ, Erdmann E, Massi-Benedetti M, Moules IK, Skene AM, Tan MH, Lefebvre PJ, Murray GD, Standl E, Wilcox RG, Wilhelmsen L, Betteridge J, Birkeland K, Golay A, Heine RJ, Koranyi L, Laakso M, Mokan M, Norkus A, Pirags V, Podar T, Scheen A, Scherbaum W, Schernthaner G, Schmitz O, Skrha J, Smith U, Taton J. Secondary prevention of macrovascular events in patients with type 2 diabetes in the PROactive Study (PROspective pioglitAzone Clinical Trial In macroVascular Events): a randomised controlled trial. *Lancet.* 2005;366(9493):1279-1289.

8. Dormandy JA, Betteridge DJ, Schernthaner G, Pirags V, Norgren L. Impact of peripheral arterial disease in patients with diabetes--results from PROactive (PROactive 11). *Atherosclerosis.* 2009;202(1):272-281.

9. Yki-Jarvinen H. Thiazolidinediones. *N Engl J Med.* 2004;351(11):1106-1118.

10. Kaul S, Bolger AF, Herrington D, Giugliano RP, Eckel RH. Thiazolidinedione drugs and cardiovascular risks: a science advisory from the American Heart Association and American College of Cardiology Foundation. *Circulation.*121(16):1868-1877.

11.   Xin X, Yang S, Kowalski J, Gerritsen ME. Peroxisome proliferator-activated receptor gamma ligands are potent inhibitors of angiogenesis in vitro and in vivo. *J Biol Chem.* 1999;274(13):9116-9121.

12.   Xu X, Chen P, Zheng Q, Wang Y, Chen W. Effect of pioglitazone on diabetic nephropathy and expression of HIF-1alpha and VEGF in the renal tissues of type 2 diabetic rats. *Diabetes Res Clin Pract.*

13.   Makino H, Miyamoto Y, Sawai K, Mori K, Mukoyama M, Nakao K, Yoshimasa Y, Suga S. Altered gene expression related to glomerulogenesis and podocyte structure in early diabetic nephropathy of db/db mice and its restoration by pioglitazone. *Diabetes.* 2006;55(10):2747-2756.

14.   Toblli JE, Cao G, Giani JF, Angerosa M, Dominici FP, Gonzalez-Cadavid NF. Antifibrotic effects of pioglitazone at low doses on the diabetic rat kidney are associated with the improvement of markers of cell turnover, tubular and endothelial integrity, and angiogenesis. *Kidney Blood Press Res.*34(1):20-33.

15.   Aljada A, O'Connor L, Fu YY, Mousa SA. PPAR gamma ligands, rosiglitazone and pioglitazone, inhibit bFGF- and VEGF-mediated angiogenesis. *Angiogenesis.* 2008;11(4):361-367.

16.   Keshamouni VG, Arenberg DA, Reddy RC, Newstead MJ, Anthwal S, Standiford TJ. PPAR-gamma activation inhibits angiogenesis by blocking ELR+CXC chemokine production in non-small cell lung cancer. *Neoplasia.* 2005;7(3):294-301.

17.   Vogt T, Hafner C, Bross K, Bataille F, Jauch KW, Berand A, Landthaler M, Andreesen R, Reichle A. Antiangiogenetic therapy with pioglitazone, rofecoxib, and metronomic trofosfamide in patients with advanced malignant vascular tumors. *Cancer.* 2003;98(10):2251-2256.

18.   Coras B, Hafner C, Reichle A, Hohenleutner U, Szeimies RM, Landthaler M, Vogt T. Antiangiogenic therapy with pioglitazone, rofecoxib, and trofosfamide in a patient with endemic kaposi sarcoma. *Arch Dermatol.* 2004;140(12):1504-1507.

19.   Sarayba MA, Li L, Tungsiripat T, Liu NH, Sweet PM, Patel AJ, Osann KE, Chittiboyina A, Benson SC, Pershadsingh HA, Chuck RS. Inhibition of corneal neovascularization by a peroxisome proliferator-activated receptor-gamma ligand. *Exp Eye Res.* 2005;80(3):435-442.

20. Huang PH, Sata M, Nishimatsu H, Sumi M, Hirata Y, Nagai R. Pioglitazone ameliorates endothelial dysfunction and restores ischemia-induced angiogenesis in diabetic mice. *Biomed Pharmacother.* 2008;62(1):46-52.

21. Kelley DE, He J, Menshikova EV, Ritov VB. Dysfunction of mitochondria in human skeletal muscle in type 2 diabetes. *Diabetes.* 2002;51(10):2944-2950.

22. Rabol R, Boushel R, Almdal T, Hansen CN, Ploug T, Haugaard SB, Prats C, Madsbad S, Dela F. Opposite effects of pioglitazone and rosiglitazone on mitochondrial respiration in skeletal muscle of patients with type 2 diabetes. *Diabetes Obes Metab.*12(9):806-814.

23. Choo HJ, Kim JH, Kwon OB, Lee CS, Mun JY, Han SS, Yoon YS, Yoon G, Choi KM, Ko YG. Mitochondria are impaired in the adipocytes of type 2 diabetic mice. *Diabetologia.* 2006;49(4):784-791.

24. Skov V, Glintborg D, Knudsen S, Tan Q, Jensen T, Kruse TA, Beck-Nielsen H, Hojlund K. Pioglitazone enhances mitochondrial biogenesis and ribosomal protein biosynthesis in skeletal muscle in polycystic ovary syndrome. *PLoS One.* 2008;3(6):e2466.

25. Bogacka I, Xie H, Bray GA, Smith SR. Pioglitazone induces mitochondrial biogenesis in human subcutaneous adipose tissue in vivo. *Diabetes.* 2005;54(5):1392-1399.

26. Semenza GL. Hypoxia-inducible factor 1 (HIF-1) pathway. *Sci STKE.* 2007;2007(407):cm8.

27. Michelakis ED, Sutendra G, Dromparis P, Webster L, Haromy A, Niven E, Maguire C, Gammer TL, Mackey JR, Fulton D, Abdulkarim B, McMurtry MS, Petruk KC. Metabolic modulation of glioblastoma with dichloroacetate. *Sci Transl Med.* 2010;2(31):31ra34.

28. Sutendra G, Dromparis P, Kinnaird A, Stenson TH, Haromy A, Parker JM, McMurtry MS, Michelakis ED. Mitochondrial activation by inhibition of PDKII suppresses HIF1a signaling and angiogenesis in cancer. *Oncogene.* 2012.

29. Wei K, Jayaweera AR, Firoozan S, Linka A, Skyba DM, Kaul S. Quantification of myocardial blood flow with ultrasound-induced destruction of microbubbles administered as a constant venous infusion. *Circulation.* 1998;97(5):473-483.

30. Motola D, Piccinni C, Biagi C, Raschi E, Marra A, Marchesini G, Poluzzi E. Cardiovascular, ocular and bone adverse reactions associated with thiazolidinediones: a disproportionality analysis of the US FDA adverse event reporting system database. *Drug Saf.* 2012;35(4):315-323.

31. Hankenson KD, Dishowitz M, Gray C, Schenker M. Angiogenesis in bone regeneration. *Injury.* 2011;42(6):556-561.

32. Bair SM, Choueiri TK, Moslehi J. Cardiovascular complications associated with novel angiogenesis inhibitors: Emerging evidence and evolving perspectives. *Trends Cardiovasc Med.* 2013.

33. Guan Y, Hao C, Cha DR, Rao R, Lu W, Kohan DE, Magnuson MA, Redha R, Zhang Y, Breyer MD. Thiazolidinediones expand body fluid volume through PPARgamma stimulation of ENaC-mediated renal salt absorption. *Nat Med.* 2005;11(8):861-866.

34. Cree MG, Zwetsloot JJ, Herndon DN, Qian T, Morio B, Fram R, Sanford AP, Aarsland A, Wolfe RR. Insulin sensitivity and mitochondrial function are improved in children with burn injury during a randomized controlled trial of fenofibrate. *Ann Surg.* 2007;245(2):214-221.

35. Abcouwer SF. Direct Effects of PPARalpha Agonists on Retinal Inflammation and Angiogenesis May Explain How Fenofibrate Lowers Risk of Severe Proliferative Diabetic Retinopathy. *Diabetes.* 2013;62(1):36-38.

36. Liu H, Zang C, Fenner MH, Liu D, Possinger K, Koeffler HP, Elstner E. Growth inhibition and apoptosis in human Philadelphia chromosome-positive lymphoblastic leukemia cell lines by treatment with the dual PPARalpha/gamma ligand TZD18. *Blood.* 2006;107(9):3683-3692.

37. Liu H, Zang C, Fenner MH, Possinger K, Elstner E. PPARgamma ligands and ATRA inhibit the invasion of human breast cancer cells in vitro. *Breast Cancer Res Treat.* 2003;79(1):63-74.

38. Panigrahy D, Singer S, Shen LQ, Butterfield CE, Freedman DA, Chen EJ, Moses MA, Kilroy S, Duensing S, Fletcher C, Fletcher JA, Hlatky L, Hahnfeldt P, Folkman J, Kaipainen A. PPARgamma ligands inhibit primary tumor growth and metastasis by inhibiting angiogenesis. *J Clin Invest.* 2002;110(7):923-932.

39. Zang C, Wachter M, Liu H, Posch MG, Fenner MH, Stadelmann C, von Deimling A, Possinger K, Black KL, Koeffler HP, Elstner E. Ligands for PPARgamma and RAR cause induction of growth inhibition and apoptosis in human glioblastomas. *J Neurooncol.* 2003;65(2):107-118.

40. Touyz RM, Schiffrin EL. Peroxisome proliferator-activated receptors in vascular biology-molecular mechanisms and clinical implications. *Vascul Pharmacol.* 2006;45(1):19-28.

41. Perez-Ortiz JM, Tranque P, Burgos M, Vaquero CF, Llopis J. Glitazones induce astroglioma cell death by releasing reactive oxygen species from mitochondria: modulation of cytotoxicity by nitric oxide. *Mol Pharmacol.* 2007;72(2):407-417.

42. Clark TA, Pierce GN. Cardiovascular complications of non-insulin-dependent diabetes: the JCR:LA-cp rat. *J Pharmacol Toxicol Methods.* 2000;43(1):1-10.

43. Vine DF, Glimm DR, Proctor SD. Intestinal lipid transport and chylomicron production: possible links to exacerbated atherogenesis in a rodent model of the metabolic syndrome. *Atheroscler Suppl.* 2008;9(2):69-76.

44. Kim KY, Cheon HG. Antiangiogenic effect of rosiglitazone is mediated via peroxisome proliferator-activated receptor gamma-activated maxi-K channel opening in human umbilical vein endothelial cells. *J Biol Chem.* 2006;281(19):13503-13512.

45. Scoditti E, Massaro M, Carluccio MA, Distante A, Storelli C, De Caterina R. PPARgamma agonists inhibit angiogenesis by suppressing PKCalpha- and CREB-mediated COX-2 expression in the human endothelium. *Cardiovasc Res.*86(2):302-310.

46. Higuchi A, Ohashi K, Shibata R, Sono-Romanelli S, Walsh K, Ouchi N. Thiazolidinediones reduce pathological neovascularization in ischemic retina via an adiponectin-dependent mechanism. *Arterioscler Thromb Vasc Biol.*30(1):46-53.

47. Murata T, Hata Y, Ishibashi T, Kim S, Hsueh WA, Law RE, Hinton DR. Response of experimental retinal neovascularization to thiazolidinediones. *Arch Ophthalmol.* 2001;119(5):709-717.

48. Herington JL, Crispens MA, Carvalho-Macedo AC, Camargos AF, Lebovic DI, Bruner-Tran KL, Osteen KG. Development and prevention of postsurgical adhesions in a chimeric mouse model of experimental endometriosis. *Fertil Steril.*95(4):1295-1301 e1291.

49. Gealekman O, Burkart A, Chouinard M, Nicoloro SM, Straubhaar J, Corvera S. Enhanced angiogenesis in obesity and in response to PPARgamma activators through adipocyte VEGF and ANGPTL4 production. *Am J Physiol Endocrinol Metab.* 2008;295(5):E1056-1064.

50.   Van Oosterhout MF, Willigers HM, Reneman RS, Prinzen FW. Fluorescent microspheres to measure organ perfusion: validation of a simplified sample processing technique. *Am J Physiol.* 1995;269(2 Pt 2):H725-733.

A version of this chapter has been submitted for publication. Dromparis P, Sutendra G, Paulin R, Proctor S, Michelakis ED and McMurtry MS. 2013.

Chapter 5

Overall Conclusions and Future Directions

5.1 Discussion and Conclusions

In this dissertation, I expand on the functional role of mitochondria in vascular oxygen sensing and the importance of ER-mitochondria crosstalk in the pulmonary vasculature. I explore the clinical implications of therapeutically targeting this unit in pulmonary vascular disease, as well as provide examples of how therapies that re-activate mitochondria may provide undesirable effects in some instances. The main conclusions of this work may be directly or indirectly relevant to basic science researchers as well as clinicians.

In chapter 1 of this dissertation, I approached the challenge of synthesizing an integrative and multifactorial presentation that provided a comprehensive model of the role of mitochondria in vascular health and disease. To summarize, the ability of mitochondria to sense changes in oxygen is contingent on adequate supply of metabolic substrates, as disruption of mitochondrial metabolism interferes with the ability of mitochondria to appropriately sense changes in oxygen. Indeed, this has been exploited by cancer cells, which actively suppress mitochondrial metabolism by inhibiting the glucose oxidation gatekeeping enzyme, PDH. This strategy not only suppresses apoptosis through several feedback mechanisms, but also modulates vascular homeostasis and tissue perfusion by activating HIF1α and promoting the formation of new blood vessels in rapidly growing tumors. Indeed, re-activation of glucose oxidation with the metabolic modulator dichloroacetate, or exogenous administration of mitochondrial-derived signals inhibits the inappropriate pseudo-hypoxic signaling. This opens the intriguing possibility that mitochondria can regulate chronic vascular homeostasis, in addition to the acute effects classically described. In addition, glucose oxidation can be suppressed is by disrupting mitochondrial calcium levels. Calcium is a necessary cofactor for PDH and the Krebs' enzymes IDH and αKGDH. In vascular cells, mitochondria are in close proximity and even form functional units with the ER, which is well recognized as the largest calcium storage organelle. Calcium released by the ER enters the mitochondria and drives ATP production. ATP produced by the mitochondria is essential for the high ATP demand of ER-calcium ATPases. Since many

vasoconstrictors also promote the release of ER-calcium, the functional proximity of the ER and mitochondria allows for exquisite matching of ATP production under times of contractile stimulation and enhanced ATP demand. However, disruption in the calcium cross-talk between the ER and mitochondria, which occurs through physical disruption under ER-stress for example, can also trigger pathological signaling, similar to that in cancer.

In chapter 2 of this thesis, we explored the effects of disrupting ER-mitochondria calcium transfer and the effects on chronic oxygen sensing in a knockout mouse model. Uncoupling protein-2 (UCP2) was recently implicated in the mitochondrial uptake of calcium specifically from the ER in vascular cells. Genetic loss (or pharmacological inhibition) of this protein resulted in reduced Ca^{2+}_m levels both at baseline and under stimulation of ER-calcium release in pulmonary artery smooth muscle cells (PASMCs). Deficiencies in UCP2 resulted in (1) suppressed activity of PDH (2) suppressed levels of Krebs' cycle intermediates (3) suppressed mROS (4) normoxic activation of HIF1α, all of which mimicked the effects of chronic hypoxia in wildtype cells. In addition, the absence of further effects by hypoxia on UCP2-deficient cells suggested that disruption of UCP2-mediated ER-calcium transport completely mimics the effects of hypoxia in all parameters studied. In vivo analysis found that mice-deficient in UCP2 developed spontaneous pulmonary hypertension due to pulmonary vascular remodeling (pulmonary hypertension is a well-documented consequence of chronic hypoxia) and had elevated hematocrit, both which mimicked the effects of chronic hypoxia on the UCP2-wildtype controls. In agreement with the in vitro data, hypoxia did not exacerbate the pulmonary hypertension or hematocrit elevation in the UCP2-deficient mice, suggesting that the pseudohypoxic signaling is maximally activated. This work supports mitochondrial-derived signals as modulators in the chronic response to hypoxia. In addition, it highlights the recently described importance of the ER-mitochondria unit in the development of pulmonary hypertension.

In chapter 3 of this dissertation, we provided evidence that targeting the functional disruption of the ER-mitochondria unit can prevent mitochondrial

suppression pulmonary vascular remodeling. We show 4-phenylbuyric acid (PBA) administered in the drinking water (1) prevents and reverses the activation of the pro-proliferative and anti-apoptotic arm of the ER-stress response (2) prevents and reverses the pulmonary vascular remodeling by suppressing apoptosis and inhibiting proliferation in the resistance pulmonary arteries and (3) prevents and reverses changes in pulmonary hemodynamics in two well-established models of pulmonary hypertension. Mechanistic studies in PASMCs showed that PBA, and a second chaperone TUDCA, prevented the ER-stress-induced reduction of mitochondrial calcium and the subsequent suppression of mitochondrial signaling that contributes to the cellular hallmark of pulmonary hypertension. This work represents a novel and previously unexplored approach to targeting metabolic signals in pulmonary vascular remodeling disease, which is particularly appealing since many of the known pulmonary hypertension-associated triggers could at least in theory involve these activation pathways. Moreover, this is work is an example of how pathobiology linked with the functional dysregulation between mitochondria and other organelles can be therapeutically targeted.

In chapter 4 of this dissertation, we explore how activating mitochondrial signaling may be undesirable in some clinical instances. Pioglitazone, a thiazolidinedione commonly used in the management of type II diabetes mellitus, impaired angiogenesis and gastrocnemius perfusion in our hind-limb ischemia model. Mechanistic studies in vitro suggested that pioglitazone increases mitochondrial-derived signals and impaired HIF1α activation, even in hypoxia. This work is in keeping with our other data and further supports the function of mitochondria in regulating the response to chronic hypoxia. Furthermore, this work highlights the potential pitfalls of mitochondria activating therapies in the inappropriate clinical setting and suggests that perhaps inhibition of mitochondrial-derived signals may in fact be therapeutic in circumstances where hypoxic signaling may be beneficial.

5.2 Future directions

This work has several new and exciting implications for future basic science, translational, and clinical research:

- Our descriptions of spontaneous pulmonary hypertension in a mouse model that mimics the in vitro cellular metabolic phenotype of human pulmonary hypertension PASMCs may be an additional and important tool for future studies in the field of pulmonary hypertension, as well as oxygen sensing in the pulmonary vasculature. Our data suggesting that UCP2-deficient mice exhibit aberrations in systemic hypoxia signaling (ie increased hematocrit) may expand future oxygen sensing studies beyond the pulmonary vasculature as well.

- The recent description of polymorphisms in the promoter/gene of UCP2 that affect both expression and function in humans has clinical relevance. Genetic studies comparing polymorphisms in idiopathic pulmonary artery patients could identify a genetic susceptibility and potentially open new avenues of therapy specifically for these patients.

- The work with chemical chaperones that are already FDA approved and are currently being used clinically allows for the rapid progression of these agents into early phase clinical trials. Rationale for this transition is particularly strong, considering the robust association between the expression of the ATF6-induced protein, Nogo, and the WHO classification of pulmonary hypertension patients. In addition, further pre-clinical trials combining these agents with direct mitochondrial activators like dichloroacetate may reveal additional synergistic benefits.

- This work uncovers a mechanism that could explain the recent clinical descriptions of adverse cardiovascular events in diabetic patients managed with the thiazolidinedione class of insulin sensitizers. Our work supports careful reconsideration of the use of these agents in high-risk populations. In addition, this work serves as a caution against the potential undesirable consequences that future mitochondrial-influencing therapies may elicit if utilized in inappropriate clinical circumstances.